



DOUBLE-DIFFUSIVE CONVECTION FLOW IN A
POROUS MEDIUM SATURATED WITH A
NANOFLUID

A DISSERTATION SUBMITTED TO THE UNIVERSITY OF
KWAZULU-NATAL FOR THE DEGREE OF MASTER OF SCIENCE
IN THE COLLEGE OF AGRICULTURE, ENGINEERING AND SCIENCE.

By

Nageeb A. H. Haroun

School of Mathematics, Statistics and Computer Sciences

Pietermaritzburg

March 2014

Contents

Abstract	iv
Declaration	v
Dedication	vi
Acknowledgment	vii
1 Introduction	1
1.1 Background and Motivation	1
1.2 Double-diffusive convection	5
1.3 The study of nanofluids	6
1.4 Empirical and numerical studies of double-diffusive convection	7
1.5 Some solution techniques	10

1.5.1	The spectral relaxation method (SRM)	11
1.5.2	The spectral quasi-linearization method (SQLM)	12
1.6	Dissertation objectives	13
2	A brief description of the SRM and SQLM	15
3	Unsteady nanofluid flow, heat and mass transfer over a stretching sheet	25
3.1	Introduction	25
3.2	Governing Equations	28
3.3	Skin friction, heat and mass transfer coefficients	31
3.4	Some particular cases of interest	33
3.5	Results and Discussion	35
3.6	Summary	51
4	Mixed convection in MHD nanofluid flow due to a stretching sheet with Soret and Dufour effects	52
4.1	Introduction	53
4.2	Mathematical formulation	55

4.3	Skin friction, heat and mass transfer coefficients	59
4.4	Some particular cases of interest	61
4.5	Results and Discussion	62
4.6	Summary	73
5	Unsteady MHD mixed convection with suction/injection due to a stretching/shrinking surface	74
5.1	Introduction	74
5.2	Governing Equations	76
5.3	Skin friction, heat and mass transfer coefficients	81
5.4	Cases of special interest	82
5.5	Results and Discussion	83
5.6	Summary	98
6	Conclusion	99
	Bibliography	103

Abstract

In this work, we studied heat and mass transfer in a nanofluid flow over a stretching sheet. Fluid flow in different flow geometries was studied and a co-ordinate transformation was used to transform the governing equations into non-dimensional non-similar boundary layer equations. These equations were then solved numerically using both established and recent techniques such as the spectral relaxation and spectral quasi-linearization methods. Numerical solutions for the heat transfer, mass transfer and skin friction coefficients have been presented for different system parameters, such as heat generation, Soret and Dufour effects, chemical reaction, thermal radiation influence, the local Grashof number, Prandtl number, Eckert number, Hartmann number and the Schmidt number. The dependency of the skin friction, heat and mass transfer coefficients on these parameters has been quantified and discussed. The accuracy, and validity of the spectral relaxation and spectral quasi-linearization methods has been established.

Declaration

I declare that this thesis presents my original work and effort. It was carried out under the supervision of Prof. P. Sibanda, in the School of Mathematics, Statistics and Computer Sciences, University of KwaZulu-Natal, Pietermaritzburg.

It has not been submitted in any form to any university or institution of learning for any degree or qualification. Where use has been made of the work of others it is duly acknowledged.

Student: _____
Nageeb. A. H. Haroun

Date

Supervisor: _____
Prof. P. Sibanda

Date

Dedication

This thesis is dedicated to my Mommy and beautiful wife, BAIEGA MOHAMED ESSA MAHMOUD.

Acknowledgment

I am most grateful to God for his grace to achieve all I have done so far. This dissertation owes its completion to a select group of family and close friends. My biggest thanks go to my supervisor Prof. P. Sibanda for his useful advice and support throughout the research. I would like to thank Prof. S.S Motsa for his advice and help on spectral methods, my brother Prof. Mahgoup Haroun, a true brother and friend, who taught me not to take life as a graduate student too seriously and my friends in the School of Mathematics, Statistics and Computer Science, especially those in applied mathematics for helping me with ideas and suggestions in my research: Sami M.S. Ahamed and his beautiful wife, Olumuyiwa Otegbeye, S. Shaw and others who have generously supported me (you know who you are). I would like to thank my great mother, Khadiga Iderise, who has always supported me in every thing I have done, and my family for the support that they gave me. Most importantly, to the one who has made it possible for me to be here, do what I have done, and has guided me, even though sometimes I did not listen; thank you Dr. Abdallah Ibrihim.

List of Tables

3.1	Thermophysical properties of water and copper and silver nanofluids.	35
3.2	Effect of various values of the Prandtl number Pr on the skin friction $-f''(0)$ and heat transfer coefficient $-\theta'(0)$, when $\delta = 0$	36
3.3	Effect of various values of the Prandtl number Pr on the skin friction $-f''(0)$ and heat transfer coefficient $-\theta'(0)$, when $\delta = 0$	37
3.4	Effect of variation of nanoparticle volume fraction ϕ on the skin friction $-f''(0)$, heat and mass transfer coefficients $-\theta'(0)$, $-\Phi'(0)$ when $\delta = 1$, $\gamma = 1$	38
3.5	Effect of variation of nanoparticle volume fraction ϕ on the skin friction $-f''(0)$, heat and mass transfer coefficients $-\theta'(0)$, $-\Phi'(0)$ when $\delta = 1$, $\gamma = 1$	39
4.1	Comparison of the values of $-f''(0,0)$ for various values of n , when $\phi = 0$, $Gr_t = Gr_c = 0$ and $\xi = 0$ (steady state).	62
4.2	Comparison of the heat transfer coefficient $-\theta'(0, \xi)$ for various values of Pr and ξ with $\phi = 0$, $Nr = Ec = D_f = n = 0$	63

4.3	Comparison of heat transfer coefficient $-\theta'(0, 0)$ for various values of Pr , when $\phi = 0$, $Nr = Ec = D_f = n = 0$ and $\xi = 0$ (steady state).	63
5.1	Comparison of $f''(0, 1)$ for various values of λ when $Ha = Gr_t = Gr_c = \delta = D_f = Sc = Sr = \gamma = 0$, $Pr = 1$ and $\phi = 0$ with $\xi = 1$ (final steady state). . .	84
5.2	Comparison of $f''(0, 1)$ for various values of λ when $Ha = Gr_t = Gr_c = \delta = D_f = Sc = Sr = \gamma = 0$, $Pr = 1$ and $\phi = 0$ with $\xi = 1$	85
5.3	Comparison of $f''(0, 1)$ for various values of λ for the both stretching/shrinking sheet when $Ha = Gr_t = Gr_c = \delta = D_f = Sc = Sr = \gamma = 0$, $Pr = 1$ and $\phi = 0$ with $\xi = 1$	85

List of Figures

3.1	Physical model and coordinate system.	28
3.2	Effect of nanoparticle volume fraction ϕ on the velocity profiles with $\xi = 0.5$, $\delta = 1, \gamma = 1$	41
3.3	Effect of nanoparticle volume fraction ϕ on tangential velocity profiles with $\xi = 0.5, \delta = 1, \gamma = 1$	41
3.4	Effect of nanoparticle volume fraction ϕ on the temperature profiles with $\xi =$ $0.5, \delta = 1, \gamma = 1$	42
3.5	Effect of nanoparticle volume fraction ϕ on the concentration profiles with $\xi = 0.5, \delta = 1, \gamma = 1$	42
3.6	Effect of the dimensionless heat generation δ on the temperature profiles with $\xi = 0.5, \phi = 0.3, \gamma = 1$	43
3.7	Effect of the dimensionless heat generation δ on the concentration profiles with $\xi = 0.5, \phi = 0.3, \gamma = 1$	44

3.8	Effect of chemical reaction parameter γ on the concentration profiles with $\xi = 0.5, \delta = 1, \phi = 0.3$	44
3.9	Effect of the Soret number Sr on the concentration profiles with $\xi = 0.5, \delta = 1, \phi = 0.3, \gamma = 1$	45
3.10	Effect of the variation nanoparticle volume fraction ϕ on the skin friction coefficient against ξ with $\delta = 1, \gamma = 1$	46
3.11	Effect of the variation nanoparticle volume fraction ϕ on heat transfer coefficient against ξ with $\delta = 1, \gamma = 1$	47
3.12	Effect of the variation nanoparticle volume fraction ϕ on mass transfer coefficient against ξ with $\delta = 1, \gamma = 1$	47
3.13	Effect of the dimensionless heat generation parameter δ on heat transfer coefficient against ξ with $\phi = 0.3, \gamma = 1$	48
3.14	Effect of the dimensionless heat generation parameter δ on mass transfer coefficient against ξ with $\phi = 0.3, \gamma = 1$	49
3.15	Effect of chemical reaction parameter γ on mass transfer coefficient against ξ with $\delta = 1, \phi = 0.3$	50
3.16	Effect of the Soret number Sr on mass transfer coefficient against ξ with $\delta = 1, \phi = 0.3, \gamma = 1$	51
4.1	Physical model and coordinate system.	55

4.2	Effect of nanoparticle volume fraction ϕ on (a) the normal and (b) tangential velocity profiles respectively, for $Gr_t = 0.01$, $n = 0$, $Gr_c = 0.01$, $Nr = 10$, $Pr = 7, Ec = 10$, $D_f = 0.01$, $\gamma = 3$, $Sc = 1, Sr = 1$ and $\xi = 0.5$	65
4.3	Effect of nanoparticle volume fraction ϕ on (a) the temperature profiles and (b) the concentration profiles for $Gr_t = 0.01$, $n = 0$, $Gr_c = 0.01$, $Nr = 10$, $Pr = 7, Ec = 10$, $D_f = 0.01$, $\gamma = 3$, $Sc = 1, Sr = 1$ and $\xi = 0.5$	65
4.4	Effect of nanoparticle volume fraction ϕ on the skin friction coefficient for $Gr_t = 0.01$, $n = 0$, $Gr_c = 0.01$, $Nr = 10$, $Pr = 7, Ec = 10$, $D_f = 0.01$, $\gamma = 3, Sc = 1$ and $Sr = 1$	66
4.5	Effect of nanoparticle volume fraction ϕ on (a) the heat transfer coefficient and (b) the mass transfer coefficient for $Gr_t = 0.01$, $n = 0$, $Gr_c = 0.01$, $Nr = 10$, $Pr = 7, Ec = 10$, $D_f = 0.01$, $\gamma = 3, Sc = 1$ and $Sr = 1$	66
4.6	Effect of the thermal radiation parameter Nr on (a) the temperature profiles and (b) the concentration profiles for $n = 0$, $\phi = 0.3$, $Gr_t = 0.01$, $Gr_c = 0.01$, $Pr = 7$, $Ec = 10$, $D_f = 0.01$, $\gamma = 3$, $Sc = 1$, $Sr = 1$ and $\xi = 0.5$	67
4.7	Effect of the thermal radiation parameter Nr on skin friction coefficient for $n = 0$, $\phi = 0.3$, $Gr_t = 0.01$, $Gr_c = 0.01$, $Pr = 7$, $Ec = 10$, $D_f = 0.01$, $\gamma = 3$, $Sc = 1$ and $Sr = 1$	68
4.8	Effect of the thermal radiation parameter Nr on (a) the heat transfer coefficient and (b) the mass transfer coefficient for $n = 0$, $\phi = 0.3$, $Gr_t = 0.01$, $Gr_c = 0.01$, $Pr = 7$, $Ec = 10$, $D_f = 0.01$, $\gamma = 3$, $Sc = 1$ and $Sr = 1$	68

4.9	Effect of the Dufour number D_f on (a) the temperature profiles and (b) the concentration profiles with nanofluid $\phi = 0.3, 0.5$	69
4.10	Effect of the Dufour number D_f on (a) the heat transfer coefficient and (b) the mass transfer coefficient with nanofluid $\phi = 0.3, 0.5$ for $n = 0$, $Gr_t = 0.05$, $Gr_c = 0.1$, $Pr = 7$, $Nr = 10$, $Ec = 9$, $\gamma = 0.3$, $Sc = 2$ and $Sr = 1$	70
4.11	Effect of the chemical reaction parameter γ on the concentration profiles for $n = 0$, $\phi = 0.3$, $Gr_t = 0.01$, $Gr_c = 0.01$, $Pr = 7$, $Nr = 10$, $Ec = 10$, $D_f = 0.01$, $Sc = 1$, $Sr = 1$ and $\xi = 0.5$	71
4.12	Effect of the chemical reaction parameter γ on the local Sherwood number for $n = 0$, $\phi = 0.3$, $Gr_t = 0.01$, $Gr_c = 0.01$, $Pr = 7$, $Nr = 10$, $Ec = 10$, $D_f = 0.01$, $Sc = 1$ and $Sr = 1$	71
4.13	Effect of the Soret number Sr on the concentration profiles with $n = 0$, $\phi = 0.3$, $Gr_t = 0.01$, $Gr_c = 0.01$, $Pr = 7$, $Nr = 10$, $Ec = 10$, $D_f = 0.01$, $Sc = 1$, $\gamma = 3$ and $\xi = 0.5$	72
4.14	Effect of the Soret number Sr on the local Sherwood number for $n = 0$, $\phi = 0.3$, $Gr_t = 0.01$, $Gr_c = 0.01$, $Pr = 7$, $Nr = 10$, $Ec = 10$, $D_f = 0.01$, $Sc = 1$ and $\gamma = 3$	73
5.1	Schematic diagram of the flow geometry.	77

5.2	Effect of the nanoparticle volume fraction ϕ on (a) the normal velocity and (b) tangential Velocity profiles respectively, for $D_f = 0.01$, $\lambda = 0.5$, $Gr_t = 0.01$, $Gr_c = 0.01$, $Ha = 2$, $\delta = 0.1$, $Sc = 1$, $Sr = 1$, $f_w = 1$, $\gamma = 0.1$ and $\xi = 0.5$. . .	87
5.3	Effect of the nanoparticle volume fraction ϕ on (a) the temperature profiles and (b) the concentration profiles for $D_f = 0.01$, $\lambda = 0.5$, $Gr_t = 0.01$, $Gr_c = 0.01$, $Ha = 2$, $\delta = 0.1$, $Sc = 1$, $Sr = 1$, $f_w = 1$, $\gamma = 0.1$ and $\xi = 0.5$	87
5.4	Effect of the nanoparticle volume fraction ϕ on the skin friction coefficient for $D_f = 0.01$, $\lambda = 0.5$, $Gr_t = 0.01$, $Gr_c = 0.01$, $Ha = 2$, $\delta = 0.1$, $Sc = 1$, $Sr = 1$, $f_w = 1$ and $\gamma = 0.1$	88
5.5	Effect of the nanoparticle volume fraction ϕ on (a) the heat transfer coefficient and (b) the mass transfer coefficient for $D_f = 0.01$, $\lambda = 0.5$, $Gr_t = 0.01$, $Gr_c = 0.01$, $Ha = 2$, $\delta = 0.1$, $Sc = 1$, $Sr = 1$, $f_w = 1$ and $\gamma = 0.1$	88
5.6	Effect of the Hartmann number Ha on (a) axial velocity and (b) tangential velocity profiles respectively, for $D_f = 0.01$, $\phi = 0.3$, $Gr_t = 0.01$, $Gr_c = 0.01$, $f_w = 1$, $\delta = 0.1$, $Sc = 1$, $Sr = 1$, $\lambda = -1.15$, $\gamma = 3$ and $\xi = 0.5$	90
5.7	Effect of the Hartmann number on the skin friction coefficient for $D_f = 0.01$, $\phi = 0.3$, $Gr_t = 0.01$, $Gr_c = 0.01$, $f_w = 1$, $\delta = 0.1$, $Sc = 1$, $Sr = 1$, $\lambda = -1.15$ and $\gamma = 3$	90
5.8	Effect of the Hartmann number on (a) the heat transfer coefficient and (b) the mass transfer coefficient when $D_f = 0.01$, $\phi = 0.3$, $Gr_t = 0.01$, $Gr_c = 0.01$, $f_w = 1$, $\delta = 0.1$, $Sc = 1$, $Sr = 1$, $\lambda = -1.15$ and $\gamma = 3$	91

5.9	Effect of suction/injection parameter f_w on (a) axial velocity and (b) tangential velocity profiles respectively, when $D_f = 0.01$, $\phi = 0.3$, $Gr_t = 0.01$, $Gr_c = 0.01$, $Ha = 2$, $\delta = 0.2$, $Sc = 1$, $Sr = 1$, $\lambda = 0.5$, $\gamma = 3$ and $\xi = 0.5$	92
5.10	Effect of suction/injection parameter f_w on (a) the temperature profiles and (b) the concentration profiles when $D_f = 0.01$, $\phi = 0.3$, $Gr_t = 0.01$, $Gr_c = 0.01$, $Ha = 2$, $\delta = 0.2$, $Sc = 1$, $Sr = 1$, $\lambda = 0.5$, $\gamma = 3$ and $\xi = 0.5$	93
5.11	Effect of suction/injection parameter f_w on the skin friction coefficient for $D_f = 0.01$, $\phi = 0.3$, $Gr_t = 0.01$, $Gr_c = 0.01$, $Ha = 2$, $\delta = 0.2$, $Sc = 1$, $Sr = 1$, $\lambda = 0.5$ and $\gamma = 3$	93
5.12	Effect of suction/injection parameter f_w on (a) the heat transfer coefficient and (b) the mass transfer coefficient for $D_f = 0.01$, $\phi = 0.3$, $Gr_t = 0.01$, $Gr_c = 0.01$, $Ha = 2$, $\delta = 0.2$, $Sc = 1$, $Sr = 1$, $\lambda = 0.5$ and $\gamma = 3$	94
5.13	Effect of various a stretching/shrinking parameter values λ on (a) axial velocity and (b) tangential velocity profiles respectively, for $D_f = 0.01$, $\phi = 0.3$, $Gr_t = 0.01$, $Gr_c = 0.01$, $Ha = 2$, $\delta = 0.1$, $Sc = 1$, $Sr = 1$, $f_w = 1$, $\gamma = 0.1$ and $\xi = 0.5$	96
5.14	Effect of various a stretching/shrinking parameter values λ on (a) the temperature profiles and (b) the concentration profiles for $D_f = 0.01$, $\phi = 0.3$, $Gr_t = 0.01$, $Gr_c = 0.01$, $Ha = 2$, $\delta = 0.1$, $Sc = 1$, $Sr = 1$, $f_w = 1$, $\gamma = 0.1$ and $\xi = 0.5$	96

5.15	Effect of various a stretching/shrinking parameter values λ on the skin friction coefficient for $D_f = 0.01$, $\phi = 0.3$, $Gr_t = 0.01$, $Gr_c = 0.01$, $Ha = 2$, $\delta = 0.1$, $Sc = 1$, $Sr = 1$, $f_w = 1$ and $\gamma = 0.1$	97
5.16	Effect of various a stretching/shrinking parameter values λ on (a) the heat transfer coefficient and (b) the mass transfer coefficient for $D_f = 0.01$, $\phi = 0.3$, $Gr_t = 0.01$, $Gr_c = 0.01$, $Ha = 2$, $\delta = 0.1$, $Sc = 1$, $Sr = 1$, $f_w = 1$ and $\gamma = 0.1$	97

Chapter 1

Introduction

1.1 Background and Motivation

Fluid flow and heat transfer occur in both natural and man-made industrial situations. Such flow or heat and mass transfer processes can be modeled mathematically by complex systems of partial differential equations, which are often nonlinear due to both the complexity of the problem and the number of variables in the problem. There are several ways to solve these differential equations, such as numerical, analytical or semi-analytical methods. Each of these methods has both advantages and disadvantages. Analytical solutions, where they can be found, often provide the best insights into the effects of different parameters that have a bearing on the solution, which is not usually the case with the other methods. Due to their complexity, there are however a lot of fluid flow, and heat and mass transfer problems that do not have exact solutions. In order to solve such problems semi-analytical and numerical methods have been introduced and used successfully. The main goal of the current study is

to introduce two numerical methods to solve nonlinear partial differential equations that arise in the flow of fluids.

Flows of practical significance, such as the spread of ground pollutants, occur over a porous medium. A porous medium consists of a solid matrix with interconnected voids. In a natural porous medium the distribution of pores, their shapes and sizes is irregular. Examples of natural porous media include beach sand, sandstone, limestone, wood and pulmonary tissue in the lungs, Bear and Bachmat [1], Corey [2], Ingham and Pop [3] and Vazquez [4]. Porous media flows have been comprehensively studied since they offer a means of separating solid materials of different sizes, Strange and Webber [5], Nield and Bejan [6]. Porous media act as highly selective screens or cages that allow access only to particles below a certain size. Porous media are generally characterized by two properties of porous media; porosity and permeability, that generally control the movement and storage of fluids. Porosity is the ratio of the void space to the total volume of the porous medium, see Lethr and Lethr [7]. Porosity is denoted by φ and represents the total storage capacity of the medium. The quantity $1 - \varphi$ therefore defines the fraction of the medium occupied by the solid. By defining φ in this way, the implicit assumption is that all the void space is connected. If, some of the pore space is disconnected from the remainder, then the concept of an effective porosity is often introduced. This is defined as the ratio of connected void to total volume, Nield and Bejan [6]. The second property, permeability, of porous media gives a sense of the ease with which a fluid can move freely through the pores. Natural flow through porous media is found in geomechanics, soil mechanics, hydrogeology, petroleum geology and geophysics. In civil engineering, this type of flow is important in geothermal energy recovery, ground water pollution, thermal energy storage and crude oil extraction, Feng [8], Vafai [9]. The significant topic investigated in this

dissertation is that of flow, or heat and mass transfer, in a porous medium saturated with a nanofluid.

Modelling fluid flow, or heat and mass transfer in a porous medium, has been investigated in various ways. Firstly, the concept of non-Darcy effects on transport equations, as will be explained further in Section 1.2, for several geometrical configurations and boundary conditions has been used, Nield and Bejan [6]. Alternatively, research on porous media has used the generalised Brinkman-Forcheimer model. In particular, Vafai [9] and Ranganatha and Viskanta [10] used this model to study convection from a vertical plate media; Nield and Kuznetsov [11; 12] studied boundary layer flows in nanofluids; while Kumari and Nath [13] studied non-Darcy natural convection in a Newtonian in a porous medium. In the present work we investigate the convective transport of heat and mass in nanofluid boundary layer flow.

In heat transfer studies, the objective is often to determine energy transfer between bodies at different temperatures and the mechanisms of heat transfer. In the eighteenth and early nineteenth centuries, researchers postulated that all bodies contained an invisible substance called the caloric. Properties assigned to the caloric included the weight. These ideas have subsequently proved to be inconsistent, but nevertheless an important feature of the caloric was that it flowed from hotter bodies to colder ones, see Behzadmehr and Azarkish [14]. Heat transfer is now understood to be the flow of thermal energy due to a non-uniform temperature field. This is commonly measured as a heat flux, see Holman [15] and Burmeister [16]. There are three modes of heat transfer between differentially heated bodies, conduction, convection and radiation, Thirumale [17].

Mass transfer occurs either via the bulk fluid motion or through the diffusion of a chemical species. The primary focus in this dissertation is on mass transfer through diffusion as a result of concentration gradients. An often mentioned example of diffusive mass transfer is the humidification that occurs when a container of water is left open leading to a mixture of air and water vapour in the atmosphere. A concentration gradient causes water to be transported from the liquid surface into the atmosphere, Wetly et al. [18]. Mass transfer has several similarities to the process of heat transfer.

The mechanisms of heat and mass transfer may be considered in terms of conduction or convection. In this regard, heat conduction is due to temperature gradients normal to the interface between two materials, and mass diffusion is due to mass gradients normal to the surface, if the fluid is at rest everywhere, see Kays and Crawford [19]. Moreover, if the fluid is moving, then its own movement as well as the two potential gradients are responsible for transferring heat and mass. Hence the transport of heat or mass is by both molecular conduction processes together with gross fluid motion.

Heat transport induced by buoyancy forces arising from a temperature gradient is called free convection, see Jaluria [20], Gorla and Zinolabedini [21; 22], Gebhart et al. [23] and Rathore and Kapuno [24]. It arises in situations such as cooling operations. Numerous scholars have studied free convection flows, among them Jaluria and Gebhart [25], Chen and Minkowycz [26] and Jaluria and Himasekhar [27]. Forced convection in porous medium was investigated by Rudramoorthy and Mayilsamy [28]. A combination of natural and forced convection was studied by Wooding [29] and Lai [30], and Lloyd and Sparrow [31]. Mixed convection with boundary layer stability and viscous dissipation over a horizontal surface was studied by,

among others, Mureithi and Mason [32] whose findings showed that the boundary layer is dominated by internal regions of super velocities.

1.2 Double-diffusive convection

In this section, we turn our attention to processes of combined heat and mass transfer that are driven by buoyancy. Double-diffusive convection describes convection driven by two different density gradients with different diffusion rates, see Siegmund and Rubinfeld [33]. Double-diffusive convection occurs in sea water, the mantle flow in the earth's crust as well as in many engineering and physical problems such as in contaminant transport in saturated soils, food processing, and the spread of pollutants, Bourich and Advani [34]. Double-diffusive convection in a fluid-saturated porous medium has been an active area of research for many years. Comprehensive reviews of the literature in this area can be found in the articles by Benzeghiba and Chikh [35], Mojtabi and Mojtabi [36], Beya and Lilia [37] and Mamou [38]. Double-diffusive convection also appears in the modeling of solar ponds, Akbarzadeh and Manins [39]. Nield [40] investigated double-diffusive convection and the in viscoelastic fluids in a porous media. Numerous previous studies have been published regarding the problem of a porous layer heated from below or the side by, among others, Baines and Gill [41], Gershuni et al. [42] and Khan and Zebib [43]. A number of studies are of particular interest, such as Raptis et al. [44] who found similarity solutions for the boundary layer flow near a vertical wall immersed in porous media with constant temperature and solute concentration. Nield et al. [45] studied convection due to inclined thermal and solutal gradients in a shallow horizontal layer in porous medium. Amahmid et al. [46] investigated double-diffusive convection in

a horizontal Brinkman porous layer with constant heat and mass fluxes. Alloui et al. [47] investigated the onset of double-diffusive convection in a rectangular porous layer on horizontal boundaries. The transition to chaos in double-diffusive Marangoni convection was investigated by Li et al. [48]. Magnetohydrodynamic (MHD) double-diffusive convective flow in a porous medium was investigated by Okedayo et al. [49] and the influence of viscous dissipation on free convection in a non-Darcy porous medium saturated with a nanofluid was studied by RamReddy et al. [50]. This review of the literature shows the importance of combined heat and mass transfer in double-diffusive convection flow. However, insufficient work has been carried out on double-diffusive convection. Consequently in this study we will consider fluid flow, and heat and mass transfer on nanofluids.

1.3 The study of nanofluids

The study of nanofluids has in recent years gained a lot of attention. Nanofluids are solid-liquid mixtures consisting of solid nanoparticles suspended in a liquid. For a fluid that is an inherently poor thermal conductor, such as ethylene glycol, high concentrations of solid particles are usually required to achieve good thermal conductivity. However, reports by Eastman et al. [51] and Choi et al. [52] show that the addition of a small amount of copper nanoparticles, less than 1% by volume, could increase the fluid's thermal conductivity by as much as 40%. Some results in this speedily evolving field include a surprisingly strong increase in the thermal conductivity of a nanofluid compared with the base fluid, Vassallo et al. [53]. Cooling by nanofluids has many potential applications. In this regard, You et al. [54] studied the feasibility of using a nanofluid to improve the cooling of nuclear reactors. Other studies

indicate that nanofluids as cooling fluids have the potential to conserve considerably amounts of energy for industries in the USA and reduce annual gas emissions by approximately 5.6-million tonnes of carbon dioxide, see Routbort [55]. Nanoparticles can also be used to cool pipes exposed to high temperatures in geothermal power and energy extraction from the earth's crust, Wong et al.[56]. Besides other mechanical applications such as in automatic transmission fluids, engine oils, lubricants and coolants, biomedical applications such as in cancer therapies, nano-drug delivery, nano-cryosurgery as well as electronic applications such as cooling microchips in computers have been reported by Boungiorno et al. [57].

1.4 Empirical and numerical studies of double-diffusive convection

Early empirical studies on double-diffusive convection (DDC) were carried out over 40 years ago. For instance, Herbert and Turner [58] studied double-diffusive convection and stratification in oceans. In a multi-compound solution, Bai et al.[59] showed that double-diffusive convection occurs in the liquid due to a coupling of temperature and concentration gradients. Other recent empirical studies include those of Mergui et al. [60] and Barman and Dutta [61].

The transport equations are nonlinear and it is not easy to find their analytical solutions because analytical techniques generally cannot handle this level of complexity. Instead, numerical solutions are usually sought. Consequently, many researchers have recognised the value of using empirical studies to validate theoretical models of DDC. One of the first to do this was Griffith [62], who studied diffusive convection experimentally using a Hele-Shaw cell

in a porous medium. He measured salt fluxes and compared the results with predictions from numerical models. In another study, Beckermann et al.[63] provided experimental validation for numerical simulations of double-diffusive natural convection in a Hele-Shaw cell. Webb et al. [64] also investigated DDC in a cylinder in a highly diffusive regime.

With the success of numerical simulations, other studies have recognised factors which may influence DDC, such as hydromagnetics, chemical reaction, heat generation, heat radiation and Soret and Dufour effects, see Gebhart and Pera [65]. Free convection with suction/injection over permeable surfaces in a porous medium was studied by Minkowycz et al.[66]. The problem of modelling fluid flow has attracted many investigations, see for instance Chamkha and El-Kabeir [67], Lai [68], Yih [69] and Cheng [70]. Of particular interest are the following three findings. Firstly, interfacial velocities due to mass diffusion are small enough to be neglected. Secondly, the heat transfer rate at the surface increases with the buoyancy parameter, unsteadiness parameter, Prandtl number, and the solid volume fraction of nanoparticles. Finally, larger values of the Grashof number have a significant effect on the momentum boundary layer flow of a nanofluid along a stretching sheet with thermal radiation and viscous dissipation, see Khan et al. [71]. A variety of methods have been used for these studies. In particular, Lai [68] obtained similarity solutions, while implicit finite differences were used by Yih [69], Mahdy [72] and Khan et al. [71]. Mixed convection flow along both vertical and inclined flat plates was investigated by Chen et al. [73], who showed that the interfacial velocities due to mass diffusion are very small and so could be neglected. Unsteady heat and mass transfer over an impulsively stretched vertical surface with chemical reaction and Soret and Dufour effects was studied by Chamkha and El-Kabeir [67]. They demonstrated the influences of the Hartmann number, Dufour number, Soret number, mixed convection parameter, suction/injection

parameter, dimensionless chemical reaction parameter, and the wall temperature and concentration exponent. Lai [68] solved the coupled heat and mass transfer problem in a vertical plate in a saturated porous medium. The results indicated that heat and mass transfer results may range from the asymptotic free convection limit to that of the forced convection limit. Yih [69] used the modified Keller box method to study mixed convection about a wedge embedded in a porous medium. Solutions for steady two-dimensional free convection and mass transfer flow of a viscous incompressible electrically conducting fluid through a porous medium were found by Acharya et al. [74]. The solution for transient heat and mass transfer from a vertical plate embedded in fluid saturated porous media were found using the cubic spline collocation method by Cheng [70]. Unsteady mixed convection boundary layer flow and heat transfer in nanofluids due to a stretching sheet was studied by Mahdy [72]. They discussed the effects of the governing parameters and different models of nanofluids and found that the heat transfer rate at the surface increases with buoyancy parameter, unsteadiness parameter, Prandtl number, and the solid volume fraction of nanoparticles. Khan et al. [71] found that larger values of the Grashof number had a significant effect on the momentum boundary layer for unsteady MHD free convection boundary layer. Implicit finite differences were used to solve nonlinear partial differential equations. In this study we will investigate unsteady and steady MHD mixed convection boundary layer flow, heat and mass transfer in a porous medium saturated with a nanofluid.

Ishak et al. [75] investigated heat transfer over an unsteady stretching permeable surface with a prescribed wall temperature. They quantified the effects of the unsteadiness parameter, suction/injection and the Prandtl number on the heat transfer characteristics. Complementing this was a study by Joshi et al. [76]. They found the effect of thermal radiation in magne-

tohydrodynamic (MHD) boundary layer flow over a stretching surface with suction/injection. Manjunatha et al. [77] used a fifth order Runge-Kutta Fehlberg method to investigate the effect of thermal radiation on boundary layer flow and heat transfer from a dusty fluid over an unsteady stretching sheet. Bhattacharyya et al.[78] studied unsteady MHD boundary layer flow with diffusion and a first order chemical reaction over a permeable stretching sheet with suction or blowing using the finite difference method and a quasi-linearization technique. From this analysis of the literature, it is clear that numerical methods, such as finite difference, fifth order Runge-Kutta Fehlberg method and the Keller-box method can be useful for solving non-linear differential equations

1.5 Some solution techniques

Numerous problems in science and engineering are governed by nonlinear differential equations. These equations are often strongly coupled and obtaining their exact solutions is not simple. For this reason we often have to resort to approximate numerical solutions. Over the years, a number of computational methods have been developed to solve non-linear equations, Adomian [79]. These include established numerical schemes like the Runge-Kutta schemes, the shooting method, the Keller-box method and the finite element method. The main disadvantage of numerical methods is that they often do not give insights into the structure of the solution, especially when the problem involves many parameters. They also give discontinuous points on the solution curve. Furthermore, some numerical methods are not stable or uniformly convergent. In such cases one is often forced to resort to either the classical series method or other perturbation methods to find approximate analytical solutions. The

disadvantage of conventional perturbation methods is that they require the presence of either a large or a small parameter in the problem, see Williams and Rhyne [80]. Many of the methods are difficult to implement, because of slow rates of convergence or are even divergent. In this work, we use at least two innovative numerical techniques to solve strongly nonlinear systems of partial differential equations that arise in the study of fluid flow problems. The methods of particular interest are; (1) the spectral relaxation method (SRM), and (2) the spectral quasi-linearization method (SQLM), see Motsa et al. [81] and Motsa [82]. These two techniques are used in conjunction with the Chebyshev pseudo-spectral collocation method which is extensively explained in Trefethen [83] and Canuto et al. [84]. Furthermore, the two approaches use ideas suggested by;

- The Gauss-Seidel relaxation technique, and
- The Taylor series expansion.

1.5.1 The spectral relaxation method (SRM)

The spectral relaxation method is based on simple iteration schemes formed by reducing large systems of nonlinear equations into smaller systems of linear equations, Motsa [82]. The method has been used to solve various nonlinear problems and has been determined to be an efficient method, see Motsa [82]. The main idea is to decouple the system of nonlinear equations using the Gauss-Seidel method. The decoupled system of equations is then integrated numerically using the Chebyshev spectral collocation method. It has been observed that the SRM gives good accuracy, even with only a few grid points, Motsa [82]. In Motsa and Makukula [85], the method was used to solve the steady von Karman flow of a Reiner-

Rivlin fluid with Joule heating and viscous dissipation. Accurate results were obtained and the speed of convergence of the method was significantly improved by using successive over relaxation (SOR) techniques. In Shateyi [86], the steady MHD flow of a Maxwell fluid past a vertical stretching sheet in a Darcy porous medium was studied. In Shateyi and Makinde [87], the SRM was used to solve the problem of steady stagnation point flow and heat transfer of an electrically conducting incompressible viscous fluid. Shateyi and Marewo [88] studied the magneto-dynamic boundary layer flow with heat and mass transfer in an incompressible upper-convected Maxwell fluid over a stretching sheet with viscous dissipation and thermal radiation. Motsa et al. [81], extended the method to a multistage technique to achieve better accuracy and computational efficiency. We use the spectral relaxation method to solve the system of nonlinear partial differential equations that describe the fluid flow and heat and mass transfer.

1.5.2 The spectral quasi-linearization method (SQLM)

The spectral quasi-linearization method (SQLM) was introduced by Motsa and Shateyi [89]. In the SQLM, the governing nonlinear equations are linearized using the Newton-Raphson based quasi-linearization method (QLM), which was developed by Bellman and Kalaba [90]. The method has been implemented extensively and shown to be efficient, simple to use and quite accurate. For instance, in Motsa and Shateyi [89], the SQLM scheme was developed and used to solve the Blasius boundary layer equation and the unsteady free convective heat and mass transfer on a stretching surface in a porous medium with suction/injection parameter. The method was compared against the local linearisation method (LLM) where it was shown that the SQLM loses accuracy when the number of collocation points is made large, see Motsa

and Sibanda [91]. The method has been used alongside other methods to try to determine its accuracy. In Dlamini et al. [92], the SQLM is compared against the compact finite difference quasi-linearization method (CFD-QLM) using both a one dimensional problem and a three dimensional problem. The results showed that SQLM had a faster computational speed than the CFD-QLM but the SQLM was less accurate for the three dimensional problem. In another example, Motsa and Sibanda [93] used the method to obtain a sequence of techniques with arbitrary higher order convergence. The techniques were used to find solutions of Falkner-Skan type boundary layer equations. We use the spectral quasi-linearization method to solve the system of nonlinear partial differential equations which describe the fluid motion and heat and mass transfer.

1.6 Dissertation objectives

The objectives of this dissertation are as follows:

- (i) To investigate unsteady nanofluid flow with heat and mass transfer over a stretching sheet in the presence of heat generation.
- (ii) To determine the effects of the Dufour and Soret parameters, the magnetic field strength, the thermal radiation parameter, buoyancy terms and the chemical reaction parameter on steady state mixed convection in a nanofluid flow over a non-isothermal wedge due to a stretching sheet.

To this end:

- We compare the accuracy rate of the SRM and SQLM.
- We compare our results with previous studies to determine the accuracy and reliability of the SRM and SQLM.

The study consists of four main chapters. In Chapter 2 we give a description of the theory under pinning the use of the SRM and SQLM methods. In Chapter 3 we study unsteady nanofluid flow, heat and mass transfer over a stretching sheet in the presence of heat generation and thermal-diffusion effects. The governing non-linear partial differential equations and the boundary conditions are transformed into a set of non-similar equations are solved numerically using both the spectral relaxation and quasi-linearization methods. The accuracy of the numerical methods is tested by determining the influences of various physical parameters and in the limiting case our results are compared with published work. In Chapter 4 we study steady state mixed convection and heat and mass transfer characteristics from a non-isothermal wedge due to a stretching sheet with the Soret and Dufour effects. The transformed coupled nonlinear partial differential equations are solved numerically using the spectral relaxation method. A comparison is made between our results and others published in the literature. In Chapter 5 we extend the work presented in Chapter 4 to study unsteady magnetohydrodynamic mixed convection boundary layer flow with suction/injection. In the analysis we include the effects of the heat generation coefficient, viscous dissipation and the Soret and Dufour effects. The spectral relaxation method is used to solve the governing non-similar equations. A parametric survey of the effects of some governing parameters is made and a representative sample of results presented graphically. A comparison of the results obtained using the SRM method for the skin friction coefficient with previously published results is given. In Chapter 6 we conclude by discussing the main findings of this dissertation.

Chapter 2

A brief description of the SRM and SQLM

In this chapter we discuss in detail the spectral relaxation and quasi-linearization methods. The methods were first introduced by Motsa and Makukula [85] for the solution of nonlinear system of equations such as arise in the study of fluid flow problems. Moreover, we used matlab program for a simulations in order to obtain the values of our parameter for this dissertation.

Over the years, a number of computational methods have been developed to solve nonlinear equations. Such higher order systems have proven to be complicated to solve analytically, hence the need to obtain numerical solutions. As was described in Section 1.5, while methods such as the Runge-Kutta schemes and the finite element method are quite efficient in terms of providing approximate solutions for system of nonlinear equations, because of slow convergence, they may however be unsuited to solve strongly nonlinear systems. Thus conventional

methods are unsuited to solving the systems of nonlinear partial differential equations that arise when modelling fluid flow. Instead, here we adopt a different approach.

The spectral relaxation method (SRM) and the spectral quasi-linearization method (SQLM) have higher rates of convergence, good accuracy with only a few grid points, and ease of application to complicated nonlinear partial differential equations. Consequently, although the methods have not been applied extensively, we use them here due to the following advantages:

- (i) They are applicable to all non-linear ODE and PDE equations.
- (ii) They are relatively easy to implement.

The methods are fully described in Motsa and Sibanda [91]. Here we present a brief description of how the methods can be implemented in practice. Let us consider a system of m nonlinear ordinary differential equations in m unknown functions $z_j(\eta)$ $j = 1, 2, 3, \dots, m$ where $\eta \in [a, b]$ is the dependent variable. Define a vector Z_j to be the vector of the derivatives of the variable z_j with respect to η , such that

$$Z_j(\eta) = [z_j^{(0)}, z_j^{(1)}, \dots, z_j^{(n_j)}], \quad (2.1)$$

where $z_j^{(0)} = z_j$, $z_j^{(p)}$ is the p th derivative of z_j with respect to η and $n_j(j = 1, 2, \dots, m)$ is the highest derivative order of the variable z_j appearing in the system of equations. Now let Z_j be denoted as a sum of its linear (L_j) and nonlinear components (N_j) as

$$L_j[Z_1, Z_2, \dots, Z_m] + N_j[Z_1, Z_2, \dots, Z_m] = H_j(\eta), \quad j = 1, 2, \dots, m, \quad (2.2)$$

where $z_j^{(0)} = z_j$, $z_j^{(p)}$ is the p th derivative of z_j with respect to η and $n_j(j = 1, 2, \dots, m)$ is the highest order derivative order of the variable z_j appearing in the system of equations. Now

the system can be written in terms of Z_j as a sum of its linear (L_j) and nonlinear components (N_j) as

$$L_j[Z_1, Z_2, \dots, Z_m] + N_j[Z_1, Z_2, \dots, Z_m] = H_j(\eta), \quad j = 1, 2, \dots, m, \quad (2.3)$$

where $H(\eta)$ is a known function of η . If the nonlinear component in (2.2) is a sum of nonlinear terms with at least one of them being a multiple of z_j , we can further split N_j into a sum of the two nonlinear functions as

$$N_j[Z_1, Z_2, \dots, Z_m] = z_j F_j[Z_1, Z_2, \dots, \hat{Z}_j, Z_m] + G_j[Z_1, Z_2, \dots, Z_m], \quad (2.4)$$

where $\hat{Z}_j(\eta) = [z_j^{(1)}, \dots, z_j^{(n_j)}]$ and F_j is a nonlinear function of Z_1, Z_2, \dots, Z_m in which z_j is either absent or appears as a nonlinear factor.

A two point boundary condition is imposed on equation (2.2) in the form

$$\sum_{j=1}^m \sum_{p=0}^{n_j-1} \beta_{v,j}^p z_j^{(p)}(\mathbf{a}) = W_{\mathbf{a},v}, v = 1, 2, \dots, m_{\mathbf{a}}, \quad (2.5)$$

$$\sum_{j=1}^m \sum_{p=0}^{n_j-1} \gamma_{c,j}^p z_j^{(p)}(\mathbf{b}) = W_{\mathbf{b},c}, c = 1, 2, \dots, m_{\mathbf{b}}, \quad (2.6)$$

where $\beta_{v,j}^{[p]}$, $\gamma_{c,j}^{[p]}$ are the constant coefficients of $z_j^{(p)}$ in the boundary conditions, and $m_{\mathbf{a}}$, $m_{\mathbf{b}}$ are the total number of prescribed boundary conditions at $\eta = \mathbf{a}$ and $\eta = \mathbf{b}$ respectively.

We use the Gauss-Seidel method to decouple systems of nonlinear equations. Given initial

$z_j(\eta)$ at the collocation points as the matrix vector product see Motsa [94]

$$\frac{dz_j}{d\eta} = \sum_{s=0}^{\bar{N}} \mathbf{D}_{\tau_s}(\tau_s) = \mathbf{D}\mathbf{Z}_i, \quad i = 0, 1, \dots, \bar{N} \quad (2.9)$$

where $\bar{N} + 1$ is the number of grid points, $\mathbf{D} = 2D/(b - a)$ and $\mathbf{Z} = [z(\tau_0), z(\tau_1), \dots, z(\tau_{\bar{N}})]^T$ is the vector function at the collocation points. Higher order derivatives are obtained as powers of \mathbf{D} , that is

$$z_j^{(p)} = \mathbf{D}^p \mathbf{Z}_j. \quad (2.10)$$

Equation (2.1) is equivalent to

$$\sum_{j=1}^m \sum_{p=0}^{n_j} \alpha_{i,j}^{[p]} z_j^{(p)} + \mathbf{N}_i[Z_1, Z_2, \dots, Z_m] = \mathbf{H}_i, \quad (2.11)$$

where $\alpha_{i,j}^{[p]}$ are the constant coefficients of $z_j^{(p)}$, the derivative of z_j , $j = 1, 2, \dots, m$ at the i th equation for $i = 1, 2, \dots, m$. The iteration scheme given in equation (2.7) can be expressed compactly as

$$\begin{aligned} & \sum_{j=1}^i \sum_{p=0}^{n_j} \alpha_{i,j}^{[p]} z_{j,r+1}^{(p)} + z_{i,r+1} F[Z_{1,r+1}, \dots, Z_{i-1,r+1}, \hat{Z}_{i,r}, Z_{i+1,r}, \dots, Z_{m,r}] \\ & = \mathbf{H}_i - \sum_{j=i+1}^m \sum_{p=0}^{n_j} \alpha_{i,j}^{[p]} z_{j,r}^{(p)} - \mathbf{G}_i[Z_{1,r+1}, \dots, Z_{i-1,r+1}, \dots, Z_{m,r}] \end{aligned} \quad (2.12)$$

for $i = 1, 2, \dots, m$. Applying equations (2.10) to (2.12) and the corresponding boundary conditions gives

$$\begin{aligned} & \sum_{j=1}^i \sum_{p=0}^{n_j} \alpha_{i,j}^{[p]} \mathbf{D}^p \mathbf{Z}_{j,r+1} + z_{i,r+1} F_i[\mathbf{Z}_{1,r+1}, \dots, \mathbf{Z}_{i-1,r+1}, \widehat{\mathbf{Z}}_{i,r}, \mathbf{Z}_{i+1,r}, \dots, \mathbf{Z}_{m,r}] \\ & = \mathbf{H}_i - \sum_{j=i+1}^m \sum_{p=0}^{n_j} \alpha_{i,j}^{[p]} \mathbf{D}^p \mathbf{Z}_{j,r} - \mathbf{G}_i[\mathbf{Z}_{1,r+1}, \dots, \mathbf{Z}_{i-1,r+1}, \mathbf{Z}_{i,r}, \dots, \mathbf{Z}_{m,r}] \end{aligned} \quad (2.13)$$

subject to

$$\sum_{j=1}^m \sum_{p=0}^{n_j-1} \beta_{v,j}^{[p]} \sum_{c=0}^{\bar{N}} \mathbf{D} \frac{p}{N_c} z_{j,r+1}(\tau_z) = C_{a,v}, \quad v = 1, 2, \dots, m_a, \quad (2.14)$$

$$\sum_{j=1}^m \sum_{p=0}^{n_j-1} \gamma_{o,j}^{[p]} \sum_{c=0}^{\bar{N}} \mathbf{D} \frac{p}{0z} z_{j,r+1}(\tau_z) = \mathbf{C}_{b,o}, \quad o = 1, 2, \dots, m_a, \quad (2.15)$$

Consider the system of m nonlinear differential equations in m unknowns functions $z_i(\eta)$, $i = 1, 2, \dots, m$ where $\eta \in [a, b]$ is the dependent variable. The system can be written in terms of z_i as a sum of it's linear (L) and nonlinear components (N)

$$L[Z_1(\eta), Z_2(\eta), \dots, Z_m(\eta)] + N[Z_1(\eta), Z_2(\eta), \dots, Z_m(\eta)] = H(\eta), \quad \eta \in (a, b) \quad (2.16)$$

subject to the boundary conditions

$$A_i[Z_1(a), Z_2(a), \dots, Z_m(a)] = W_{a,i}, \quad B_i[Z_1(b), Z_2(b), \dots, Z_m(b)] = W_{b,i}, \quad (2.17)$$

where A_i and B_i are linear operators and $W_{a,i}$ and $W_{b,i}$ are constants for $i = 1, 2, \dots, m$. A vector Z_j is defined as

$$Z_j = [z_j^{(0)}, z_j^{(1)}, \dots, z_j^{(n_j)}], \quad (2.18)$$

where $z_j^{(0)} = z_j$, $z_j^{(p)}$ is the p th derivative of z_j with respect to η and n_i ($i = 1, 2, \dots, m$) is the highest derivative order of the variable z_j and (2.17) becomes

$$L_i[Z_1, Z_2, \dots, Z_m] + N_i[Z_1, Z_2, \dots, Z_m] = \sum_{j=1}^m \sum_{p=0}^{n_j} \alpha_{i,j}^{[p]} z_j^{(p)} + N_i[Z_1, Z_2, \dots, Z_m] \quad (2.19)$$

where $\alpha_{i,j}^{[p]}$ are the constant coefficient of $z_j^{(p)}$.

The derivatives in the boundary conditions are at most one less than the highest derivative of z_j in the governing system (2.20). We define the vector \check{Z}_j to be the vector of the derivatives of the variables z_j with respect to the dependent variable η from 0 up to $n_j - 1$, that is,

$$\check{Z}_j = [z_j^{(0)}, z_j^{(1)}, \dots, z_j^{(n_j-1)}] \quad (2.20)$$

The boundary conditions (2.17) are written as

$$\begin{aligned} & A_\nu[\check{Z}_1(\mathbf{a}), \check{Z}_2(\mathbf{a}), \dots, \check{Z}_m(\mathbf{a})] \\ &= \sum_{j=1}^m \sum_{p=0}^{n_j-1} \beta_{\nu,j}^{[p]} z_j^{(p)}(\mathbf{a}) = Q_{\mathbf{a},\nu}, \quad \nu = 1, 2, \dots, m_{\mathbf{a}}, \end{aligned} \quad (2.21)$$

$$\begin{aligned} & B_\sigma[\check{Z}_1(\mathbf{b}), \check{Z}_2(\mathbf{b}), \dots, \check{Z}_m(\mathbf{b})] \\ &= \sum_{j=1}^m \sum_{p=0}^{n_j-1} \gamma_{\sigma,j}^{[p]} z_j^{(p)}(\mathbf{b}) = Q_{\mathbf{b},\sigma}, \quad \sigma = 1, 2, \dots, m_{\mathbf{b}}. \end{aligned} \quad (2.22)$$

where $\beta_{\nu,j}^{[p]}$ and $\gamma_{\sigma,j}^{[p]}$ are the constant coefficients of $Z_j^{(p)}$ in the boundary conditions, and $m_{\mathbf{a}}$, $m_{\mathbf{b}}$ are the total number of prescribed boundary conditions at $\mathbf{x} = \mathbf{a}$ and $\mathbf{x} = \mathbf{b}$ respectively where

$$m_{\mathbf{a}} + m_{\mathbf{b}} = \sum_{j=1}^m n_j \quad (2.23)$$

Assume that the solution $z_i(\eta)$ of (2.19) at the $(r+1)$ th iteration is $z_{i,r+1}$. If the solution at the previous iteration $z_{i,r}(\eta)$ is sufficiently close to $z_{i,r+1}$, the nonlinear component N_i of equation (2.19) can be linearized using a one term Taylor series expansion for multiple variables so that equation (2.19) can be approximated as

$$L_i[Z_{1,r+1}, Z_{2,r+1}, \dots, Z_{m,r+1}] + N_i[Z_{1,r}, \dots, Z_{m,r}] + \sum_{j=1}^m \sum_{p=0}^{n_j} (z_{j,r+1}^{(p)} - z_{j,r}^{(p)}) \frac{\partial N_i}{\partial z_j^{(p)}}[\dots] = H_i(\eta), \quad (2.24)$$

subject to conditions

$$\sum_{j=1}^m \sum_{p=0}^{n_j-1} \beta_{\nu,j}^{[p]} z_{j,r+1}^{(p)}(\mathbf{a}) = 0, \quad \nu = 1, 2, \dots, m_{\mathbf{a}}, \quad (2.25)$$

$$\sum_{j=1}^m \sum_{p=0}^{n_j-1} \gamma_{\sigma,j}^{[p]} z_{j,r+1}^{(p)}(\mathbf{b}) = 0, \quad \sigma = 1, 2, \dots, m_{\mathbf{b}}. \quad (2.26)$$

where

$$\begin{bmatrix} \cdot & \cdot & \cdot \end{bmatrix} = \begin{bmatrix} Z_{1,r} & Z_{2,r} & \cdot & \cdot & \cdot & Z_{m,r} \end{bmatrix}. \quad (2.27)$$

Equation (2.24) can be re-written as

$$L_i[Z_{1,r+1}, \dots, Z_{m,r+1}] + \sum_{j=1}^m \sum_{p=0}^{n_j} z_{j,r+1}^{(p)} \frac{\partial N_i}{\partial z_j^{(p)}} [\dots] = H_i(\eta) + \sum_{j=1}^m \sum_{p=0}^{n_j} z_{j,r}^{(p)} \frac{\partial N_i}{\partial z_j^{(p)}} [\dots] - N_i [\dots] \quad (2.28)$$

The initial approximation is obtained as a solution of the linear part of equation (2.16) subject to the boundary conditions equation (2.17), in other words, we solve

$$\sum_{j=1}^m \sum_{p=0}^{n_j} \alpha_{i,j}^{[p]} z_{j,0}^{(p)} = H_i(\eta), \quad (2.29)$$

subject to

$$\sum_{j=1}^m \sum_{p=0}^{n_j-1} \beta_{\nu,j}^{[p]} z_{j,0}^{(p)}(\mathbf{a}) = W_{\mathbf{a},\nu}, \quad \nu = 1, 2, \dots, m_a \quad (2.30)$$

$$\sum_{j=1}^m \sum_{p=0}^{n_j-1} \gamma_{\sigma,j}^{[p]} z_{j,0}^{(p)}(\mathbf{b}) = W_{\nu,\mathbf{b}}, \quad \sigma = 1, 2, \dots, m_b. \quad (2.31)$$

The differentiation matrix \mathbf{D} is used to approximate the derivatives of the unknown variables $z_i(\eta)$ at the grid points as the matrix vector product

$$\frac{dZ_j}{d\eta} = \sum_{k=0}^{\bar{N}} \mathbf{D}_{lk} Z_i(\tau_k) = \mathbf{D}\mathbf{Z}_i, \quad l = 0, 1, \dots, \bar{N} \quad (2.32)$$

where $\bar{N}+1$ is the number of collocation points, $\mathbf{D} = 2\mathbf{D}/(\mathbf{b}-\mathbf{a})$, and $\mathbf{Z} = [z(\tau_0), z(\tau_1), \dots, z(\tau_{\bar{N}})]^T$ is the vector function at the collocation points. Higher order derivatives are obtained as powers of \mathbf{D} , that is

$$Z_j^{(p)} = \mathbf{D}^p \mathbf{Z}_j. \quad (2.33)$$

Applying the Chebyshev spectral method on the initial approximation equations (2.29)-(2.31), we obtain,

$$\sum_{j=1}^m \sum_{p=0}^{n_j} \alpha_{i,j}^{[p]} \mathbf{D}^p \mathbf{Z}_{j,0} = \mathbf{H}_i(\eta), \quad (2.34)$$

subject to

$$\sum_{j=1}^m \sum_{p=0}^{n_j-1} \beta_{\nu,j}^{[p]} \sum_{k=0}^N \mathbf{D}_{N_q}^p z_{j,0}(\tau_k) = W_{\alpha,\nu}, \quad \nu = 1, 2, \dots, m_a \quad (2.35)$$

$$\sum_{j=1}^m \sum_{p=0}^{n_j-1} \gamma_{\sigma,j}^{[p]} \sum_{k=0}^N \mathbf{D}_{0_q}^p z_{j,0}(\tau_k) = W_{\beta,\sigma}, \quad \sigma = 1, 2, \dots, m_b \quad (2.36)$$

Equations (2.34) can be written in matrix form

$$\begin{bmatrix} A_{1,1} & A_{1,2} & \cdot & \cdot & \cdot & A_{1,m} \\ A_{2,1} & A_{2,2} & \cdot & \cdot & \cdot & A_{2,m} \\ \cdot & \cdot & \cdot & \cdot & \cdot & \cdot \\ \cdot & \cdot & \cdot & \cdot & \cdot & \cdot \\ \cdot & \cdot & \cdot & \cdot & \cdot & \cdot \\ A_{m,1} & A_{m,2} & \cdot & \cdot & \cdot & A_{m,m} \end{bmatrix} \begin{bmatrix} Z_{1,0} \\ Z_{2,0} \\ \cdot \\ \cdot \\ \cdot \\ Z_{m,0} \end{bmatrix} = \begin{bmatrix} H_1 \\ H_2 \\ \cdot \\ \cdot \\ \cdot \\ H_m \end{bmatrix} \quad (2.37)$$

where $Z_{i,0}$ are vectors of size $(\bar{N} + 1) \times 1$ and $A_{i,j}$ are $(\bar{N} + 1) \times (\bar{N} + 1)$ matrices which are, respectively, defined as

$$\begin{aligned} Z_{i,0} &= [z_{i,0}(\tau_0), z_{i,0}(\tau_1), \dots, z_{i,0}(\tau_N)]^T, \\ A_{i,j} &= \sum_{p=0}^{n_j} \alpha_{i,j}^p D^p, \quad i, j = 1, 2, \dots, m. \end{aligned} \quad (2.38)$$

Applying the Chebyshev spectral collocation on the recursive iteration scheme (2.28) gives

$$\sum_{j=1}^m [A_{i,j} + \Pi_{i,j}] Z_{j,r+1} = \Phi_{i,r}, \quad i, j = 1, 2, \dots, m, \quad (2.39)$$

where $Z_{i,r+1} = [z_{i,r+1}(\tau_0), z_{i,r+1}(\tau_1), \dots, z_{i,r+1}(\tau_N)]^T$, $A_{i,j} = \sum_{p=0}^{n_j} \alpha_{i,j}^p D^p$, $i, j = 1, 2, \dots, m$ and

$\Pi_{i,j}$ and Φ_i are given by

$$\Pi_{i,j} = \sum_{p=0}^{n_j} \left[\frac{\partial N_i}{\partial Z_j^{(p)}} \right]_d D^p, \quad (2.40)$$

and

$$\Phi_{i,r} = H_i(\eta) + \sum_{j=1}^m \sum_{p=0}^{n_j} Z_{j,r}^{(p)} \frac{\partial N_i}{\partial Z_j^{(p)}} [\dots]_d - N_i[Z_{1,r}, Z_{2,r}, \dots, Z_{m,r}], \quad (2.41)$$

respectively, where $[\dots]_d$ denotes a diagonal matrix. We let $\Delta = \mathbf{A} + \mathbf{\Pi}$, and rewrite the equation (2.39) in matrix form

$$\begin{bmatrix} \Delta_{1,1} & \Delta_{1,2} & \cdot & \cdot & \cdot & \Delta_{1,m} \\ \Delta_{2,1} & \Delta_{2,2} & \cdot & \cdot & \cdot & \Delta_{2,m} \\ \cdot & \cdot & \cdot & & & \cdot \\ \cdot & \cdot & & \cdot & & \cdot \\ \cdot & \cdot & & & \cdot & \cdot \\ \Delta_{m,1} & \Delta_{m,2} & \cdot & \cdot & \cdot & \Delta_{m,m} \end{bmatrix} \begin{bmatrix} Z_{1,r+1} \\ Z_{2,r+1} \\ \cdot \\ \cdot \\ \cdot \\ Z_{m,r+1} \end{bmatrix} = \begin{bmatrix} \Phi_{1,r} \\ \Phi_{2,r} \\ \cdot \\ \cdot \\ \cdot \\ \Phi_{m,r} \end{bmatrix} \quad (2.42)$$

where $Z_{i,r}$ and $\Phi_{i,r}$ are vectors of size $(\bar{N} + 1) \times 1$ and $\Delta_{i,j}$ are $(\bar{N} + 1) \times (\bar{N} + 1)$ matrices.

Starting from $Z_{i,0}$, the recursive sequence (2.42) is solved iteratively for $r = 0, 1, 2, 3, \dots$

In this Chapter we gave a description of two methods that can be used in the numerical solution of both ordinary and nonlinear partial differential equations, which often arise in fluid mechanics and other engineering applications. The goal is to highlight the advantages of these methods over traditional methods of solving the PDE problems in fluid mechanics. In the next chapter we study the problem of unsteady nanofluid flow, heat and mass transfer due to a stretching sheet in order to set up a system of equations to which we can apply these methods.

Chapter 3

Unsteady nanofluid flow, heat and mass transfer over a stretching sheet

In this chapter we study unsteady nanofluid flow and heat and mass transfer over a stretching sheet in the presence of heat generation, thermal-diffusion effects and a homogeneous chemical reaction parameter. The transformed nonlinear partial differential equations are solved numerically using spectral relaxation and quasi-linearization methods.

3.1 Introduction

There has been a great deal of investigative interest in the study of boundary flow and heat transfer characteristics due to the impulsive motion of a stretching sheet. An assortment of technical processes involve the production of stretching materials including both metallic and polymer sheets. The final product is, in general, dependent on the heat transfer at the sheet

surface.

Over a century ago, Blasius [95] presented report on the boundary layer flow over a flat plate in a uniform free stream. It was 30 years before Howarth [96], provided a numerical solution to the Blasius problem. Boundary layer flow over a continuously moving plate in a quiescent ambient fluid was the first to studied by Sakiadis [97]. Crane [98] expanded this study to a sheet which stretched with a velocity that was linearly proportional to the distance from the origin. Since Crane's pioneering work, the literature concerning boundary layer flow past a stretching sheet has grown enormously. Indeed, Crane's problem has been expanded to include many other features such as porosity, heat and mass transfer, magnetic field effects and viscoelasticity or permeable surfaces, Gupta and Gupta [99].

Early work based on Crane's model includes that of Chen and Strob [100] and Grubka and Bobba [101]. More recently contributions have come from Gireesha et al. [102], Aiyesimi et al. [103], Bhattacharyya and Vajravelu [104], Ramesh et al. [105], Joshi et al. [106], Mondal and Pal [107] and Vajravelu [108]. Of significance, because of the importance of boundary layer flow over stretching sheets, are studies concerned with aspects of unsteady flow past a stretching sheet by Andersson et al. [109], Ali and Mehmood [110], Ishak et al. [111], Ishak et al. [112], Hayat et al. [113], Sharma et al. [114], Sharma [115], Bachok et al. [116], Bhattacharyy [117], Manjunatha et al. [118] and Bhattacharyya et al. [119]. Liao [120] and Xu et al. [121] obtained series solutions of the unsteady boundary layer equations and studied heat transfer in boundary layer over an impulsively stretching plate.

As explained in Section 1.3, nanofluids are dilute suspensions of nanoparticles with critical dimension smaller than 100 nm dispensed in a base fluid. Thermal conductivity rates in common fluids such as water, oils and ethylene glycol are very poor but can be improved by adding these nanoparticles, mostly metals or metal oxides, Choi and Eastman [122]. Much attention has been paid in the past decade to nanofluids because of their enhanced thermal properties, Yulong et al. [123]. Nanofluids have higher thermal conductivity rates than common fluids such as water, and have been considered for application as advanced heat transfer fluids, Sheikholeslami et al. [124]. The most important properties of nanofluids are enhanced effective fluid thermal conductivity and heat transfer coefficient, see Choi [125] and Khan and Pop [126]. Later, Das [127], Zheng et al. [128], Mustafa et al. [129] and Kameswaran et al. [130] provided further examples of problems relating to nanofluid flow on stretching surfaces. Studies on unsteady nanofluid flow due to stretching sheet have also been reported by Rohni et al. [131], Narayana and Sibanda [132], Bachok et al.[133], Chamkha et al.[134] and Mustafa et al. [135].

The goal of this study is thus, to present solutions of the boundary layer momentum, energy and concentration equations for unsteady nanofluid flow over a stretching sheet with heat generation, thermo-diffusivity (Soret effects) and a chemical reaction. We use the spectral relaxation method (SRM) together with the spectral quasi-linearization method (SQLM) suggested by Motsa et al. [85; 136] to obtain accurate numerical solutions of the governing non-linear equations.

3.2 Governing Equations

Consider the unsteady two-dimensional laminar free, convective flow of an incompressible nanofluid over a stretching sheet (situated $y = 0$). As shown in Figure 3.1, the x and y coordinates are taken along and perpendicular to the sheet respectively with the flow confined to $y \geq 0$. The sheet stretches with velocity $u = \alpha x$ where α is a positive constant. The temperature and nanoparticle concentration at the stretching surface are T_w and C_w , and those of the ambient nanofluid are T_∞ and C_∞ respectively. The momentum, energy and concentration equations for the laminar boundary layer flow can be written as (Chamkha et al. [134]);

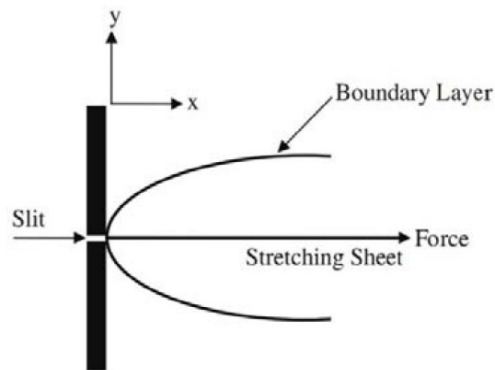


Figure 3.1: Physical model and coordinate system.

$$\frac{\partial u}{\partial x} + \frac{\partial v}{\partial y} = 0, \quad (3.1)$$

$$\frac{\partial u}{\partial t} + u \frac{\partial u}{\partial x} + v \frac{\partial u}{\partial y} = \frac{\mu_{nf}}{\rho_{nf}} \frac{\partial^2 u}{\partial y^2}, \quad (3.2)$$

$$\frac{\partial T}{\partial t} + u \frac{\partial T}{\partial x} + v \frac{\partial T}{\partial y} = \alpha_{nf} \frac{\partial^2 T}{\partial y^2} + \frac{Q}{(\rho c_p)_{nf}} (T - T_\infty), \quad (3.3)$$

$$\frac{\partial C}{\partial t} + u \frac{\partial C}{\partial x} + v \frac{\partial C}{\partial y} = D_m \frac{\partial^2 C}{\partial y^2} + \frac{D_m K_T}{T_m} \frac{\partial^2 T}{\partial y^2} - k_0 (C - C_\infty), \quad (3.4)$$

where t , u and v are the time and tangential and normal velocity components along the x and y axes respectively, T and C are the temperature and concentration, μ_{nf} is the effective dynamic viscosity of the nanofluid, ρ_{nf} is the nanofluid density, α_{nf} is the thermal diffusivity of the nanofluid, $(\rho c_p)_{nf}$ is the heat capacity of the nanofluid, ρ is the density of the fluid, c_p is the heat capacity of the base fluid at constant pressure, Q is the volumetric rate of heat generation/absorption, D_m is the chemical molecular diffusivity, K_T , T_m and k_0 are the thermal diffusion ratio, the mean fluid temperature and a chemical reaction parameter respectively.

The flow is subject to the boundary conditions:

$$t \geq 0 : u = \alpha x, \quad v = 0, \quad T = T_w = T_\infty + bx, \quad C = C_w = C_\infty + dx \quad \text{at} \quad y = 0,$$

$$t \geq 0 : u \rightarrow 0, \quad T \rightarrow T_\infty, \quad C \rightarrow C_\infty \quad \text{as} \quad y \rightarrow \infty, \quad (3.5)$$

and initial conditions

$$t < 0 : u = 0, \quad v = 0, \quad T = T_w, \quad C = C_w, \quad \forall x, y, \quad (3.6)$$

where α , b and d are positive constants.

The effective dynamic viscosity of the nanofluid was given by Brinkman [137] as

$$\mu_{nf} = \frac{\mu_f}{(1 - \phi)^{2.5}}, \quad (3.7)$$

where ϕ is the solid volume fraction of nanoparticles, μ_f is the dynamic viscosity of the base

fluid. In equations (3.1) - (3.4)

$$\begin{aligned}
(\rho c_p)_{nf} &= (1 - \phi)(\rho c_p)_f + \phi(\rho c_p)_s, \\
\rho_{nf} &= (1 - \phi)\rho_f + \phi\rho_s, \quad \nu_{nf} = \frac{\mu_{nf}}{\rho_{nf}}, \\
\alpha_{nf} &= \frac{k_{nf}}{(\rho c_p)_{nf}}, \quad \frac{k_{nf}}{k_f} = \frac{(k_s + 2k_f) - 2\phi(k_f - k_s)}{(k_s + 2k_f) + \phi(k_f - k_s)},
\end{aligned} \tag{3.8}$$

where ν_{nf} is the kinematic viscosity of nanofluid, $(\rho c_p)_f$ is heat capacity of the base fluid, k_{nf} is the thermal conductivity of the nanofluid, k_f and k_s are the thermal conductivities of the fluid and of the solid fractions, respectively, and ρ_f and ρ_s are the densities of the fluid and of the solid fractions, respectively, see Abu-Nada [138].

It is convenient to introduce the stream function ψ defined by

$$\mathbf{u} = \frac{\partial \psi}{\partial y}, \quad \mathbf{v} = -\frac{\partial \psi}{\partial x}, \tag{3.9}$$

and the following non-dimensional variables, see Liao [139]

$$\begin{aligned}
\eta &= \sqrt{\frac{\mathbf{a}}{\nu_f \xi}} y, \quad \xi = 1 - \exp(-\tau), \quad \tau = \mathbf{a}t, \quad \psi = \sqrt{\mathbf{a}\nu_f \xi} x f(\xi, \eta), \\
\theta(\xi, \eta) &= \frac{T - T_\infty}{T_w - T_\infty}, \quad \Phi(\xi, \eta) = \frac{C - C_\infty}{C_w - C_\infty}.
\end{aligned} \tag{3.10}$$

The governing equations (3.1) - (3.4) along with the boundary conditions (3.5) can then be presented in the form

$$f''' + \phi_1 \left[\frac{\eta}{2}(1 - \xi)f'' + \xi (ff'' - f'^2) \right] = \phi_1 \xi (1 - \xi) \frac{\partial f'}{\partial \xi}, \tag{3.11}$$

$$\theta'' + \frac{k_f}{k_{nf}} \text{Pr} \phi_2 \left[\frac{\eta}{2}(1 - \xi)\theta' + \xi (f\theta' - f'\theta + \delta\theta) \right] = \frac{k_f}{k_{nf}} \text{Pr} \phi_2 \xi (1 - \xi) \frac{\partial \theta}{\partial \xi}, \tag{3.12}$$

$$\Phi'' + \text{Sc} \left[\frac{\eta}{2}(1 - \xi)\Phi' + \xi (f\Phi' - f'\Phi - \gamma\Phi) + \text{Sr}\theta'' \right] = \text{Sc} \xi (1 - \xi) \frac{\partial \Phi}{\partial \xi}, \tag{3.13}$$

subject to the boundary conditions

$$\begin{aligned}
f(\xi, 0) &= 0, \quad f'(\xi, 0) = 1, \quad \theta(\xi, 0) = 1, \quad \Phi(\xi, 0) = 1, \quad \xi \geq 0, \\
f'(\xi, \infty) &= 0, \quad \theta(\xi, \infty) = 0, \quad \Phi(\xi, \infty) = 0, \quad \xi \geq 0,
\end{aligned} \tag{3.14}$$

where

$$\phi_1 = (1 - \phi)^{2.5} \left[1 - \phi + \phi \left(\frac{\rho_s}{\rho_f} \right) \right], \quad \phi_2 = \left[1 - \phi + \phi \frac{(\rho c)_s}{(\rho c)_f} \right], \quad (3.15)$$

and

$$\begin{aligned} \text{Pr} &= \frac{\nu_f}{\alpha_f}, \quad \alpha_f = \frac{k_f}{(\rho c_p)_f}, \quad \nu_f = \frac{\mu_f}{\rho_f}, \quad \text{Sc} = \frac{\nu_f}{D}, \quad \gamma = \frac{k_1}{a}, \\ \text{Sr} &= \frac{D_m K_T}{T_m} \frac{(T_w - T_\infty)}{\nu_f (C_w - C_\infty)}, \quad \delta = \frac{Q}{a(\rho c_p)_{nf}}. \end{aligned} \quad (3.16)$$

The parameters Pr , Sc , Sr , α_f , δ , γ and ν_f represent the Prandtl number, Schmidt number, Soret number, coefficient of thermal diffusivity of the base fluid, dimensionless heat generation, scaled chemical reaction parameter and the kinematic viscosity of base fluid respectively.

The Prandtl number Pr is a dimensionless number; and it represents the ratio of momentum diffusivity to thermal diffusivity. The Prandtl number controls the relative thickness of the momentum and thermal boundary layers. When Pr is small, the heat diffuses very quickly compared to the velocity. The mass transfer analog of the Prandtl number is the Schmidt number Sc , which is the ratio of momentum diffusivity to the mass diffusivity. The Soret number represents the ratio of the thermal diffusion coefficient to the ordinary diffusion coefficient.

3.3 Skin friction, heat and mass transfer coefficients

In heat and mass transport problems, we are particularly interested in the skin friction coefficient C_f , the local Nusselt number Nu_x and the local Sherwood number Sh_x . These parameters respectively characterize the surface drag and the wall heat and mass transfer rates respectively.

The shearing stress at the surface of the wall τ_w is given by

$$\tau_w = -\mu_{nf} \left(\frac{\partial u}{\partial y} \right)_{y=0} = -\frac{\alpha x \mu_f}{(1-\phi)^{2.5}} \sqrt{\frac{a}{\nu_f \xi}} f''(0, \xi), \quad (3.17)$$

where μ_{nf} is the coefficient of viscosity.

The skin friction coefficient is defined as

$$C_f^x = \frac{2\tau_w}{\rho_f a^2 x^2}. \quad (3.18)$$

Hence

$$(1-\phi)^{2.5} \sqrt{\xi \text{Re}_x} C_f^x = -2f''(0, \xi). \quad (3.19)$$

where Re_x is the local Reynolds number given by

$$\text{Re}_x = \frac{\alpha x^2}{\nu_f}. \quad (3.20)$$

The heat transfer rate at the surface is given by

$$q_w = -k_{nf} \left(\frac{\partial T}{\partial y} \right)_{y=0} = -k_{nf} (T_w - T_\infty) \sqrt{\frac{a}{\nu_f \xi}} \theta'(0, \xi), \quad (3.21)$$

where k_{nf} is the thermal conductivity of the nanofluid.

The Nusselt number is defined as

$$\text{Nu}_x = \frac{x q_w}{k_f (T_w - T_\infty)}, \quad (3.22)$$

so that

$$\frac{\text{Nu}_x}{\sqrt{\xi \text{Re}_x}} \left(\frac{k_f}{k_{nf}} \right) = -\theta'(0, \xi). \quad (3.23)$$

The mass flux at the surface is given by

$$q_m = -D \left(\frac{\partial C}{\partial y} \right)_{y=0} = -D (C_w - C_\infty) \sqrt{\frac{a}{\nu_f \xi}} \Phi'(0, \xi), \quad (3.24)$$

and the Sherwood number is given by

$$\text{Sh}_x = \frac{xq_m}{D(C_w - C_\infty)}, \quad (3.25)$$

so that

$$\frac{\text{Sh}_x}{\sqrt{\xi \text{Re}_x}} = -\Phi'(0, \xi). \quad (3.26)$$

3.4 Some particular cases of interest

In this section we present some limiting cases of equations (3.11)-(3.13) where the equations reduce to ordinary differential equations.

Case(1): Initial steady state flow

For steady flow we have $\xi = 0$ corresponding to $t = 0$. Thus $f(\eta, 0) = f_i(\eta)$, $\theta(\eta, 0) = \theta_i(\eta)$ and $\Phi(\eta, 0) = \Phi_i(\eta)$. In this case equations (3.11) - (3.13) reduce to

$$f_i''' + \frac{1}{2}\phi_1\eta f_i'' = 0, \quad (3.27)$$

$$\theta_i'' + \frac{1}{2}\frac{k_f}{k_{nf}}\text{Pr}\phi_2\eta\theta_i' = 0, \quad (3.28)$$

$$\Phi_i'' + \frac{1}{2}\text{Sc}\eta\Phi_i' + \text{ScSr}\theta_i'' = 0, \quad (3.29)$$

subject to boundary conditions (3.38).

In the case $\phi_1 = 1$, equation (3.27) reduces to (see Ishak et al. [111], Mustafa et al. [135] and Liao [139])

$$f_i''' + \frac{1}{2}\eta f_i'' = 0, \quad (3.30)$$

subject to

$$f_i(0) = 0, \quad f_i'(0) = 1, \quad f_i'(\infty) = 0. \quad (3.31)$$

Equation (3.30) admits the exact solution, see Liao [139]

$$f_i(\eta) = \eta \operatorname{erfc}\left(\frac{\eta}{2}\right) + \frac{2}{\sqrt{\pi}} \left[1 - \exp\left(\frac{-\eta^2}{4}\right) \right], \quad (3.32)$$

where the complementary error function erfc , is defined as

$$\operatorname{erfc}(\eta) = 1 - \operatorname{erf}(\eta) = 1 - \frac{2}{\sqrt{\pi}} \int_0^\eta e^{-t^2} dt = \frac{2}{\sqrt{\pi}} \int_\eta^\infty e^{-t^2} dt. \quad (3.33)$$

The skin friction in the initial steady state is

$$\sqrt{\xi \operatorname{Re}_x} \quad C_f^x = -\frac{1}{\sqrt{\pi}}. \quad (3.34)$$

The exact solution plays an important role in the proper understanding of qualitative features of the model and the validation of numerical solutions.

Case(2): Final steady state flow

In this case, $\xi = 1$ as $t \rightarrow \infty$, corresponding to $f(\eta, 1) = f_s(\eta)$, $\theta(\eta, 1) = \theta_s(\eta)$ and $\Phi(\eta, 1) = \Phi_s(\eta)$. Equations (3.11) - (3.13) reduce to the following forms

$$f_s''' + \phi_1 (f_s f_s'' - f_s'^2) = 0, \quad (3.35)$$

$$\theta_s'' + \frac{k_f}{k_{nf}} \operatorname{Pr} \phi_2 (f_s \theta_s' - f_s' \theta_s + \delta \theta_s) = 0, \quad (3.36)$$

$$\Phi_s'' + \operatorname{Sc} (f_s \Phi_s' - f_s' \Phi_s - \gamma \Phi_s + \operatorname{Sr} \theta_s'') = 0, \quad (3.37)$$

subject to the boundary conditions

$$f(0) = 0, \quad f'(0) = 1, \quad \theta(0) = 1, \quad \Phi(0) = 1, \quad f'(\infty) = 0, \quad \theta(\infty) = 0, \quad \Phi(\infty) = 0. \quad (3.38)$$

Equation (3.35) reduces to the equation (3.39) below when $\phi_1 = 1$ and $\xi = 1$

$$f_s''' + f_s f_s'' - f_s'^2 = 0, \quad (3.39)$$

subject to boundary conditions (3.38). This equation has the exact solution, see Liao [139]

$$f_s = 1 - e^{-\eta}. \quad (3.40)$$

3.5 Results and Discussion

The nonlinear partial differential equations (3.1) - (3.4) with the boundary conditions (3.5) were transformed to the nonlinear forms (3.11) - (3.13). These equations were solved using the spectral relaxation method SRM together with the spectral quasi-linearization method SQLM. In this section we used the parameters given previously in literature and compared the results with those published previously. The thermophysical properties, together with those of the base fluid, are given in Table 3.1, see Oztop and Abu-Nada [140].

Table 3.1: Thermophysical properties of water and copper and silver nanofluids.

Physical properties	Base fluid (Water)	Copper (Cu)	Silver (Ag)
$C_p(\text{J/kgK})$	4179	385	235
$\rho(\text{Kg/m}^3)$	997.1	8933	10500
$k(\text{W/mK})$	0.613	401	429
$\alpha \times 10^7(\text{m}^2/\text{s})$	1.47	1163.1	1738.6
$\beta \times 10^5(\text{K}^{-1})$	21	1.67	1.89

The case when the heat generation term in equation (3.12) is absent with $\phi = 0$ (regular fluid) has been considered and compared with the results reported by Chamkha and El-Kabeir [67]. The results are shown in Tables 3.2 and 3.3 for various values of the Prandtl number and $\lambda = 0$. From the Tables, it can be seen that heat transfer coefficient increases for increasing Prandtl numbers. This increase suggests that the heat diffuses much slower compared to the velocity. Thus, momentum diffusivity dominates. Moreover, the present results show that the values for both skin friction and heat transfer coefficients are in good agreement with those from Chamkha and El-Kabeir [67]. We may, therefore, conclude that the present numerical methods (SRM and SQLM) can be used with confidence to solve systems of coupled nonlinear equations of the type presented in this study.

Table 3.2: Effect of various values of the Prandtl number Pr on the skin friction $-f''(0)$ and heat transfer coefficient $-\theta'(0)$, when $\delta = 0$.

Pr	Chamkha and El-Kabeir [67]		Present result SRM	
	$f''(0, 1)$	$-\theta'(0, 1)$	$f''(0, 1)$	$-\theta'(0, 1)$
0.7	-1.00000	0.79371	-1.00005852	0.79415181
1.0	-1.00000	1.00000	-1.00005852	1.00005852
3.0	-1.00000	1.92374	-1.00005852	1.92364300
7.0	-1.00000	3.07221	-1.00005852	3.07221790

Table 3.3: Effect of various values of the Prandtl number Pr on the skin friction $-f''(0)$ and heat transfer coefficient $-\theta'(0)$, when $\delta = 0$.

Pr	Chamkha and El-Kabeir [67]		Present result SQLM	
	$f''(0,1)$	$-\theta'(0,1)$	$f''(0,1)$	$-\theta'(0,1)$
0.7	-1.00000	0.79371	-1.00005852	0.79415181
1.0	-1.00000	1.00000	-1.00005852	1.00005852
3.0	-1.00000	1.92374	-1.00005852	1.92364300
7.0	-1.00000	3.07221	-1.00005852	3.07221790

The results for both a Cu-water and a Ag-water were found by both SRM and SQLM, as shown in Tables 3.4 - 3.5. In the analysis we note that $\phi = 0$ represents a regular fluid and $\xi = 1$ represents the final steady state. In the numerical simulations we have used mostly $Pr = 7$ which represents water-based fluids. We used the values $Sc = 0.6$, $Sr = 0.4$ and $Pr = 7$; as have been used previously by Afify [141] and Gbadeyan et al.[142]. The results obtained by both the SRM and SQLM are typically of the same orders, This means that these methods are good enough for solving complicated nonlinear partial differential equations.

Table 3.4: Effect of variation of nanoparticle volume fraction ϕ on the skin friction $-f''(0)$, heat and mass transfer coefficients $-\theta'(0)$, $-\Phi'(0)$ when $\delta = 1$, $\gamma = 1$.

SRM							
ϕ	ξ	Cu - Water			Ag - Water		
		$-f''(0, \xi)$	$-\theta'(0, \xi)$	$-\Phi'(0, \xi)$	$-f''(0, \xi)$	$-\theta'(0, \xi)$	$-\Phi'(0, \xi)$
0.0	0.3	0.70127	1.96885	0.29914	0.70127	1.96885	0.29914
	0.5	0.78983	2.00842	0.44555	0.78983	2.00842	0.44555
	0.7	0.87627	2.04601	0.58441	0.87627	2.04601	0.58441
	1.0	1.00024	2.09309	0.78086	1.00024	2.09309	0.78086
0.3	0.3	0.82643	1.22051	0.45328	0.88207	1.16354	0.46148
	0.5	0.93080	1.19782	0.60359	0.99346	1.13098	0.61132
	0.7	1.03267	1.15065	0.75169	1.10219	1.06903	0.76016
	1.0	1.17877	0.60768	1.04850	1.25813	0.21711	1.10588
0.5	0.3	0.65794	0.90136	0.53081	0.70795	0.83012	0.54082
	0.5	0.74103	0.87907	0.68432	0.79736	0.79794	0.69329
	0.7	0.82213	0.83564	0.83329	0.88462	0.73967	0.84231
	1.0	0.93845	0.27724	1.11972	1.00978	-0.28592	1.18603

Table 3.5: Effect of variation of nanoparticle volume fraction ϕ on the skin friction $-f''(0)$, heat and mass transfer coefficients $-\theta'(0)$, $-\Phi'(0)$ when $\delta = 1$, $\gamma = 1$.

SQLM							
ϕ	ξ	Cu - Water			Ag - Water		
		$-f''(0, \xi)$	$-\theta'(0, \xi)$	$-\Phi'(0, \xi)$	$-f''(0, \xi)$	$-\theta'(0, \xi)$	$-\Phi'(0, \xi)$
0.0	0.3	0.70127	1.96885	0.29914	0.70127	1.96885	0.29914
	0.5	0.78983	2.00842	0.44555	0.78983	2.00842	0.44555
	0.7	0.87627	2.04601	0.58441	0.87627	2.04601	0.58441
	1.0	1.00024	2.09309	0.78086	1.00024	2.09309	0.78086
0.3	0.3	0.82643	1.22051	0.45328	0.88207	1.16354	0.46148
	0.5	0.93080	1.19782	0.60359	0.99346	1.13098	0.61132
	0.7	1.03267	1.15065	0.75169	1.10219	1.06903	0.76016
	1.0	1.17877	0.60768	1.04850	1.25813	0.21711	1.10588
0.5	0.3	0.65794	0.90136	0.53081	0.70795	0.83012	0.54082
	0.5	0.74103	0.87907	0.68432	0.79736	0.79794	0.69329
	0.7	0.82213	0.83564	0.83329	0.88462	0.73967	0.84231
	1.0	0.93845	0.27724	1.11972	1.00978	-0.28592	1.18603

The effect of the various fluid and physical parameters are presented graphically in Figures 3.2 - 3.16. Here we have assumed Prandtl number $Pr = 7$ for both Ag-water and Cu-water nanofluids, see Afify [141], Hasegawa and Kasagi [143] and Kafoussias and Williams [144]. The graphical results show the local skin friction coefficient $-f''(0, \xi)$, the local heat transfer coefficient $-\theta'(0, \xi)$ and the local mass transfer coefficient $-\Phi'(0, \xi)$ for different physical and fluid parameter values. We have excluded any analysis of the effects of Pr and Sc because these have been discussed extensively in the literature.

Figures 3.2 - 3.5 show typical fluid velocity profiles, temperature and concentration profiles for different nanoparticle volume fraction ϕ . As can be seen from the figures, increasing ϕ increases both the nanofluid velocity profiles and the temperature profiles. By contrast, it causes the solute concentration profiles to decrease. Thus, we can conclude that the conductivity of the nanofluid increases as the nanoparticle volume fraction increases, so leading to a broadening of the thermal boundary layer profiles. This increases momentum thinning and decreases the nanoparticle volume fraction. Furthermore, the results in Figures 3.2 and 3.3 indicate that the effect of the nanoparticle volume fraction is more pronounced in the case of a Cu-water nanofluid compared to a Ag-water nanofluid. However, in Figure 3.4 we note that the reverse; the effect of the nanoparticle volume fraction is greater in the case of an Ag-water nanofluid compared to an Cu-water nanofluid. Moreover, in Figure 3.4 as the nanoparticle volume fraction increases, the temperature of the nanofluid decreases. Physically, an increase in the nanoparticle volume fraction leads to an increase in the thermal conductivity of the nanofluid, and hence the thickness of the thermal boundary layer increases. Overall, the results show a good agreement with Vajravelu et al.[145] and Kameswaran et al. [146].

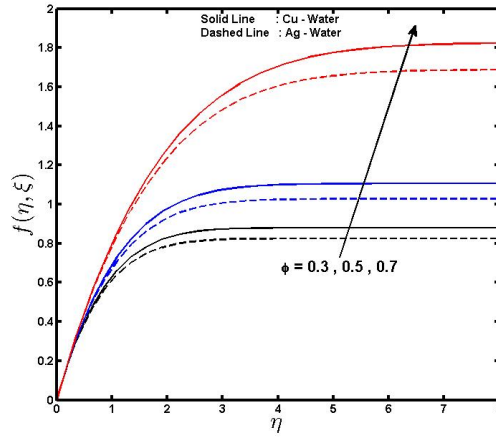


Figure 3.2: Effect of nanoparticle volume fraction ϕ on the velocity profiles with $\xi = 0.5$, $\delta = 1$, $\gamma = 1$.

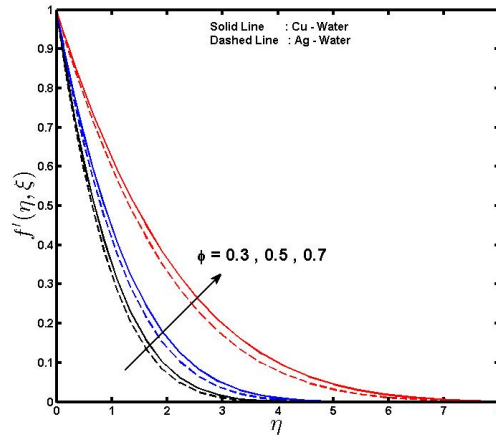


Figure 3.3: Effect of nanoparticle volume fraction ϕ on tangential velocity profiles with $\xi = 0.5$, $\delta = 1$, $\gamma = 1$.

We note from Figure 3.5 that the effect of the nanoparticle volume fraction is greater in the case of a Ag-water nanofluid compared to a Cu-water nanofluid. However, when $\phi = 0.7$ we get the opposite effect. The results show a good agreement with Kameswaran et al.[147].

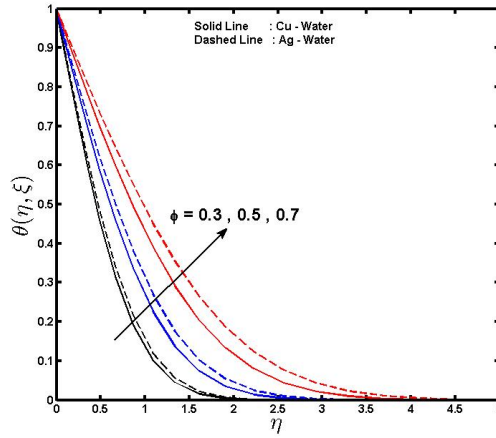


Figure 3.4: Effect of nanoparticle volume fraction ϕ on the temperature profiles with $\xi = 0.5$, $\delta = 1$, $\gamma = 1$.

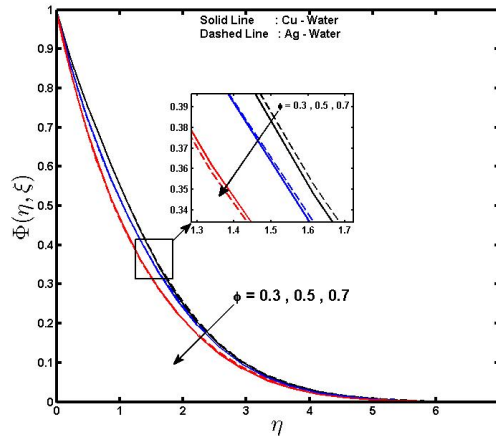


Figure 3.5: Effect of nanoparticle volume fraction ϕ on the concentration profiles with $\xi = 0.5$, $\delta = 1$, $\gamma = 1$.

Figures 3.6 and 3.7 show the influence of the heat generation parameter on the temperature and concentration profiles. Increasing the heat generation parameter tends to increase the nanofluid temperature significantly. The presence of a heat source causes the thermal boundary layer to increase. The result is expected because heat generation in the fluid increases the temperature within the boundary layer which accelerates the convection as well as increas-

ing the flow within the boundary layer at the same time as the solute concentration profiles increase. Therefore, the concentration boundary layer thickness decreases as the heat generation parameter increases due to the new product. Again, the effect of the dimensionless heat generation is more significant in the case of a Ag-water nanofluid compared to a Cu-water nanofluid, which is a similar result to that of Alam and Mollah[148].

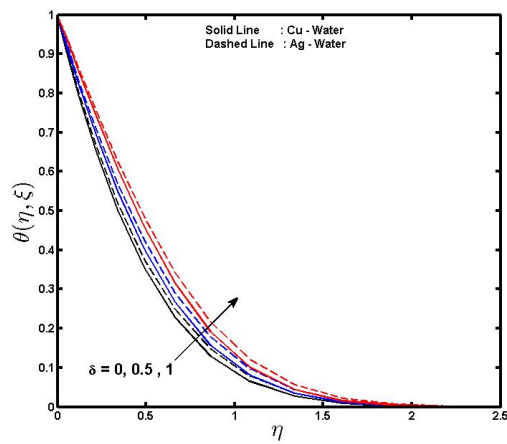


Figure 3.6: Effect of the dimensionless heat generation δ on the temperature profiles with $\xi = 0.5$, $\phi = 0.3$, $\gamma = 1$.

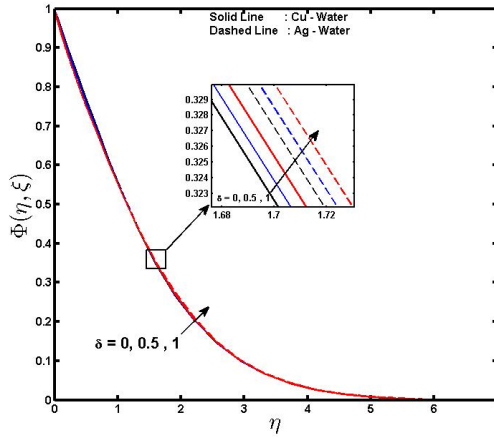


Figure 3.7: Effect of the dimensionless heat generation δ on the concentration profiles with $\xi = 0.5$, $\phi = 0.3$, $\gamma = 1$.

Figure 3.8 shows the effect of the chemical reaction parameter on the solute concentration profiles. As the chemical reaction increases, the solute concentration in the nanofluid decreases due to the conversion of solute to form a new product. This result shows that the solute concentration thickness is reduced as the reaction progresses.

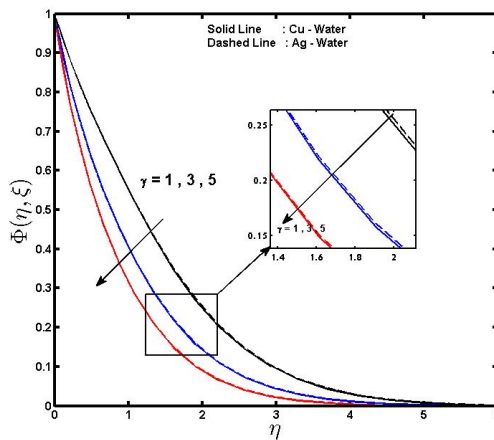


Figure 3.8: Effect of chemical reaction parameter γ on the concentration profiles with $\xi = 0.5$, $\delta = 1$, $\phi = 0.3$.

Figure 3.9 shows the impact of the Soret number on the concentration profiles. The Figure shows that as the Soret number increases, the nanofluid boundary layer thickness increases, more significantly in the case of a Ag-water nanofluid than for a Cu-water nanofluid.

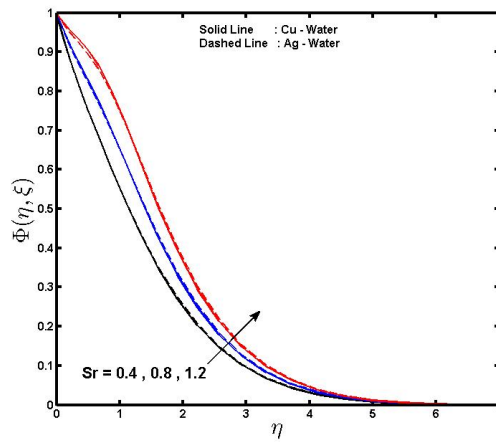


Figure 3.9: Effect of the Soret number Sr on the concentration profiles with $\xi = 0.5$, $\delta = 1$, $\phi = 0.3$, $\gamma = 1$.

Figures 3.10 - 3.12 show the effect of various values of the nanoparticle volume fraction on the skin friction, heat and mass transfer coefficient. Increasing the nanoparticle volume fraction value causes the skin friction and the heat transfer coefficients to decrease, while the mass transfer coefficient increases. We obtain higher values of the skin friction and mass transfer coefficients at $\xi = 1$, see Figures (3.10 and 3.12), but at $\xi = 0$ we get higher values of heat transfer coefficient, see Figure 3.11. This indicates that changes in heat transfer rates are associated with the nanoparticle volume fraction, which highlights the possible use of nanofluids in heat transfer processes.

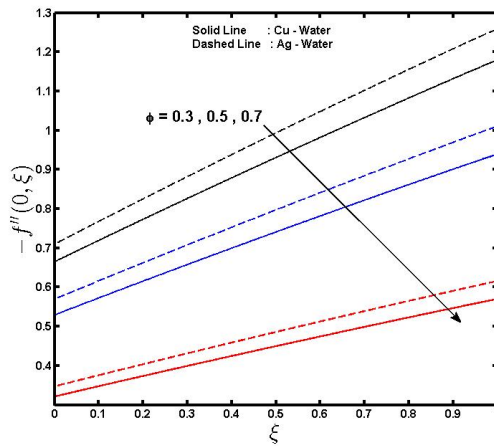


Figure 3.10: Effect of the variation nanoparticle volume fraction ϕ on the skin friction coefficient against ξ with $\delta = 1$, $\gamma = 1$.

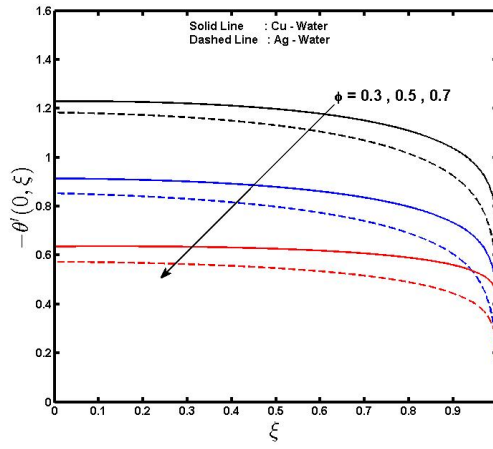


Figure 3.11: Effect of the variation nanoparticle volume fraction ϕ on heat transfer coefficient against ξ with $\delta = 1$, $\gamma = 1$.

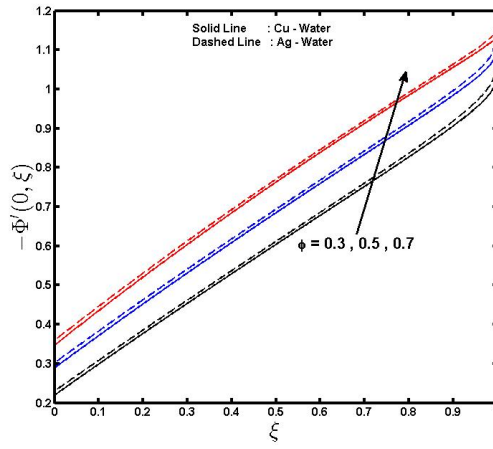


Figure 3.12: Effect of the variation nanoparticle volume fraction ϕ on mass transfer coefficient against ξ with $\delta = 1$, $\gamma = 1$.

Figures 3.13 and 3.14 show the impact of heat generation on the heat and mass transfer coefficients. For both Cu-water and Ag-water nanofluids, the heat transfer coefficient $-\theta'(0, \xi)$ decreases with the heat generation parameter while increasing with ξ . The mass transfer coefficient $-\phi'(0, \xi)$ increases with ξ and the heat generation parameter. With increasing heat generation parameter δ and ξ , we obtain higher values of the mass transfer coefficient. In particular, when $\delta = 0, 0.5$ with $\xi = 1$, the heat transfer coefficient is higher than when $\delta = 1$ and $\xi = 1$. For the heat transfer coefficient (see Figure 3.13), the effect of the heat generation parameter is more significant in the case of a Cu-water nanofluid compared to a Ag-water nanofluid. However, the opposite is true for the mass transfer coefficient in Figure 3.14. These results are qualitatively similar to those obtained by Ali et al.[149].

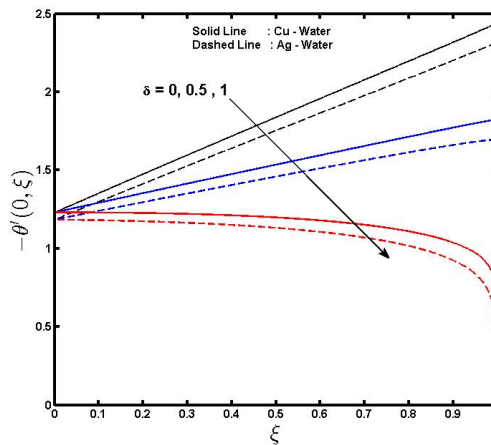


Figure 3.13: Effect of the dimensionless heat generation parameter δ on heat transfer coefficient against ξ with $\phi = 0.3$, $\gamma = 1$.

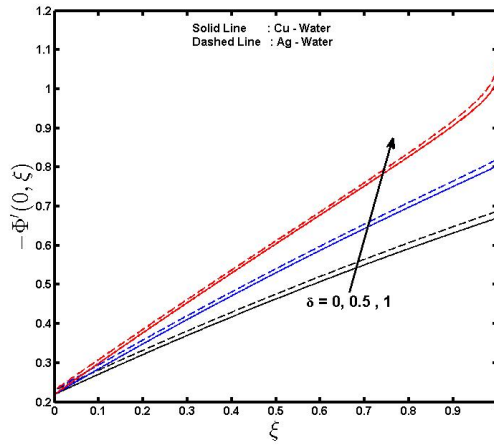


Figure 3.14: Effect of the dimensionless heat generation parameter δ on mass transfer coefficient against ξ with $\phi = 0.3$, $\gamma = 1$.

Figure 3.15 shows the influence of the chemical reaction parameter on the mass transfer coefficient. As the chemical reaction increases, the mass transfer coefficient also increases and we get higher values of mass transfer as ξ increases. We note that the effect of chemical reaction parameter is marginally greater in the case of a Ag-water nanofluid compared to a Cu-water nanofluid.

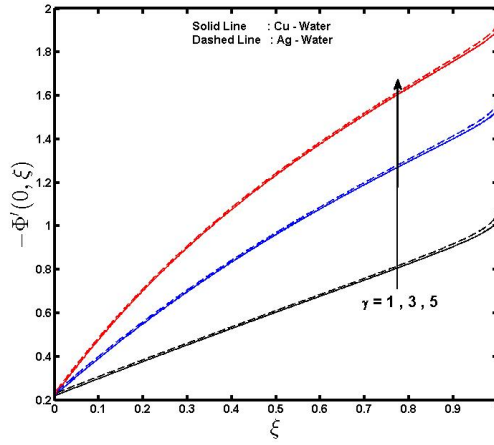


Figure 3.15: Effect of chemical reaction parameter γ on mass transfer coefficient against ξ with $\delta = 1$ $\phi = 0.3$.

Figure 3.16 illustrates the effect of the Soret number on the mass transfer rate. We observe that increasing the Soret number tends to reduce the nanoparticle volume fraction boundary layer thickness. We observe that $-\Phi'(0, \xi)$ increases with variable ξ and decreases with the Soret parameter. The effect of the Soret parameter is greater for a Ag-water nanofluid than a Cu-water nanofluid. Thus, we note that increasing the Soret number tends to reduce the volume fraction boundary layer thickness.

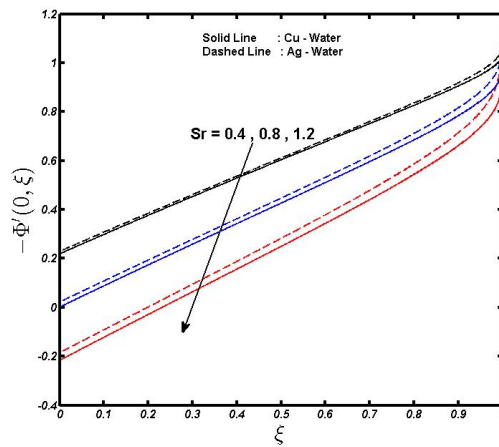


Figure 3.16: Effect of the Soret number Sr on mass transfer coefficient against ξ with $\delta = 1$, $\phi = 0.3$, $\gamma = 1$.

3.6 Summary

In this chapter we investigated unsteady nanofluid flow and convection from a stretching sheet in the presence of heat generation and Soret effects. The accuracy was tested by comparing with published literature for the special cases. We found that our results for limiting case are in line with those previously published. In Chapter 4 we study steady MHD mixed convection a nanofluid flow and heat and mass transfer from a stretching sheet.

Chapter 4

Mixed convection in MHD nanofluid flow due to a stretching sheet with Soret and Dufour effects

In this chapter we investigate Soret and Dufour effects on steady mixed convection in a nanofluid flow. The incompressible fluid flow is subject to temperature dependent viscosity, thermal radiation influences and a chemical reaction parameter. The transformed governing partial differential equations are solved numerically using the spectral relaxation method (SRM).

4.1 Introduction

The problem of steady magneto-hydrodynamics(MHD) flow and heat and mass transfer over a stretching surface has applications in polymer technology, glass-fiber production and in metallurgy. In particular, many metallurgical processes involve cooling continuous strips or filaments by drawing them through a quiescent fluid. The properties of the final product depend on the rate of cooling which can be controlled by drawing such strips in an electrically conducting fluid subject to a magnetic field to achieve the desired characteristics in the final product. Indeed, many engineering processes, on conveyor belts, possess the characteristics of a moving continuous surface, see Abel and Veena [150], Prasad et al. [151].

As was outlined in Chapter 3, Blasius [95] was the first to report the boundary layer flow over a flat plate in a uniform free stream. Howarth [96], provided a numerical solution to the Blasius problem and a continuously moving plate in a quiescent ambient fluid was the first studied by Sakiadis [97]. Crane [98] expanded this study stretched sheet. Since Crane's pioneering work, the literature concerning boundary layer flow due to a stretching sheet has grown enormously. Indeed, Crane's problem has been expanded to include many other features such as porosity, heat and mass transfer, magnetic field effects and viscoelasticity or permeable surfaces, extended by Gupta and Gupta [99].

Early work based on Crane's model includes that of Chen and Strob [100] and Grubka and Bobba [101]. More recently contributions have come from Aiyesimi et al. [103] and Aminraza et al. [152]. of significance, because of the importance of boundary layer flow over a stretching sheets, are studies concerned with aspects of unsteady flow past a stretching surface by Hamad

and Ferdows [153] and Dulal and Mondal [154]. In particular, Liao [120] and Xu et al. [121] obtained series solutions of the unsteady boundary layer equations.

As previously explained in Chapter 3, nanofluids have higher thermal conductivity rates compared to common fluids such as water and have been considered for application as advanced heat transfer fluids. Masuda et al. [155] and Buongiorno [156] suggested the use of nanofluids in cooling advanced nuclear systems. The most important properties of nanofluids are enhanced effective fluid thermal conductivity and heat transfer coefficient, see Choi [125]. Studies on steady nanofluid flow due to stretching sheet have also been reported by Gbadeyan et al. [157], Seddeek [158], Subhakar and Gangadhar [159], Shakhaoath et al. [160] and Singh et al. [161]. A benchmark study on the enhancement of thermal conductivity in nanofluids was made by Buongiorno [162]. Venerus et al. [163] investigated the viscosity effects on colloidal dispersions in heat transfer applications. Gharagozloo et al. [164] investigated aggregation and the thermal conductivity in nanofluids and Philip et al. [165] proposed a nanofluid with tunable thermal properties.

The aim of the present study is to analyze the combined effects of Soret and Dufour parameters on steady mixed convection in boundary layer flow of a nanofluid with magneto-hydrodynamics (MHD) over a non-isothermal wedge. The flow is subject to a chemical reaction, thermal radiation and viscous dissipation. A special case of this study is, that obtained by Yih [166]. The spectral relaxation method (SMR) is used to solve the governing equations.

4.2 Mathematical formulation

Consider steady two-dimensional incompressible nanofluid flow over a non-isothermal stretching wedge. The temperature and nanoparticles concentration at the stretching surface are T_w and C_w , and those of the ambient nanofluid are T_∞ and C_∞ , respectively. The radiation heat flux in the x -direction is negligible compared to the flux in the y -direction. The x -axis is along the plate and the y -axis is normal to this, as shown in Figure 4.1. Introducing the boundary layer approximation, the governing equations are given by Tiwari and Das [167];

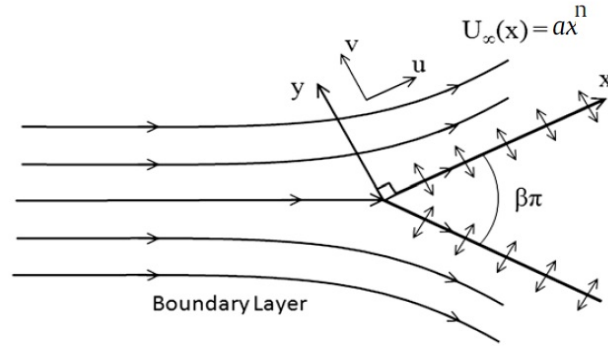


Figure 4.1: Physical model and coordinate system.

$$\frac{\partial u}{\partial x} + \frac{\partial v}{\partial y} = 0, \quad (4.1)$$

$$u \frac{\partial u}{\partial x} + v \frac{\partial u}{\partial y} = \nu_{nf} \frac{\partial^2 u}{\partial y^2} - \frac{1}{\rho_{nf}} \frac{\partial p}{\partial x} - u \left\{ \frac{\sigma B_0^2}{\rho_{nf}} \right\} + g\beta_T(T - T_\infty) + g\beta_C(C - C_\infty), \quad (4.2)$$

$$u \frac{\partial T}{\partial x} + v \frac{\partial T}{\partial y} = \alpha_{nf} \frac{\partial^2 T}{\partial y^2} - \frac{1}{(\rho c_p)_{nf}} \frac{\partial q_r}{\partial y} + \frac{\rho_f D_m K_T}{C_s (\rho c_p)_{nf}} \frac{\partial^2 C}{\partial y^2} + \frac{\nu_{nf}}{(c_p)_{nf}} \left(\frac{\partial u}{\partial y} \right)^2, \quad (4.3)$$

$$u \frac{\partial C}{\partial x} + v \frac{\partial C}{\partial y} = D_m \frac{\partial^2 C}{\partial y^2} + \frac{D_m K_T}{T_m} \frac{\partial^2 T}{\partial y^2} - R(C - C_\infty), \quad (4.4)$$

where u and v are the fluid velocity and normal velocity components in the x and y directions,

respectively, ν_{nf} is the nanofluid kinematic viscosity, p is the pressure, σ an electrical conductivity, B_0 is the externally imposed magnetic field in the y -direction, ρ_{nf} is the nanofluid density, g is the gravitational acceleration, β_T is the volumetric thermal expansion coefficient, β_C is the volumetric solutal expansion coefficient, T is the temperature of fluid in the boundary layer, C is the fluid solutal concentration, α_{nf} is the thermal diffusivity of the nanofluid, $(\rho c_p)_{nf}$ is the nanofluid heat capacitance, ρ_f is the density of the base fluid, D_m is the mass diffusivity of the concentration, K_T is the thermal diffusion ratio, C_s is the concentration susceptibility, $(c_p)_{nf}$ is the specific heat of fluid at constant pressure, T_m is the mean fluid temperature, R is the chemical reaction parameter and q_r is the radiation heat flux given by

$$q_r = -\frac{4\sigma^*}{3K^*} \frac{\partial T^4}{\partial y}, \quad (4.5)$$

where σ^* is the Stefan-Boltzmann constant and K^* is the Rosseland mean absorption coefficient. We assume that the temperature variation T^4 may be expanded in a Taylor series. Neglecting higher order terms and expanding T^4 about T_∞ we obtain, $T^4 \cong 4T_\infty^3 T - 3T_\infty^4$, see Singh et al.[161].

For a free - stream, the momentum equation (4.2) becomes

$$U_\infty \frac{dU_\infty}{dx} = -\frac{1}{\rho_{nf}} \frac{\partial p}{\partial x} - \frac{\sigma B_0^2}{\rho_{nf}} U_\infty, \quad (4.6)$$

where $U_\infty = ax^n$ is the velocity of the potential flow outside the boundary layer, $n = \beta/(2-\beta)$, and β is the Hartree pressure gradient parameter which corresponds to $\beta = \Omega/\pi$, the angle of the wedge, and a is a positive real number.

Substituting (4.6) in (4.2) and (4.5) in (4.3), the transport written as

$$u \frac{\partial u}{\partial x} + v \frac{\partial u}{\partial y} = \nu_{nf} \frac{\partial^2 u}{\partial y^2} + U_\infty \frac{dU_\infty}{dx} + (U_\infty - u) \left\{ \frac{\sigma B_0^2}{\rho_{nf}} \right\} + g\beta_T(T - T_\infty) + g\beta_C(C - C_\infty), \quad (4.7)$$

$$u \frac{\partial T}{\partial x} + v \frac{\partial T}{\partial y} = \alpha_{nf} \frac{\partial^2 T}{\partial y^2} + \frac{1}{(\rho c_p)_{nf}} \frac{16\sigma^* T_\infty^3}{3K^*} \frac{\partial^2 T}{\partial y^2} + \frac{\rho_f D_m K_T}{C_s (\rho c_p)_{nf}} \frac{\partial^2 C}{\partial y^2} + \frac{\nu_{nf}}{(c_p)_{nf}} \left(\frac{\partial u}{\partial y} \right)^2, \quad (4.8)$$

subject to the boundary conditions

$$\begin{aligned} \mathbf{u} = \mathbf{v} = 0, \quad T = T_w(x) = T_\infty + T_0 x^{2n}, \quad C = C_w(x) = C_\infty + C_0 x^{2n} \quad \text{at} \quad \mathbf{y} = 0, \\ \mathbf{u} \rightarrow \mathbf{U}_\infty(x) = \alpha x^n, \quad T = T_\infty, \quad C = C_\infty \quad \text{as} \quad \mathbf{y} \rightarrow \infty, \end{aligned} \quad (4.9)$$

and initial conditions

$$\mathbf{u} = 0, \quad \mathbf{v} = 0, \quad T = T_w, \quad C = C_w, \quad \forall x, y, \quad (4.10)$$

where T_0 and C_0 , are positive real numbers. We note that $0 \leq n \leq 1$ with $n = 0$ for the boundary- layer flow over a stationary flat plate and $n = 1$ for the flow near the stagnation point on an infinite wall.

The effective viscosity of the nanofluid, see Brinkman [137] is

$$\mu_{nf} = \frac{\mu_f}{(1 - \phi)^{2.5}}, \quad (4.11)$$

where ϕ is the solid volume fraction of nanoparticles, μ_f is the dynamic viscosity of the base fluid. In equations (4.1) - (4.4);

$$\begin{aligned} (\rho c_p)_{nf} &= (1 - \phi)(\rho c_p)_f + \phi(\rho c_p)_s \\ \rho_{nf} &= (1 - \phi)\rho_f + \phi\rho_s, \quad \nu_{nf} = \frac{\mu_{nf}}{\rho_{nf}} \\ \alpha_{nf} &= \frac{k_{nf}}{(\rho c_p)_{nf}}, \quad \frac{k_{nf}}{k_f} = \frac{(k_s + k_f) - 2\phi(k_f - k_s)}{(k_s + k_f) + \phi(k_f - k_s)}, \end{aligned} \quad (4.12)$$

where k_{nf} is the thermal conductivity of the nanofluid, k_f and k_s are the thermal conductivities of the fluid and of the solid fractions, respectively, and ρ_s is the density of the solid fractions, $(\rho c_p)_f$ and $(\rho c_p)_s$ are the heat capacity of base fluid and effective heat capacity of nanoparticles respectively, k_{nf} is the thermal conductivity of the nanofluid, see Abu-Nada [138].

It is convenient to introduce the stream function ψ where

$$\mathbf{u} = \frac{\partial \psi}{\partial y}, \quad \mathbf{v} = -\frac{\partial \psi}{\partial x}. \quad (4.13)$$

We use the following dimensionless variables, Yih [166]

$$\eta = \sqrt{\frac{U_\infty x}{\nu_f \xi}} \frac{y}{x}, \quad \xi = \frac{\sigma B_0^2}{\rho_{nf} U_\infty} x, \quad \psi = \sqrt{U_\infty \nu_f x} f(\xi, \eta), \quad \theta(\xi, \eta) = \frac{T - T_\infty}{T_w - T_\infty}, \quad \Phi(\xi, \eta) = \frac{C - C_\infty}{C_w - C_\infty}. \quad (4.14)$$

The governing equations (4.4), (4.7) and (4.8) with the boundary conditions (4.9) and (4.14)

can be presented in the form

$$f''' + \phi_1 \left[\frac{n+1}{2} f f'' + n(1-f'^2) + \xi(1-f') + Gr_t \theta + Gr_c \Phi \right] = \phi_1 (1-n) \xi \left[f' \frac{\partial f'}{\partial \xi} - f'' \frac{\partial f}{\partial \xi} \right], \quad (4.15)$$

$$\begin{aligned} \left(\frac{k_{nf}}{k_f} \frac{1}{Pr} + Nr \right) \theta'' + \phi_2 \left[\frac{n+1}{2} f \theta' - 2n f' \theta \right] + \frac{Ec}{(1-\phi)^{2.5}} (f'')^2 \\ + D_f \Phi'' = \phi_2 (1-n) \xi \left[f' \frac{\partial \theta}{\partial \xi} - \theta' \frac{\partial f}{\partial \xi} \right], \end{aligned} \quad (4.16)$$

$$\Phi'' + Sc \left[\frac{n+1}{2} f \Phi' - 2n f' \Phi - \gamma \Phi + Sr \theta'' \right] = Sc (1-n) \xi \left[f' \frac{\partial \Phi}{\partial \xi} - \Phi' \frac{\partial f}{\partial \xi} \right], \quad (4.17)$$

subject to the boundary conditions

$$\begin{aligned} f(\xi, 0) = f'(\xi, 0) = 0, \quad \theta(\xi, 0) = 1, \quad \Phi(\xi, 0) = 1, \quad \eta = 0, \quad \xi \geq 0, \\ f'(\xi, \infty) = 1, \quad \theta(\xi, \infty) = 0, \quad \Phi(\xi, \infty) = 0, \quad \eta \longrightarrow \infty, \quad \xi \geq 0, \end{aligned} \quad (4.18)$$

where

$$\phi_1 = (1-\phi)^{2.5} \left[1 - \phi + \phi \left(\frac{\rho_s}{\rho_f} \right) \right], \quad \phi_2 = \left[1 - \phi + \phi \left(\frac{(\rho c)_s}{(\rho c)_f} \right) \right]. \quad (4.19)$$

Here

$$\begin{aligned} Gr_t = \frac{g \beta_T (T_w - T_\infty) x}{U_\infty^2}, \quad Gr_c = \frac{g \beta_C (C_w - C_\infty) x}{U_\infty^2}, \quad Pr = \frac{\nu_f}{\alpha_f}, \quad Nr = \frac{16 \sigma^* T_\infty^3}{3 K^* (\rho c p)_f \nu_f}, \\ Ec = \frac{U_\infty^2}{(cp)_f (T_w - T_\infty)}, \quad Sc = \frac{\nu_f}{D_m}, \quad D_f = \frac{D_m K_T (C_w - C_\infty)}{C_s C_p \nu_f (T_w - T_\infty)}, \quad \alpha_f = \frac{k_f}{(\rho c p)_f}, \\ \nu_f = \frac{\mu_f}{\rho_f}, \quad \gamma = \frac{Rx}{U_\infty}, \quad Sr = \frac{D_m K_T (T_w - T_\infty)}{\nu_f T_m (C_w - C_\infty)}, \end{aligned} \quad (4.20)$$

where Gr_t is the local Grashof number, Gr_c is the local solutal Grashof number, Pr is the Prandtl number, Nr is the thermal radiation parameter, Ec is the Eckert number, Sc is the

Schmidt number, D_f is the Dufour number, α_f is the coefficient of the thermal diffusivity of the base fluid, ν_f is the kinematic viscosity of base fluid, γ is the scaled chemical reaction parameter and Sr is the Soret number.

The Eckert number represents the kinetic energy of the flow relative to the boundary layer enthalpy difference. The Dufour effect describes the energy flux created when a chemical system is under a concentration gradient.

4.3 Skin friction, heat and mass transfer coefficients

Parameters of engineering interest include the skin friction coefficient C_f , the local Nusselt number Nu_x , and the local Sherwood number Sh_x .

The shearing stress at the surface τ_w is given by

$$\tau_w = -\mu_{nf} \left(\frac{\partial u}{\partial y} \right)_{y=0} = -\frac{\mu_f}{(1-\phi)^{2.5}} \frac{U_\infty}{x} \sqrt{\frac{U_\infty x}{\nu_f}} f''(0, \xi), \quad (4.21)$$

where μ_{nf} is the nanofluid coefficient of viscosity.

The skin friction coefficient is defined as

$$C_f = \frac{2\tau_w}{\rho_f U_\infty^2}, \quad (4.22)$$

and using (4.21) in (4.22) we obtain

$$\frac{1}{2} (1-\phi)^{2.5} \sqrt{Re_x} C_f = -f''(0, \xi), \quad (4.23)$$

where Re_x is the local Reynolds number given by

$$Re_x = \frac{U_\infty x}{\nu_f}. \quad (4.24)$$

The heat transfer rate at the surface is given by

$$q_w = -k_{nf} \left(\frac{\partial T}{\partial y} \right)_{y=0} = -k_{nf} \frac{(T_w - T_\infty)}{x} \sqrt{\frac{U_\infty x}{\nu_f}} \theta'(0, \xi), \quad (4.25)$$

where k_{nf} is the thermal conductivity of the nanofluid.

The Nusselt number is defined as

$$Nu_x = \frac{x q_w}{k_f (T_w - T_\infty)}. \quad (4.26)$$

Using (4.25) in (4.26), the dimensionless wall heat transfer rate is obtained as

$$\frac{Nu_x}{\sqrt{Re_x}} \left(\frac{k_f}{k_{nf}} \right) = -\theta'(0, \xi). \quad (4.27)$$

The mass flux at the wall surface is given by

$$q_m = -D \left(\frac{\partial C}{\partial y} \right)_{y=0} = -D \frac{(C_w - C_\infty)}{x} \sqrt{\frac{U_\infty x}{\nu_f}} \Phi'(0, \xi), \quad (4.28)$$

and the Sherwood number is defined as

$$Sh_x = \frac{x q_m}{D (C_w - C_\infty)}. \quad (4.29)$$

Using (4.28) in (4.29) the dimensionless wall mass transfer rate is obtained as

$$\frac{Sh_x}{\sqrt{Re_x}} = -\Phi'(0, \xi). \quad (4.30)$$

4.4 Some particular cases of interest

In this section we present some limiting cases of equations (4.15) - (4.17) where the equations reduce to ordinary differential equations.

Case(1) For steady-state flow when $\phi = 0$ (regular fluid) we have $\xi = 0$, $\text{Gr}_t = 0$ and $\text{Gr}_c = 0$. In this case, equation (4.15) reduces to that given in Yih [166]

$$f''' + \frac{n+1}{2}ff'' + n(1-f'^2) = 0. \quad (4.31)$$

The solution of equation (4.31) is presented later in Table 4.1 for the skin friction for various values of n .

Case(2) For a regular fluid and $\xi = 0$, $n = 0$, $\text{Nr} = 0$, $\text{Ec} = 0$, $\text{D}_f = 0$, and Gr_t and Gr_c are set to be zero. Equations (4.15) and (4.16) reduce to

$$f''' + \frac{1}{2}ff'' = 0. \quad (4.32)$$

$$\frac{1}{\text{Pr}}\theta'' + \frac{1}{2}f\theta' = 0. \quad (4.33)$$

Equation (4.32) is decoupled from the energy equation (4.33).

Case(3): For the nanoparticle volume fraction $\phi = 0$; if we substitute the physical parameters $n = 0$, $\text{Nr} = 0$, $\text{Ec} = 0$, $\text{D}_f = 0$, and Gr_t and Gr_c are set to be zero. If we substitute into equations (4.15) - (4.16) we obtain (see Yih [166]):

$$f''' + \frac{1}{2}ff'' + \xi(1-f') = \xi \left[f' \frac{\partial f'}{\partial \xi} - f'' \frac{\partial f}{\partial \xi} \right], \quad (4.34)$$

$$\frac{1}{\text{Pr}}\theta'' + \frac{1}{2}f\theta' = \xi \left[f' \frac{\partial \theta}{\partial \xi} - \theta' \frac{\partial f}{\partial \xi} \right]. \quad (4.35)$$

The Nusselt number for various values of the Prandtl number Pr and ξ is given in Table 4.3.

4.5 Results and Discussion

As was shown in Sections 4.2 and 4.3, equations (4.2) - (4.4) and boundary conditions (4.9) were transformed into nonlinear partial differential equations (4.15) - (4.17). These were then solved numerically using the spectral relaxation method for $0 \leq \xi \leq 1$. The thermophysical properties of the nanofluids and the base fluid water, are given in Table 3.1. We have compared our results for the local skin friction coefficient $f''(0,0)$, and local Nusselt number $\theta'(0,0)$ with the previous results by Yih [166]. The results are shown in Tables 4.1 - 4.3. There is good agreement between Yih's [166] work and our values for both the local skin friction coefficient and the heat transfer coefficient. This shows the validity of our approach.

Table 4.1: Comparison of the values of $-f''(0,0)$ for various values of n , when $\phi = 0$, $Gr_t = Gr_c = 0$ and $\xi = 0$ (steady state).

n	Yih [166]	Present result (SRM)
	$-f''(0,0)$	$-f''(0,0)$
-0.05	0.213484	0.213685
0.0	0.332057	0.332058
1/3	0.757448	0.757406

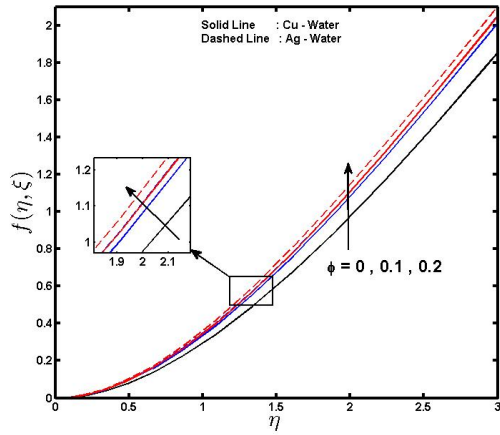
Table 4.2: Comparison of the heat transfer coefficient $-\theta'(0, \xi)$ for various values of Pr and ξ with $\phi = 0$, $\text{Nr} = \text{Ec} = \text{D}_f = \mathbf{n} = 0$.

Pr	ξ	Yih [166]	Present results
		$-\theta'(0, \xi)$	$-\theta'(0, \xi)$
	0.0	0.297526	0.297526
	0.5	0.357022	0.356986
0.733	1.0	0.382588	0.382558
	0.0	0.332057	0.332057
	0.5	0.402864	0.402822
1.0	1.0	0.433607	0.433572

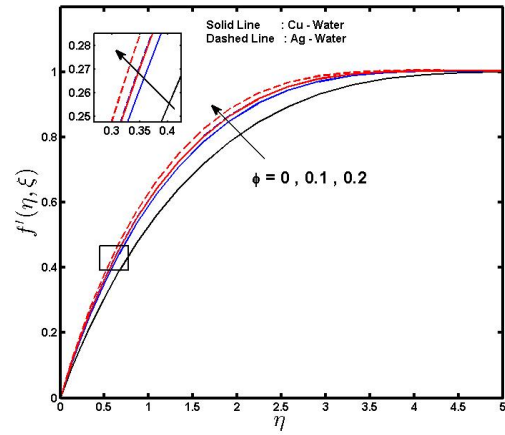
Table 4.3: Comparison of heat transfer coefficient $-\theta'(0, 0)$ for various values of Pr , when $\phi = 0$, $\text{Nr} = \text{Ec} = \text{D}_f = \mathbf{n} = 0$ and $\xi = 0$ (steady state).

Pr	Yih [166]	Present result (SRM)
	$-\theta'(0, 0)$	$-\theta'(0, 0)$
0.1	0.140034	0.140034
1.0	0.332057	0.332057
10	0.728141	0.728141
100	1.571831	1.571658
1000	3.387083	3.396962
10000	7.297402	7.351156

Figures 4.2 - 4.5 we show the effect of nanoparticle volume fraction on the velocity profiles, temperature profiles, concentration profiles, skin friction coefficient, heat transfer coefficient and the mass transfer coefficient respectively. Increased nanoparticle volume fraction leads to an increase in the fluid velocity, temperature profiles and the mass transfer coefficient, while, the concentration profiles, skin friction coefficient and heat transfer coefficients are reduced. Figures 4.4 and 4.5, show that the skin friction and the heat transfer coefficient decrease with ξ , whereas the mass transfer coefficient increases. This is due to the fact that increased nanoparticle volume fraction enhances the thermal conductivity causing higher flow rates at the surface. Comparing the effect of the nanoparticle volume fraction on Cu-water and Ag-water nanofluids, (Figures 4.2, 4.3(a) and 4.5(b)) we note that the effect is greater in the case of a Ag-water nanofluid than in a Cu-water nanofluid. The reverse is true for solutal concentration profiles, skin friction coefficient and the heat transfer coefficient, where the effect is greater for Cu-water nanofluids. These finding are similar to the results reported by Kameswaran et al.[147].

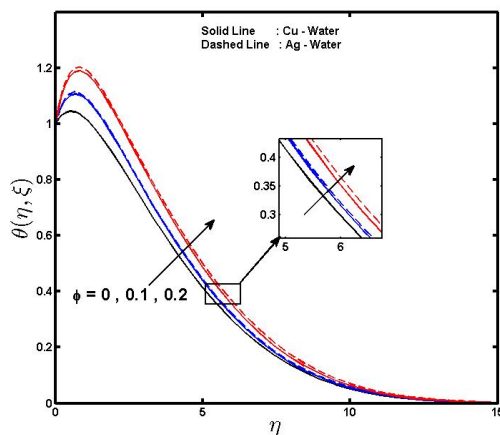


(a)

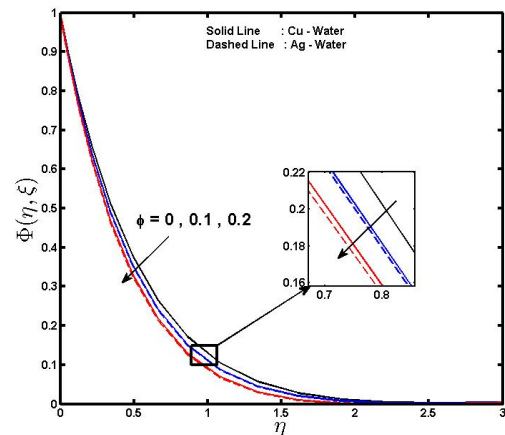


(b)

Figure 4.2: Effect of nanoparticle volume fraction ϕ on (a) the normal and (b) tangential velocity profiles respectively, for $Gr_t = 0.01$, $n = 0$, $Gr_c = 0.01$, $Nr = 10$, $Pr = 7$, $Ec = 10$, $D_f = 0.01$, $\gamma = 3$, $Sc = 1$, $Sr = 1$ and $\xi = 0.5$.



(a)



(b)

Figure 4.3: Effect of nanoparticle volume fraction ϕ on (a) the temperature profiles and (b) the concentration profiles for $Gr_t = 0.01$, $n = 0$, $Gr_c = 0.01$, $Nr = 10$, $Pr = 7$, $Ec = 10$, $D_f = 0.01$, $\gamma = 3$, $Sc = 1$, $Sr = 1$ and $\xi = 0.5$.

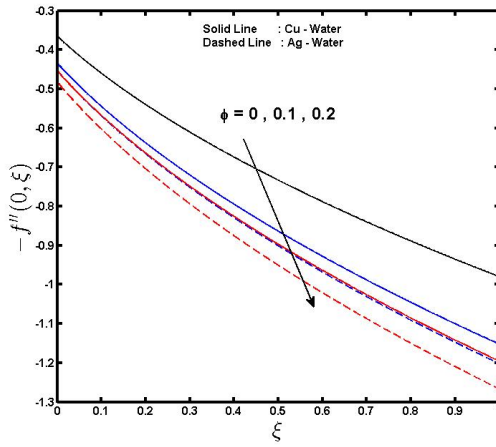


Figure 4.4: Effect of nanoparticle volume fraction ϕ on the skin friction coefficient for $Gr_t = 0.01$, $n = 0$, $Gr_c = 0.01$, $Nr = 10$, $Pr = 7$, $Ec = 10$, $D_f = 0.01$, $\gamma = 3$, $Sc = 1$ and $Sr = 1$.

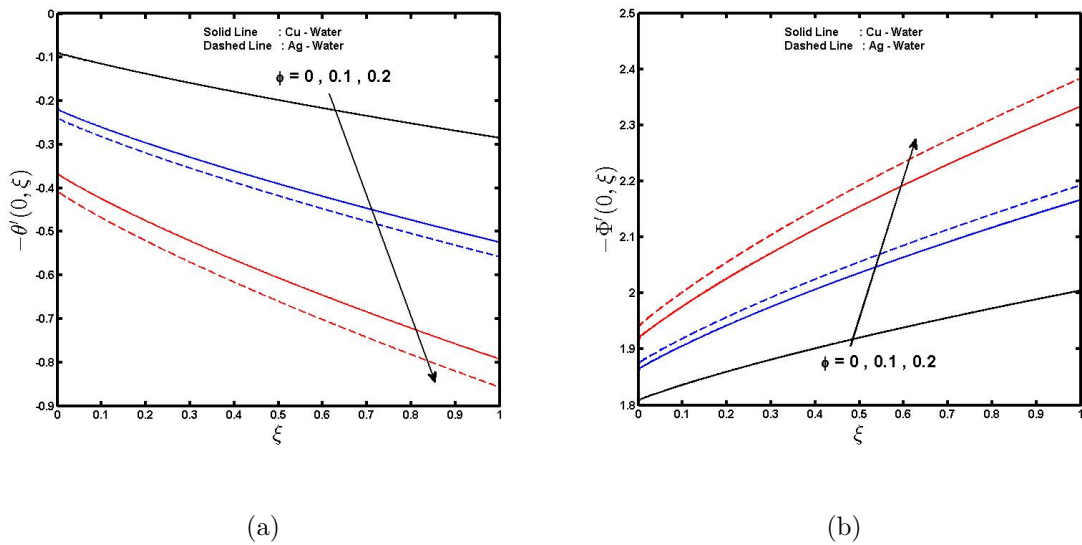


Figure 4.5: Effect of nanoparticle volume fraction ϕ on (a) the heat transfer coefficient and (b) the mass transfer coefficient for $Gr_t = 0.01$, $n = 0$, $Gr_c = 0.01$, $Nr = 10$, $Pr = 7$, $Ec = 10$, $D_f = 0.01$, $\gamma = 3$, $Sc = 1$ and $Sr = 1$.

In Figures 4.6 - 4.8, we illustrate the influence of the thermal radiation parameter on the temperature profiles, concentration profiles, skin friction coefficient, heat transfer coefficient and mass transfer coefficient. Figure 4.6(a) indicates that as η increases, the temperature profile increases correspondingly and then decreases. The results show a greater sensitivity for an Ag-water nanofluid regarding the temperature profiles, and mass transfer coefficient while Cu-water nanofluid is more sensitive for concentration profile, the skin friction coefficient and the heat transfer coefficient. These results are qualitatively similar to those obtained by Kameswaran and Sibanda [168].

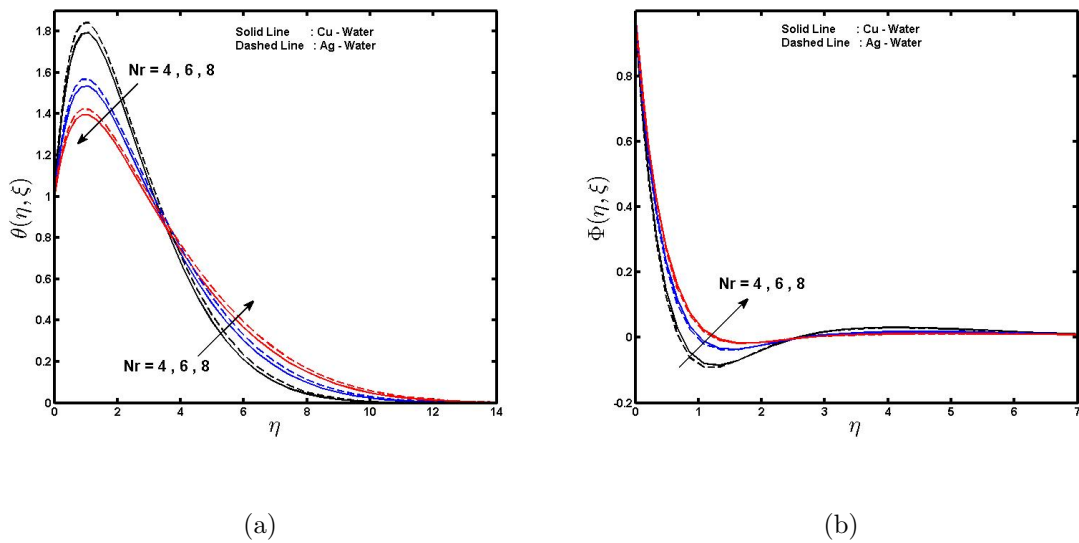


Figure 4.6: Effect of the thermal radiation parameter Nr on (a) the temperature profiles and (b) the concentration profiles for $n = 0$, $\phi = 0.3$, $Gr_t = 0.01$, $Gr_c = 0.01$, $Pr = 7$, $Ec = 10$, $D_f = 0.01$, $\gamma = 3$, $Sc = 1$, $Sr = 1$ and $\xi = 0.5$.

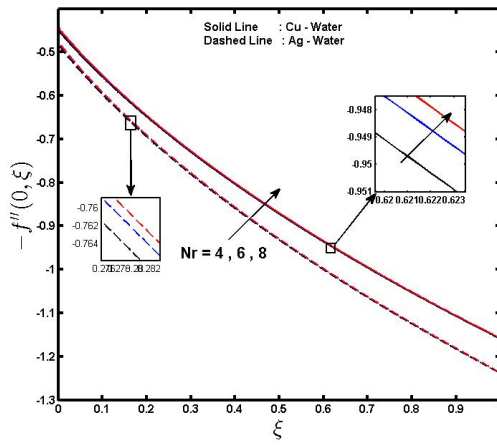


Figure 4.7: Effect of the thermal radiation parameter Nr on skin friction coefficient for $n = 0$, $\phi = 0.3$, $Gr_t = 0.01$, $Gr_c = 0.01$, $Pr = 7$, $Ec = 10$, $D_f = 0.01$, $\gamma = 3$, $Sc = 1$ and $Sr = 1$.

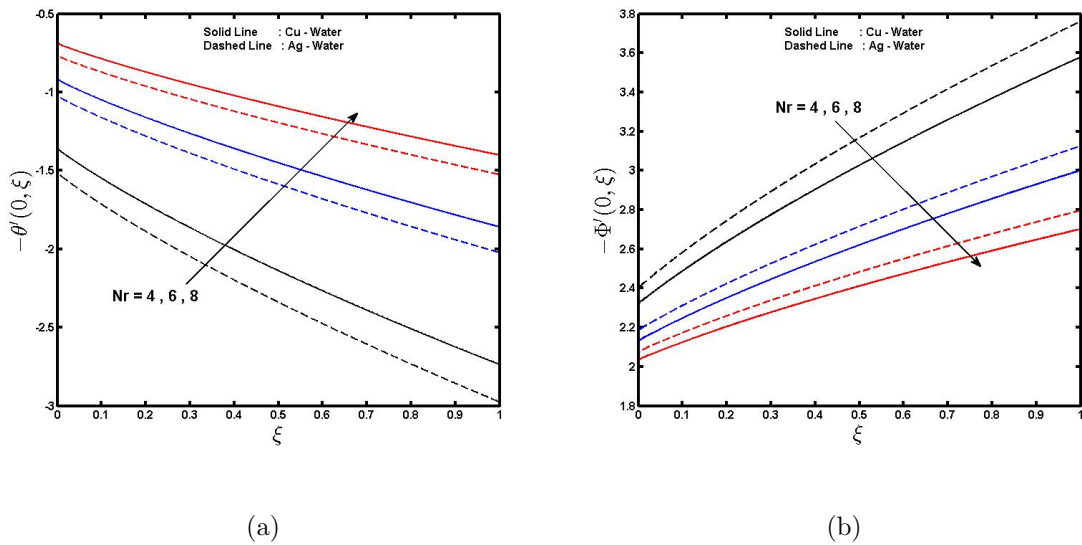


Figure 4.8: Effect of the thermal radiation parameter Nr on (a) the heat transfer coefficient and (b) the mass transfer coefficient for $n = 0$, $\phi = 0.3$, $Gr_t = 0.01$, $Gr_c = 0.01$, $Pr = 7$, $Ec = 10$, $D_f = 0.01$, $\gamma = 3$, $Sc = 1$ and $Sr = 1$.

Figures 4.9 - 4.10, show the effects of the Dufour number for different values of the nanoparticle volume fraction ($\phi = 0.3$ and 0.5) on the temperature profiles, concentration profiles, heat transfer coefficient and mass transfer coefficient, respectively. With increases in the Dufour number, the temperature profiles and mass transfer coefficient increase while the concentration profiles and heat transfer coefficient are reduced. As with the previous set of graphs, a Ag-water nanofluid show a greater sensitivity to increases in the Dufour number compared to a Cu-water nanofluid. The heat transfer coefficient is greater for a Cu-water nanofluid.

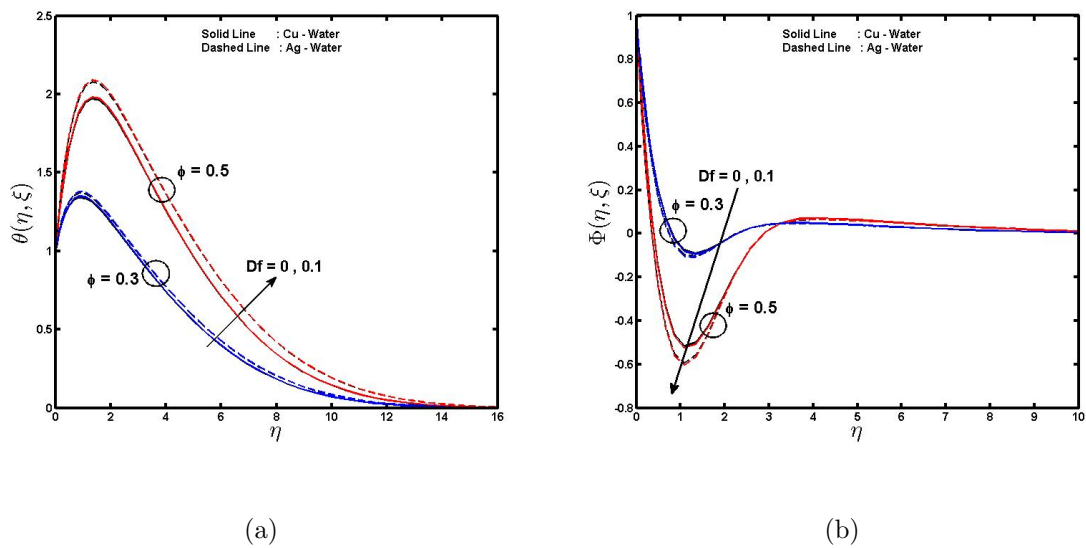


Figure 4.9: Effect of the Dufour number D_f on (a) the temperature profiles and (b) the concentration profiles with nanofluid $\phi = 0.3, 0.5$.

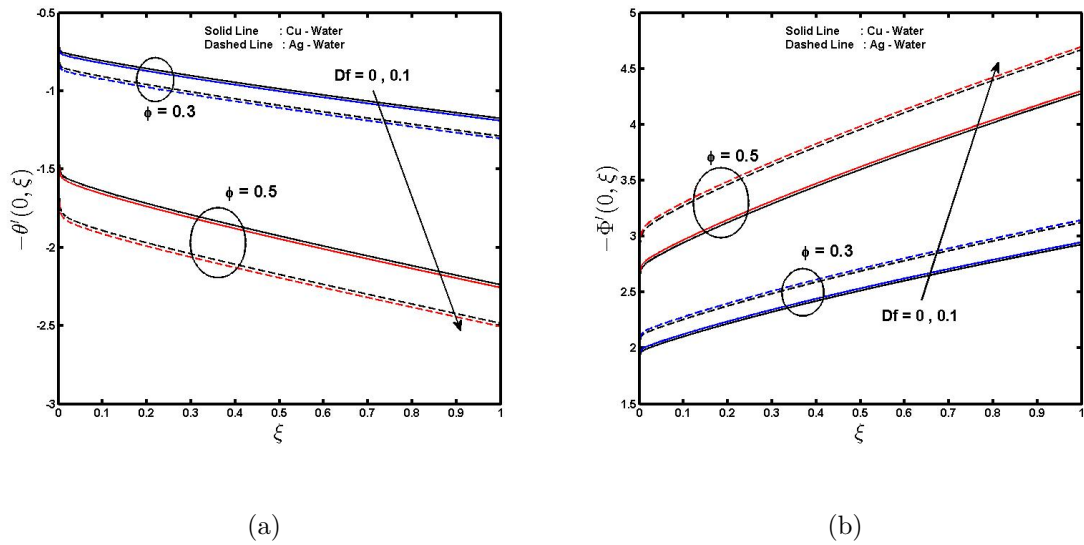


Figure 4.10: Effect of the Dufour number D_f on (a) the heat transfer coefficient and (b) the mass transfer coefficient with nanofluid $\phi = 0.3, 0.5$ for $n = 0$, $Gr_t = 0.05$, $Gr_c = 0.1$, $Pr = 7$, $Nr = 10$, $Ec = 9$, $\gamma = 0.3$, $Sc = 2$ and $Sr = 1$.

Figures 4.11 and 4.12, show the effect of the chemical reaction parameter on the concentration profiles and the mass transfer coefficient. The chemical reaction increases the rate of interfacial mass transfer. The reaction rate reduces the local solute concentration. With an increase in the chemical reaction parameter, the concentration profiles decrease whereas the mass transfer coefficient increases. The mass transfer coefficient increase as ξ increases.

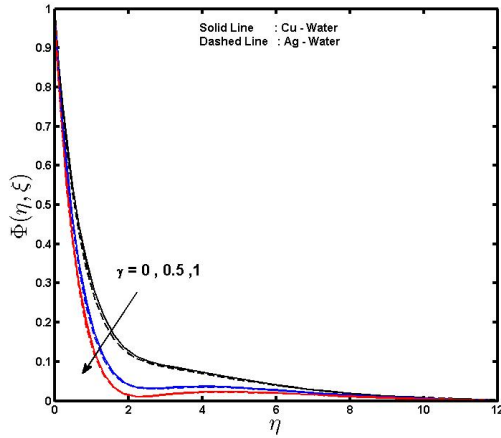


Figure 4.11: Effect of the chemical reaction parameter γ on the concentration profiles for $n = 0$, $\phi = 0.3$, $Gr_t = 0.01$, $Gr_c = 0.01$, $Pr = 7$, $Nr = 10$, $Ec = 10$, $D_f = 0.01$, $Sc = 1$, $Sr = 1$ and $\xi = 0.5$.

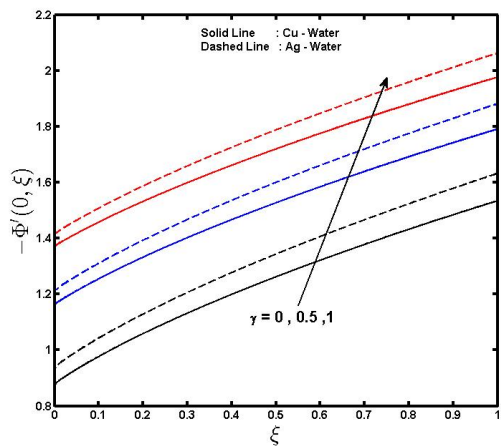


Figure 4.12: Effect of the chemical reaction parameter γ on the local Sherwood number for $n = 0$, $\phi = 0.3$, $Gr_t = 0.01$, $Gr_c = 0.01$, $Pr = 7$, $Nr = 10$, $Ec = 10$, $D_f = 0.01$, $Sc = 1$ and $Sr = 1$.

Figures 4.13 and 4.14, show the impact of the Soret number on the concentration profiles and the mass transfer coefficient. Where the concentration profiles grow less while the mass transfer coefficient increases with an increase in the Soret number. We note from Figures 4.13 and 4.14 that increasing the Soret number reduces the boundary layer thickness for the solute concentration. The mass transfer coefficient is increasing when the Soret number is positive.

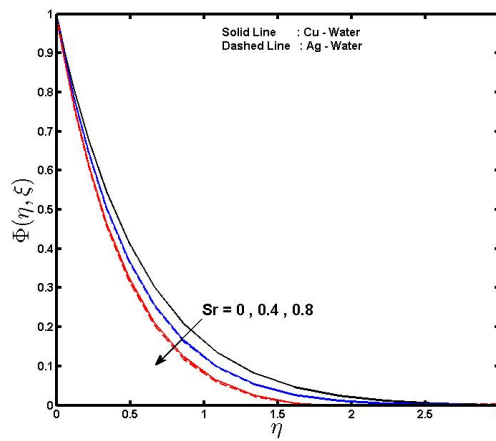


Figure 4.13: Effect of the Soret number Sr on the concentration profiles with $n = 0$, $\phi = 0.3$, $Gr_t = 0.01$, $Gr_c = 0.01$, $Pr = 7$, $Nr = 10$, $Ec = 10$, $D_f = 0.01$, $Sc = 1$, $\gamma = 3$ and $\xi = 0.5$.

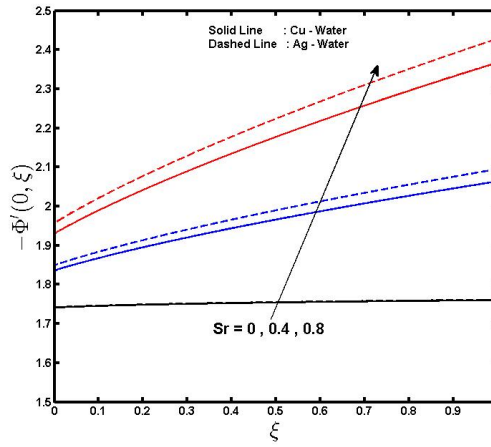


Figure 4.14: Effect of the Soret number Sr on the local Sherwood number for $n = 0$, $\phi = 0.3$, $Gr_t = 0.01$, $Gr_c = 0.01$, $Pr = 7$, $Nr = 10$, $Ec = 10$, $D_f = 0.01$, $Sc = 1$ and $\gamma = 3$.

4.6 Summary

In this chapter we have studied MHD mixed convection in a nanofluid flow due to a stretching sheet. The effects of thermal-diffusion and diffusion thermo have been investigated. The set of nonlinear governing equations and the boundary condition were reduced to coupled nonlinear partial differential equations and solved numerically using the SRM. We have qualitatively compared our present results with published results. The results show a good agreement with Yih [166]. In Chapter 5 we study unsteady MHD mixed convection in boundary layer flow with suction/injection due to a stretching/shrinking sheet.

Chapter 5

Unsteady MHD mixed convection with suction/injection due to a stretching/shrinking surface

In this Chapter, we extend the study reported in Chapter 4 to unsteady magnetohydrodynamic (MHD) mixed convection with suction/injection, heat generation, viscous dissipation, and Soret and Dufour effects. The spectral relaxation method is used to solve the non-similar differential equations that describe the flow.

5.1 Introduction

Nanofluids have been previously described in Section 2.1. Their application as a means of improving heat transfer rates in liquids has led to a considerable research interest, see collections

by Kuznetsov and Nield [169], Ishak et al. [75]. and Das [127]. The majority of the previous studies have been restricted to boundary layer flow and heat transfer in nanofluids. Following the early work by Crane [98], Khan and Pop [126] were the first to work on nanofluid flow due to stretching sheet. Other writers have studied various aspects of flow and heat transfer in a fluid of infinite extent, see for instance Chen [170] and Abo-Eldahab and El Aziz [171]. A mathematical analysis of momentum and heat transfer characteristics of the boundary layer flow of an incompressible and electrically conducting viscoelastic fluid over a linear stretching sheet was carried out by El Aziz [172]. In addition, radiation effects on the viscous flow of a nanofluid and heat transfer over a nonlinearly stretching sheet were studied by Hady et al. [173]. Theoretical studies have featured even more recently, for example, modelling unsteady boundary layer flow of a nanofluid over a permeable stretching/shrinking sheet by Bachok et al. [174]. Rohni et al. [175] developed a numerical solution for the unsteady flow over a continuously shrinking surface with wall mass suction using the nanofluid model proposed by Buongiorno [176].

The effect of magnetic field effects on nanofluids has substantial application in chemistry, physics and engineering. These include cooling of continuous filaments, in the process of drawing, annealing and thinning of copper wire. Drawing such strips through an electrically conducting fluid subject to a magnetic field can control the rate of cooling and stretching, thereby furthering the desired characteristics of the final product. Such an application of a linearly stretching sheet of incompressible viscous flow of MHD was discussed by Pavlov [177]. In other work, Jafar et al. [178] studied the effects of magnetohydrodynamic(MHD) flow and heat transfer due to a stretching/shrinking sheet with an external magnetic field, viscous dissipation and joule effects. A model for magnetohydrodynamic flow over a uniformly stretched

vertical permeable surface subject to a chemical reaction implemented by Chamkha [179]. An analysis of the effects of chemical reactions on heat and mass transfer on a magnetohydrodynamic boundary layer flow over a wedge with ohmic heating and viscous dissipation in a porous medium was carried out by Kandasamy and Palanimani [180]. The effect of a transverse magnetic field on the flow and heat transfer over a stretching surface were examined by Anjali and Thiyagarajan [181].

Despite all this prior work, there is still a lot that is known about nanofluids. In this Chapter we examine the unsteady of MHD mixed convection boundary layer with suction/injection in the presence of Soret and Dufour effects, heat generation, magnetic field, viscous dissipation and a chemical reaction. The spectral relaxation method (SRM) proposed by Motsa and his group [81; 85; 182] is used to solve the governing partial differential equations. This method has been successfully applied to other problems in fluid mechanics. In the previous two Chapters we have shown that it gives results which are comparable to those in the literature.

5.2 Governing Equations

Consider the unsteady two-dimensional laminar MHD mixed convective incompressible flow of nanofluid due to a stretching/shrinking sheet (situated $y = 0$) with velocity $u = ax$ where a is positive constant, the temperature and nanoparticles concentration at stretching surface are T_w and C_w respectively, and those of the ambient nanofluid are T_∞ and C_∞ , respectively. The x and y directions are taken in the plane of and perpendicular to the sheet, respectively, see Figure 5.1. The continuity, momentum, energy and concentration equation of an unsteady,

incompressible nanofluid boundary layer flow, as given by Suali et al. [183] and Yang [184], can be written as

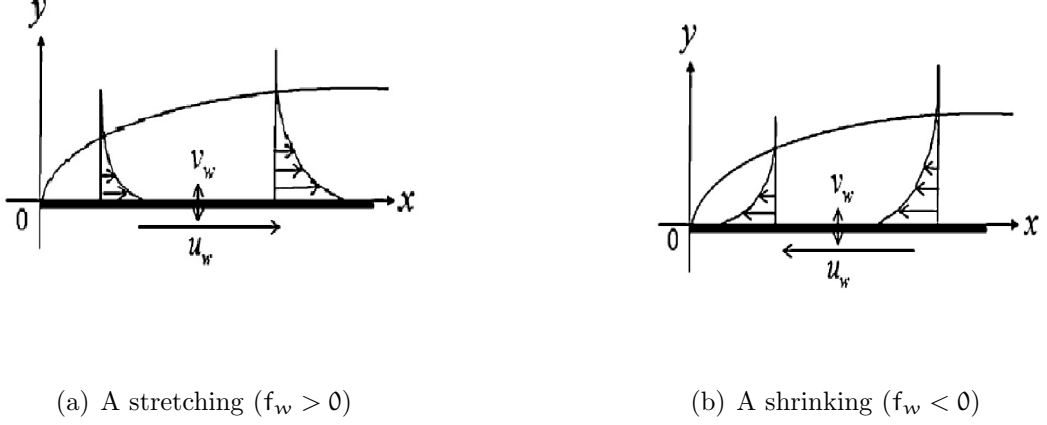


Figure 5.1: Schematic diagram of the flow geometry.

$$\frac{\partial u}{\partial x} + \frac{\partial v}{\partial y} = 0, \quad (5.1)$$

$$\frac{\partial u}{\partial t} + u \frac{\partial u}{\partial x} + v \frac{\partial u}{\partial y} = -\frac{1}{\rho_{nf}} \frac{\partial p}{\partial x} + \frac{\mu_{nf}}{\rho_{nf}} \frac{\partial^2 u}{\partial y^2} + g\beta_T(T - T_\infty) + g\beta_C(C - C_\infty) - \frac{\sigma B_0^2}{\rho_{nf}} u, \quad (5.2)$$

$$\frac{\partial T}{\partial t} + u \frac{\partial T}{\partial x} + v \frac{\partial T}{\partial y} = \alpha_{nf} \frac{\partial^2 T}{\partial y^2} + \frac{Q}{(\rho c_p)_{nf}} (T - T_\infty) + \frac{\rho_f D_m K_T}{C_s (\rho c_p)_{nf}} \frac{\partial^2 C}{\partial y^2}, \quad (5.3)$$

$$\frac{\partial C}{\partial t} + u \frac{\partial C}{\partial x} + v \frac{\partial C}{\partial y} = D_m \frac{\partial^2 C}{\partial y^2} + \frac{D_m K_m}{T_m} \frac{\partial^2 T}{\partial y^2} - R(C - C_\infty), \quad (5.4)$$

where x and y are the coordinates measured along and perpendicular to the sheet, consequently, where t , u and v are the time and the fluid velocity and normal velocity components in the x and y orientations respectively. ν_{nf} is the nanofluid kinematic viscosity, p is the pressure, ρ_{nf} nanofluid density, σ an electrical conductivity, B_0 is the uniform magnetic field in the y -direction, μ_{nf} is the effective dynamic viscosity of the nanofluid, g is gravitational acceleration, β_T is volumetric thermal expansion coefficient, β_C is volumetric solutal expansion coefficient, T is temperature of fluid in the boundary layer, C is fluid solutal concentration, α_{nf} is the thermal diffusivity of the nanofluid, $(\rho c_p)_{nf}$ is the nanofluid heat capacitance, Q is the volumetric rate of heat generation, ρ_f is the density of the base fluid, D_m is the mass dif-

fusivity of the concentration, K_T is thermal diffusion ratio, C_s is concentration susceptibility, $(cp)_{nf}$ specific heat of fluid at constant pressure, T_m is mean fluid temperature and R is the chemical reaction parameter,

subject to the boundary conditions are

$$\begin{aligned} t \geq 0 : u = U_w = ax, v = v_w, T = T_w, C = C_w \quad \text{at } y = 0, \\ t \geq 0 : u = U_\infty = a_\infty x, v = 0, T = T_\infty, C = C_\infty \quad \text{as } y \rightarrow \infty. \end{aligned} \quad (5.5)$$

The initial conditions are

$$t < 0 : u(x, y, t) = 0, v(x, y, t) = 0, T(x, y, t) = T_w, C(x, y, t) = C_w, \quad \forall x, y, \quad (5.6)$$

where a and $a_\infty (> 0)$ are the stretching/shrinking rate of the sheet and stagnation flow rate parameters, respectively, with $a < 0$ for shrinking, $a > 0$ for a stretching. Here v_w is a prescribed suction velocity ($v_w < 0$) or blowing velocity ($v_w > 0$). In case of free - stream the momentum equation (5.2) becomes

$$U_\infty \frac{dU_\infty}{dx} = -\frac{1}{\rho_{nf}} \frac{\partial p}{\partial x} - \frac{\sigma B_0^2}{\rho_{nf}} U_\infty, \quad (5.7)$$

substituting (5.7) in (5.2) the momentum equation written as

$$\begin{aligned} \frac{\partial u}{\partial t} + u \frac{\partial u}{\partial x} + v \frac{\partial u}{\partial y} = \nu_{nf} \frac{\partial^2 u}{\partial y^2} + U_\infty \frac{dU_\infty}{dx} + (U_\infty - u) \frac{\sigma B_0^2}{\rho_{nf}} + g\beta_T(T - T_\infty) \\ + g\beta_C(C - C_\infty). \end{aligned} \quad (5.8)$$

The effective dynamic viscosity of the nanofluid was given by Brinkman [137] as

$$\mu_{nf} = \frac{\mu_f}{(1 - \phi)^{2.5}}, \quad (5.9)$$

where ϕ is the solid volume fraction of nanoparticles, μ_f is the dynamic viscosity of the base fluid. In equations (5.1) - (5.4).

$$\begin{aligned}
(\rho c_p)_{nf} &= (1 - \phi)(\rho c_p)_f + \phi(\rho c_p)_s \\
\rho_{nf} &= (1 - \phi)\rho_f + \phi\rho_s \quad , \quad \nu_{nf} = \frac{\mu_{nf}}{\rho_{nf}} \\
\alpha_{nf} &= \frac{k_{nf}}{(\rho c_p)_{nf}} \quad , \quad \frac{k_{nf}}{k_f} = \frac{(k_s + k_f) - 2\phi(k_f - k_s)}{(k_s + k_f) + \phi(k_f - k_s)}.
\end{aligned} \tag{5.10}$$

where k_{nf} is the thermal conductivity of the nanofluid, k_f and k_s are the thermal conductivities of the fluid and of the solid fractions, respectively, and ρ_s is the density of the solid fractions, $(\rho c_p)_f$ and $(\rho c_p)_s$ are the heat capacity of base fluid and effective heat capacity of nanoparticle respectively, k_{nf} is the thermal conductivity of the nanofluid.

The continuity equation (5.1) is satisfied by introducing a stream function $\psi(x, y)$ such that

$$\mathbf{u} = \frac{\partial \psi}{\partial y}, \quad \mathbf{v} = -\frac{\partial \psi}{\partial x}. \tag{5.11}$$

We introduce the following non-dimensional variables, see Liao [139]

$$\eta = \left[\frac{\mathbf{a}_\infty}{\nu_f \xi} \right]^{\frac{1}{2}} y, \quad \xi = 1 - \exp(-\tau), \quad \tau = \mathbf{a}_\infty t, \quad \psi = [\mathbf{a}_\infty \nu_f \xi]^{\frac{1}{2}} x f(\xi, \eta), \tag{5.12}$$

$$\theta(\xi, \eta) = \frac{T - T_\infty}{T_w - T_\infty}, \quad \Phi(\xi, \eta) = \frac{C - C_\infty}{C_w - C_\infty}, \tag{5.13}$$

where η and ξ are similarity variables, $f(\xi, \eta)$ is the dimensionless stream function, $\theta(\xi, \eta)$ is the dimensionless temperature and $\Phi(\xi, \eta)$ is the dimensionless solute concentration. By using (5.12) and (5.13), the governing equations (5.3), (5.4) and (5.8) along with the boundary

conditions (5.5) are reduced to the following two-point boundary value problem

$$f''' + \phi_1 \left[\frac{\eta}{2}(1 - \xi)f'' + \xi (ff'' - f'^2 + 1 + \text{Ha}^2(1 - f') + \text{Gr}_t\theta + \text{Gr}_c\Phi) \right] = \phi_1\xi(1 - \xi)\frac{\partial f'}{\partial \xi}, \quad (5.14)$$

$$\theta'' + \frac{k_f}{k_{nf}} \text{Pr}\phi_2 \left[\frac{\eta}{2}(1 - \xi)\theta' + \xi (f\theta' + \delta\theta) + \frac{D_f}{\phi_2}\Phi'' \right] = \frac{k_f}{k_{nf}} \text{Pr}\phi_2\xi(1 - \xi)\frac{\partial \theta}{\partial \xi}, \quad (5.15)$$

$$\Phi'' + \text{Sc} \left[\frac{\eta}{2}(1 - \xi)\Phi' + \xi (f\Phi' - \gamma\Phi) + \text{Sr}\theta'' \right] = \text{Sc}\xi(1 - \xi)\frac{\partial \Phi}{\partial \xi}, \quad (5.16)$$

subject to the boundary conditions

$$f(\xi, 0) = f_w, \quad f'(\xi, 0) = \lambda, \quad \theta(\xi, 0) = 1, \quad \Phi(\xi, 0) = 1 \quad \text{at } \eta = 0, \quad \xi \geq 0,$$

$$f'(\xi, \infty) = 1, \quad \theta(\xi, \infty) = 0, \quad \Phi(\xi, \infty) = 0 \quad \text{as } \eta \rightarrow \infty, \quad \xi \geq 0 \quad (5.17)$$

The prime denotes differentiation with respect to η , while $\alpha_f = k_f/(\rho c_p)_f$ and $\nu_f = \mu_f/\rho_f$ are the thermal diffusivity and kinetic viscosity of the base fluid, respectively. Other non-dimensional parameters appearing in equations (5.14) - (5.16) are the Hartmann number Ha , the local temperature Grashof number Gr_t , the local concentration Grashof number Gr_c , the Prandtl number Pr , the dimensionless heat generation parameter δ , Dufour number D_f , Schmidt number Sc , scaled chemical reaction parameter γ and Soret number Sr . These are defined as

$$\begin{aligned} \text{Ha}^2 &= \frac{\sigma B_0^2}{\alpha_\infty \rho_{nf}}, \quad \text{Gr}_t = \frac{g\beta_T(T_w - T_\infty)}{\alpha_\infty^2 x}, \quad \text{Gr}_c = \frac{g\beta_C(C_w - C_\infty)}{\alpha_\infty^2 x}, \quad \text{Pr} = \frac{\nu_f}{\alpha_f}, \quad \delta = \frac{Q}{\alpha_\infty(\rho C_p)_{nf}}, \\ D_f &= \frac{D_m K_T (C_w - C_\infty)}{C_s (C_p)_f \nu_f (T_w - T_\infty)}, \quad \text{Sc} = \frac{\nu_f}{D_m}, \quad \gamma = \frac{R}{\alpha_\infty}, \quad \text{Sr} = \frac{D_m K_T (T_w - T_\infty)}{T_m \nu_f (C_w - C_\infty)}. \end{aligned} \quad (5.18)$$

The nanoparticle volume fractions ϕ_1 and ϕ_2 are defined as

$$\phi_1 = (1 - \phi)^{2.5} \left[1 - \phi + \phi \left(\frac{\rho_s}{\rho_f} \right) \right], \quad \phi_2 = \left[1 - \phi + \phi \left(\frac{(\rho c)_s}{(\rho c)_f} \right) \right], \quad (5.19)$$

In equations (5.17), $f_w = -v_w/\sqrt{a_\infty \nu_f \xi}$ represents suction ($f_w > 0$) or injection ($f_w < 0$) and $\lambda(= a/a_\infty)$ is the stretching/shrinking parameter.

5.3 Skin friction, heat and mass transfer coefficients

The skin friction coefficient C_f , the local Nusselt number Nu_x and the local Sherwood number Sh_x characterize the surface drag, wall heat and mass transfer rates, respectively.

The shearing stress at the surface of the wall τ_w is given by

$$\tau_w = -\mu_{nf} \left(\frac{\partial u}{\partial y} \right)_{y=0} = -\frac{U_\infty \mu_f}{(1-\phi)^{2.5} x} \sqrt{\frac{U_\infty x}{\nu_f \xi}} f''(0, \xi), \quad (5.20)$$

where μ_{nf} is the coefficient of viscosity.

The skin friction coefficient is defined as

$$C_{fx} = \frac{2\tau_w}{\rho_f U_\infty^2}, \quad (5.21)$$

and using equation (5.20) in Equation (5.21) we obtain

$$\frac{1}{2} (1-\phi)^{2.5} C_{fx} = -\xi^{-\frac{1}{2}} Re_x^{-\frac{1}{2}} f''(0, \xi). \quad (5.22)$$

The heat transfer rate at the surface flux at the wall is given by

$$q_w = -k_{nf} \left(\frac{\partial T}{\partial y} \right)_{y=0} = -k_{nf} \frac{(T_w - T_\infty)}{x} \sqrt{\frac{U_\infty x}{\nu_f \xi}} \theta'(0, \xi), \quad (5.23)$$

where k_{nf} is the thermal conductivity of the nanofluid. The local Nusselt number (heat transfer coefficient) is defined as

$$Nu_x = \frac{x q_w}{k_f (T_w - T_\infty)}. \quad (5.24)$$

Using equation (5.23) in equation (5.24), the dimensionless wall heat transfer rate is obtained as

$$\left(\frac{k_f}{k_{nf}}\right) Nu_x = -\xi^{-\frac{1}{2}} Re_x^{\frac{1}{2}} \theta'(0, \xi). \quad (5.25)$$

The mass flux at the wall surface is given by

$$q_m = -D \left(\frac{\partial C}{\partial y}\right)_{y=0} = -D \frac{(C_w - C_\infty)}{x} \sqrt{\frac{U_\infty x}{\nu_f \xi}} \Phi'(0, \xi), \quad (5.26)$$

and the local Sherwood number (mass transfer coefficient) is defined as

$$Sh_x = \frac{x q_m}{D(C_w - C_\infty)}. \quad (5.27)$$

The dimensionless wall mass transfer rate is obtained as

$$Sh_x = -\xi^{-\frac{1}{2}} Re_x^{\frac{1}{2}} \Phi'(0, \xi). \quad (5.28)$$

Where Re_x represents the local Reynolds number defined as

$$Re_x = \frac{x u_\infty}{\nu_f}. \quad (5.29)$$

5.4 Cases of special interest

In this section we can obtain some particular cases of of equations (5.16) - (5.14) where the equations reduce to ordinary differential equations.

Case(1): for initial steady-state flow

For steady flow when $\phi = 0$ (regular fluid) we have $\xi = 0$ corresponding to $t = 0$, thus $f(\eta, 0) = f(\eta)$, $\theta(\eta, 0) = \theta(\eta)$ and $\Phi(\eta, 0) = \Phi(\eta)$. In this case equations (5.14) - (5.16) reduce to

$$f''' + \frac{1}{2}\phi_1\eta f'' = 0. \quad (5.30)$$

$$\theta'' + \frac{1}{2}\frac{k_f}{k_{nf}}Pr \phi_2 \eta \theta' + \frac{k_f}{k_{nf}}PrD_f \Phi'' = 0. \quad (5.31)$$

$$\Phi'' + \frac{1}{2}Sc \eta \Phi' + Sc Sr \theta'' = 0. \quad (5.32)$$

We cannot obtain the exact solutions of these equations because of their boundary conditions.

Case(2):final steady state flow

In this case, we have $\xi = 1$ when $t \rightarrow \infty$, corresponding to that $f(\eta, 1) = f(\eta)$, $\theta(\eta, 1) = \theta(\eta)$ and $\Phi(\eta, 1) = \Phi(\eta)$. Equations (5.14) - (5.16) reduce to the following forms

$$f''' + ff'' - f'^2 + 1 + Ha^2(1 - f') + GR_t\theta + Gr_c\Phi = 0, \quad (5.33)$$

$$\theta'' + \frac{k_f}{k_{nf}}Pr \phi_2(f \theta' + \delta \theta) + \frac{k_f}{k_{nf}}PrD_f \Phi'' = 0, \quad (5.34)$$

$$\Phi'' + Sc (f\Phi' - \gamma \Phi + Sr \theta'') = 0. \quad (5.35)$$

The two cases above are subject to the boundary conditions (5.17). In this Chapter the equations will be solved using the SRM.

5.5 Results and Discussion

The system of partial differential equations (5.14) - (5.16) subject to boundary conditions (5.17) was solved numerically using the spectral relaxation method (SRM). We considered both Cu-water and Ag-water nanofluids. The thermophysical properties of the nanofluids used in this dissertation are given in Table 3.1. In order to determine the accuracy of our

numerical results, the present results for the skin friction coefficient were compared with the results previously published by Jafar et al. [178], Wang and Mujumdar [185] and Suali et al. [183], as shown in Tables 5.1 to 5.3. The results in the three tables show that our values for the coefficient $f''(0, 1)$ for different parameter values, are all in very good agreement with those in the literature.

Table 5.1: Comparison of $f''(0, 1)$ for various values of λ when $\text{Ha} = \text{Gr}_t = \text{Gr}_c = \delta = \text{D}_f = \text{Sc} = \text{Sr} = \gamma = 0$, $\text{Pr} = 1$ and $\phi = 0$ with $\xi = 1$ (final steady state).

	Wang and Mujumdar [185]	Jafar et al.[178]	Present result (SRM)
λ	$f''(0, 1)$	$f''(0, 1)$	$f''(0, 1)$
0	1.232588	1.2326	1.23258
0.1	1.14656	1.1466	1.14655
0.2	1.05113	1.0511	1.05112
0.5	0.71330	0.7133	0.71328
1	0.00000	0.00000	0.00000
2	-1.88731	-1.8873	-1.88690
5	-10.26475	-10.2648	-10.24531

Table 5.2: Comparison of $f''(0, 1)$ for various values of λ when $\text{Ha} = \text{Gr}_t = \text{Gr}_c = \delta = \text{D}_f = \text{Sc} = \text{Sr} = \gamma = 0$, $\text{Pr} = 1$ and $\phi = 0$ with $\xi = 1$.

λ	-0.25	-0.5	-0.75	-1
Wang and Mujumdar [185]	1.40224	1.49576	1.48930	1.32882
Jafar et al.[178]	1.4022	1.4957	1.4893	1.3288
Present result (SRM)	1.40224	1.49565	1.48913	1.32795

Table 5.3: Comparison of $f''(0, 1)$ for various values of λ for the both stretching/shrinking sheet when $\text{Ha} = \text{Gr}_t = \text{Gr}_c = \delta = \text{D}_f = \text{Sc} = \text{Sr} = \gamma = 0$, $\text{Pr} = 1$ and $\phi = 0$ with $\xi = 1$.

λ	Suali et al. [183]	Present result (SRM)
	$f''(0, 1)$	$f''(0, 1)$
4	-7.086378	-7.086378
3	-4.276545	-4.276542
0.2	1.051130	1.051130
0.1	1.146561	1.146561
-0.2	1.373886	1.373886
-0.5	1.495672	1.495670

The effect of the nanoparticle volume fraction on the nanofluid velocity profiles, temperature, concentration profiles, skin friction, the wall heat and mass transfer rates respectively are

shown in Figures 5.2 - 5.5 for both Cu-water and Ag-water nanofluids. As nanoparticle volume fraction increases, the velocity, solute concentration profiles and the wall heat transfer rates decrease while the temperature profile, skin friction and the wall mass rate increase. The findings are in agreement with those of Vajravelu et al. [145]. Increasing the nanoparticle volume fraction increases the thermal conductivity of the nanofluid resulting in a thickening of the thermal boundary layer while the momentum boundary layer thickness decreases. We also observe that for a Ag-water nanofluid the axial velocity is comparatively higher than that of a Cu-water nanofluid. We further note that the thermal conductivity of Ag-water nanofluid is more than that of Cu-water nanofluid. The temperature distribution in a Ag-water nanofluid is higher than that of a Cu-water nanofluid. The boundary layer thickness decreases with the nanoparticle volume fraction in both cases of the nanofluids. The results show a good agreement for tangential profiles and temperature profiles with Kameswaran et al.[147]. When the nanoparticle volume fraction increases, the solute boundary layer thickness decreases. In the same vein we note that the momentum boundary layer thickness increases. The findings are similar to those obtained by Hamad and Pop [186]. Figure 5.4 shows that the skin friction coefficient decreases monotonically with increasing values of the dimensionless variable ξ . The maximum value of the skin friction in the case of a Cu-water nanofluid is achieved at a smaller value of ξ compared to a Ag-water nanofluid. Furthermore, the Ag-water nanofluid shows less drag as compared to a Cu-water nanofluid. The wall heat transfer and the mass transfer rates are shown as a functions of ξ in Figures 5.5(a) and (b) respectively. The wall heat transfer rate decreases while the opposite is true for the wall mass transfer rate. The Cu-water nanofluid exhibits a higher wall heat transfer rate as compared to an Ag-water nanofluid. Thus the presence of nanoparticles tends to increase the wall heat transfer rate and to reduce the wall mass transfer rates with increasing values of ξ , in accordance with results reported by Affy

[141].

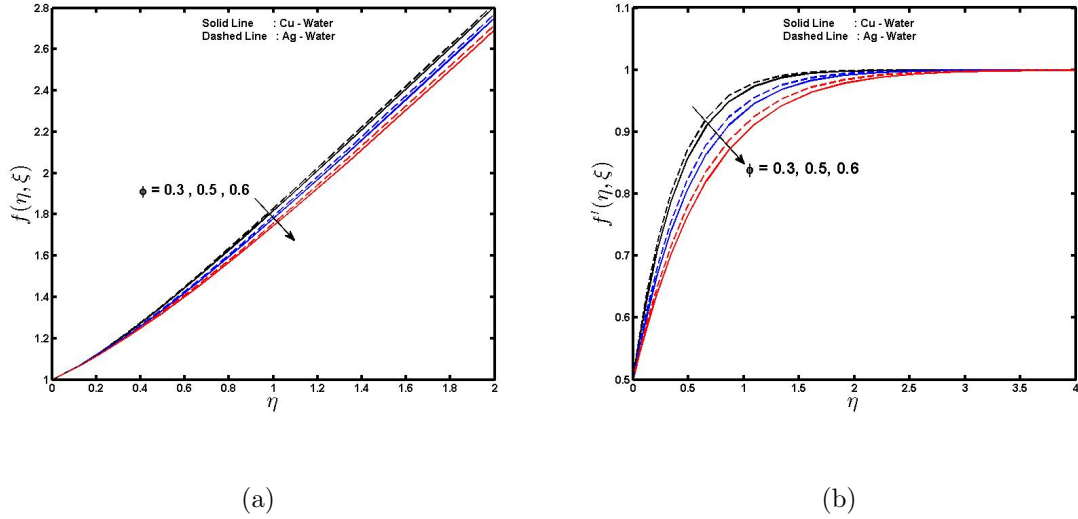


Figure 5.2: Effect of the nanoparticle volume fraction ϕ on (a) the normal velocity and (b) tangential Velocity profiles respectively, for $D_f = 0.01$, $\lambda = 0.5$, $Gr_t = 0.01$, $Gr_c = 0.01$, $Ha = 2$, $\delta = 0.1$, $Sc = 1$, $Sr = 1$, $f_w = 1$, $\gamma = 0.1$ and $\xi = 0.5$.

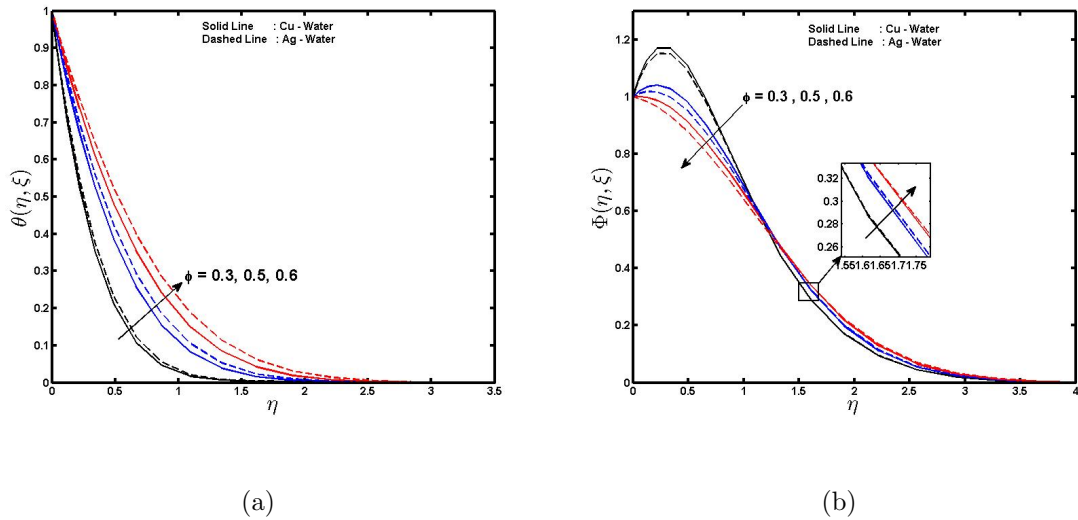


Figure 5.3: Effect of the nanoparticle volume fraction ϕ on (a) the temperature profiles and (b) the concentration profiles for $D_f = 0.01$, $\lambda = 0.5$, $Gr_t = 0.01$, $Gr_c = 0.01$, $Ha = 2$, $\delta = 0.1$, $Sc = 1$, $Sr = 1$, $f_w = 1$, $\gamma = 0.1$ and $\xi = 0.5$.

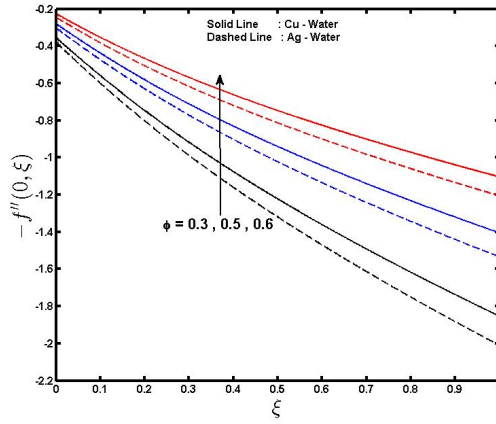


Figure 5.4: Effect of the nanoparticle volume fraction ϕ on the skin friction coefficient for $D_f = 0.01$, $\lambda = 0.5$, $Gr_t = 0.01$, $Gr_c = 0.01$, $Ha = 2$, $\delta = 0.1$, $Sc = 1$, $Sr = 1$, $f_w = 1$ and $\gamma = 0.1$.

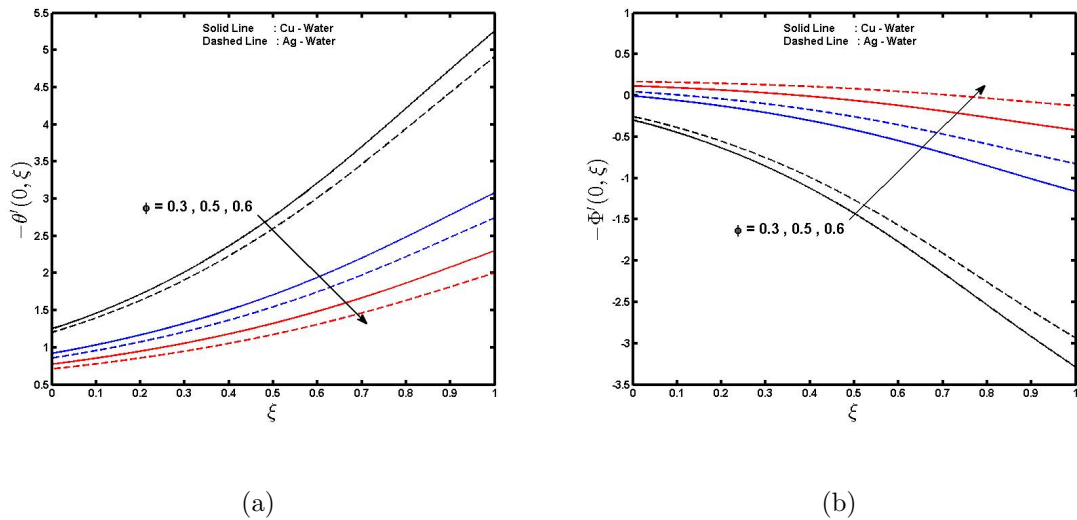


Figure 5.5: Effect of the nanoparticle volume fraction ϕ on (a) the heat transfer coefficient and (b) the mass transfer coefficient for $D_f = 0.01$, $\lambda = 0.5$, $Gr_t = 0.01$, $Gr_c = 0.01$, $Ha = 2$, $\delta = 0.1$, $Sc = 1$, $Sr = 1$, $f_w = 1$ and $\gamma = 0.1$.

Figures 5.6 to 5.8 show the nanofluid velocity, skin friction coefficient, the wall heat and mass transfer rates, respectively, for various values of the Harmann number Ha in the case of Cu-water nanofluid and Ag-water nanofluid. The effect of the Harmann number is to increase the nanofluid velocity and the wall heat transfer rate whilst reducing the skin friction coefficient and the wall mass transfer rate. The momentum boundary layer thickness increases with increases in the Harmann number. In the case of a Cu-water nanofluid the velocity is relatively less than that in an Ag-water nanofluid. Figure 5.7 shows the skin friction coefficient as a function of the dimensionless variable ξ . It is clear that the value of skin friction reduces when ξ increases. We see that the Cu-water nanofluid exhibits a higher drag on the flow as compared to the Ag-water nanofluid. Figures 5.8 (a) and (b) show that the wall heat and mass transfer rates for different values of the Hartmann number. The wall heat transfer rate increases with ξ in the case of an Ag-water nanofluid although it is less than that of a Cu-water nanofluid. Further, the values of the wall mass transfer rate increase up to certain value of ξ before decreasing.

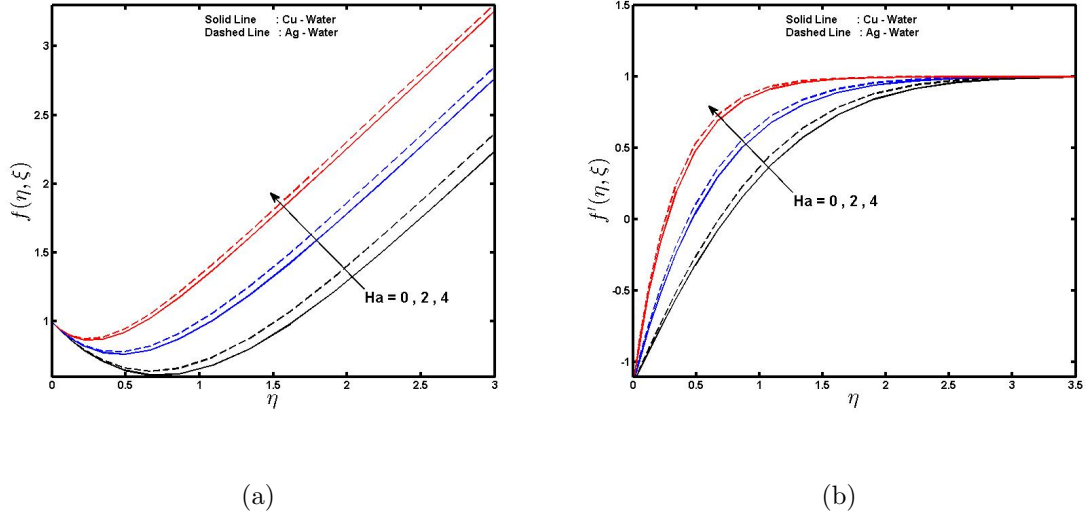


Figure 5.6: Effect of the Hartmann number Ha on (a) axial velocity and (b) tangential velocity profiles respectively, for $D_f = 0.01$, $\phi = 0.3$, $Gr_t = 0.01$, $Gr_c = 0.01$, $f_w = 1$, $\delta = 0.1$, $Sc = 1$, $Sr = 1$, $\lambda = -1.15$, $\gamma = 3$ and $\xi = 0.5$.

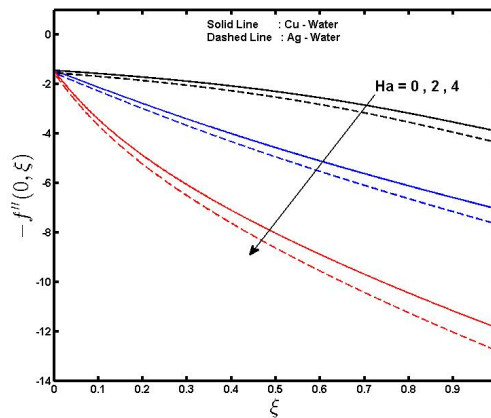


Figure 5.7: Effect of the Hartmann number on the skin friction coefficient for $D_f = 0.01$, $\phi = 0.3$, $Gr_t = 0.01$, $Gr_c = 0.01$, $f_w = 1$, $\delta = 0.1$, $Sc = 1$, $Sr = 1$, $\lambda = -1.15$ and $\gamma = 3$.

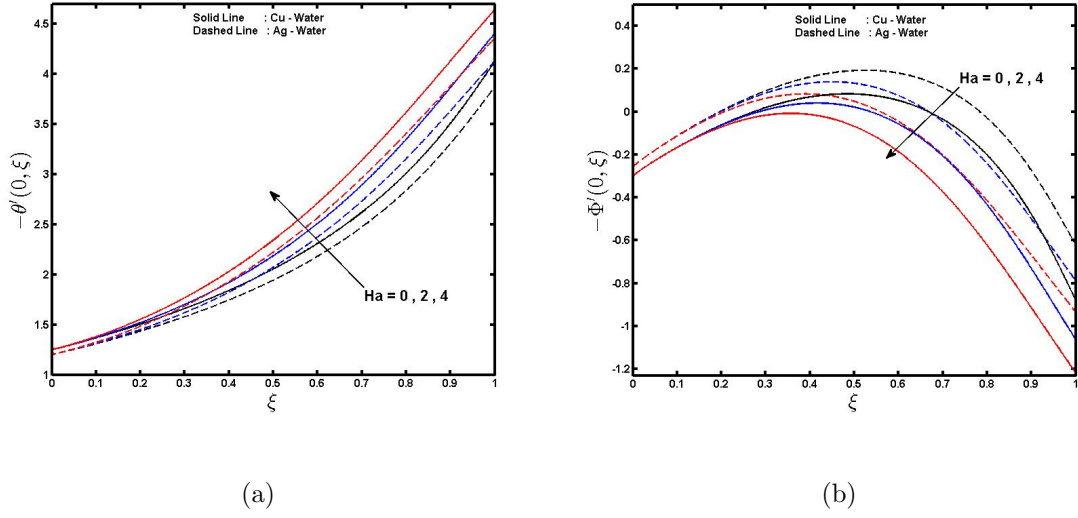


Figure 5.8: Effect of the Hartmann number on (a) the heat transfer coefficient and (b) the mass transfer coefficient when $D_f = 0.01$, $\phi = 0.3$, $Gr_t = 0.01$, $Gr_c = 0.01$, $f_w = 1$, $\delta = 0.1$, $Sc = 1$, $Sr = 1$, $\lambda = -1.15$ and $\gamma = 3$.

The effect of suction ($f_w > 0$) and injection ($f_w < 0$) parameters on the nanofluid velocity, temperature profile, concentration profile, skin friction coefficient, the wall heat and mass transfer rates are shown in Figures 5.9 - 5.12. It can be seen that ncreasing the suction/injection parameter increases the nanofluid velocity profiles and the wall heat transfer rate, while the temperature profile, skin friction coefficient and the wall mass transfer rate decrease. This means that the effect of the suction parameter is to increase the concentration profiles at the surface. Beyond this critical η value, the concentration profiles decrease with increasing injection parameter f_w . The momentum boundary layer thickness increases. In the case of a Cu-water nanofluid the increase is less than that observed for an Ag-water nanofluid. The results show a good agreement with those obtained by Motsa and Shateyi [187]. Figure 5.11 shows that the skin friction coefficient decreases with increasing ξ . Which indicates that the axial distribution of the wall heat and mass transfer rates are shown in Figures 5.12 (a) and (b), respectively, where we can see that the wall heat transfer rate increased as ξ increases.

This increase is higher in the case of a Cu-water nanofluid than that in a Ag-water nanofluid. The results reported with respect to the wall mass transfer rate hold for both nanofluids. When the suction/injection parameter $f_w = -1$, the Ag-water nanofluid values are higher than those of a Cu-water nanofluid up to a certain value of ξ , before this critical value, those for an Ag-water nanofluid are less than those of a Cu-water nanofluid, see Figure 5.12(b). For the values of the parameters, see Afify [141] and Chamkha and El-Kabeir [67]. These results show good agreement with those obtained by Alam and Mollah [148], see Figure 5.9.

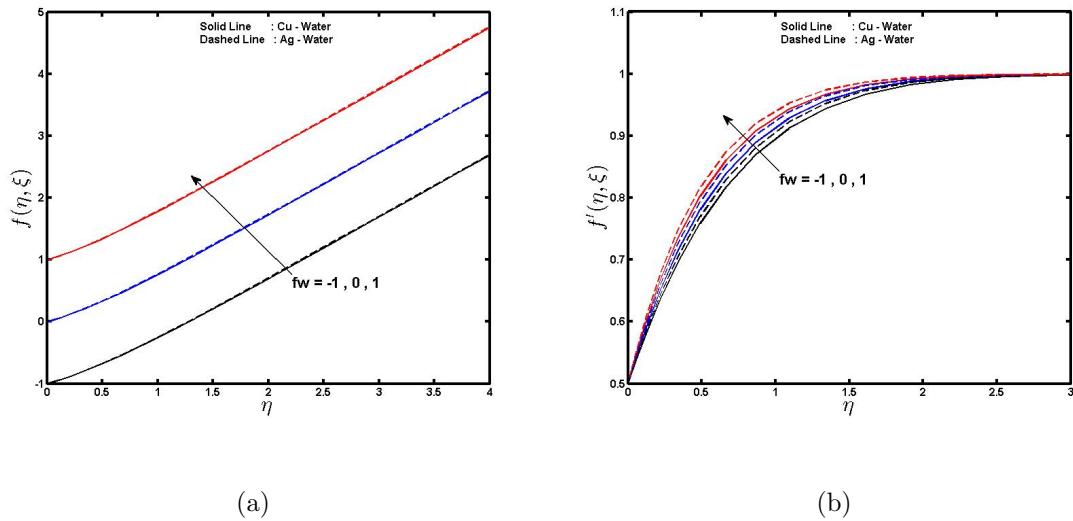


Figure 5.9: Effect of suction/injection parameter f_w on (a) axial velocity and (b) tangential velocity profiles respectively, when $D_f = 0.01$, $\phi = 0.3$, $Gr_t = 0.01$, $Gr_c = 0.01$, $Ha = 2$, $\delta = 0.2$, $Sc = 1$, $Sr = 1$, $\lambda = 0.5$, $\gamma = 3$ and $\xi = 0.5$.

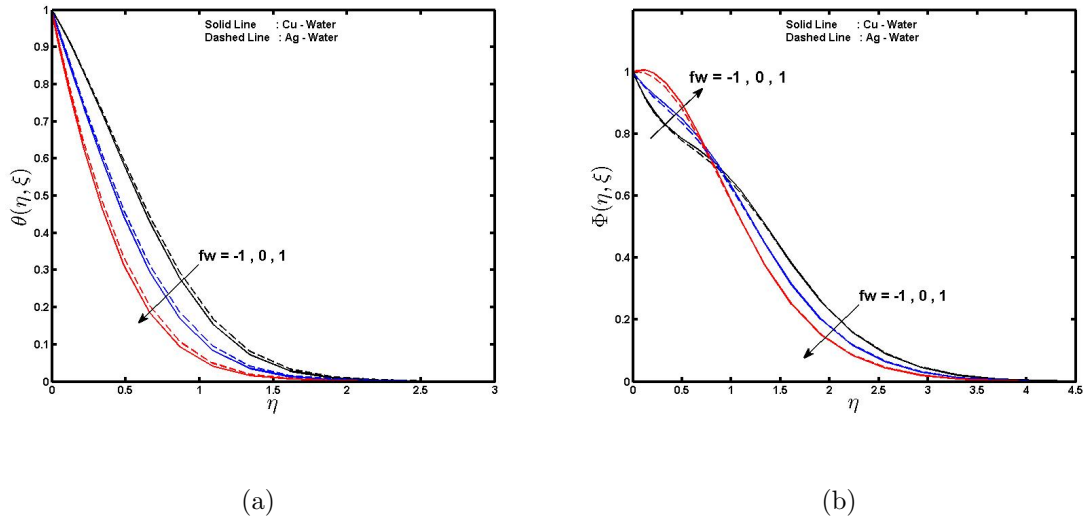


Figure 5.10: Effect of suction/injection parameter f_w on (a) the temperature profiles and (b) the concentration profiles when $D_f = 0.01$, $\phi = 0.3$, $Gr_t = 0.01$, $Gr_c = 0.01$, $Ha = 2$, $\delta = 0.2$, $Sc = 1$, $Sr = 1$, $\lambda = 0.5$, $\gamma = 3$ and $\xi = 0.5$.

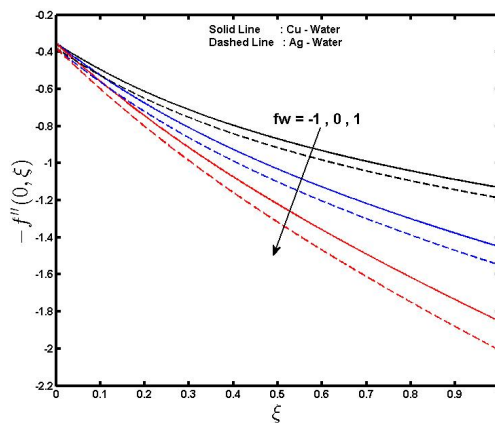


Figure 5.11: Effect of suction/injection parameter f_w on the skin friction coefficient for $D_f = 0.01$, $\phi = 0.3$, $Gr_t = 0.01$, $Gr_c = 0.01$, $Ha = 2$, $\delta = 0.2$, $Sc = 1$, $Sr = 1$, $\lambda = 0.5$ and $\gamma = 3$.

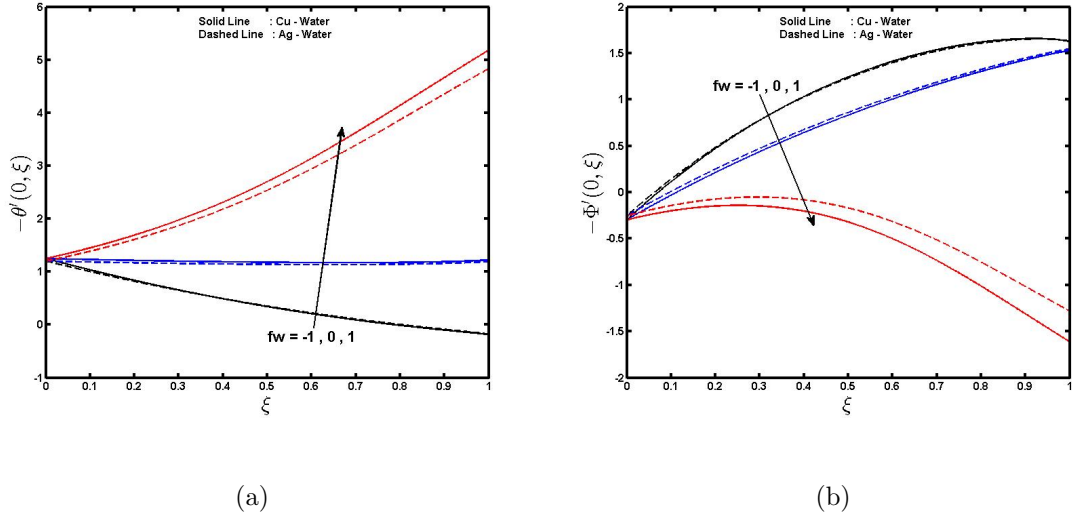
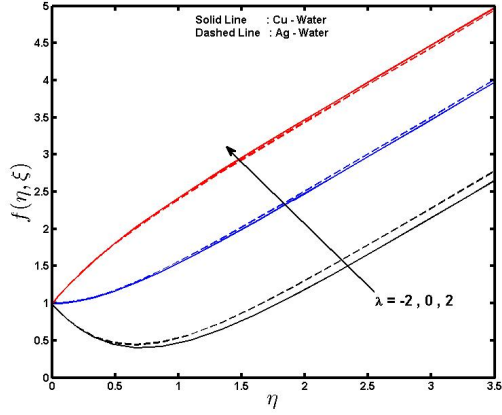


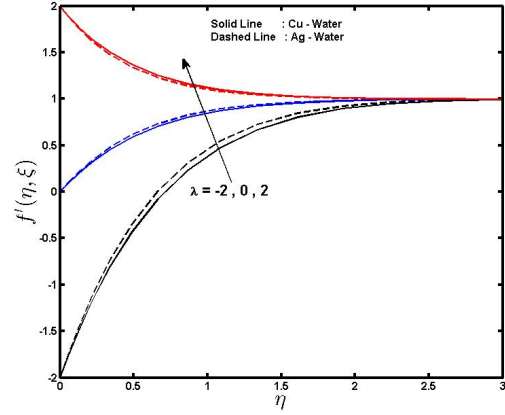
Figure 5.12: Effect of suction/injection parameter f_w on (a) the heat transfer coefficient and (b) the mass transfer coefficient for $D_f = 0.01$, $\phi = 0.3$, $Gr_t = 0.01$, $Gr_c = 0.01$, $Ha = 2$, $\delta = 0.2$, $Sc = 1$, $Sr = 1$, $\lambda = 0.5$ and $\gamma = 3$.

Figures 5.13 - 5.16 show the influence of the stretching/shrinking parameter λ on the velocity profiles, temperature profiles, solutal concentration profiles, skin friction coefficient, the wall heat and mass transfer rates are, for both nanofluids. We notice that increasing the stretching/shrinking parameter λ causes an increase in the velocity profiles, skin friction and heat transfer coefficient. On the other hand the temperature profiles, solutal concentration profiles and the mass transfer coefficient decrease with increasing λ . It can be seen from Figure 5.13 that the momentum boundary layer thickness increases with increases in the stretching/shrinking parameter λ . When $\lambda = -2$ (shrinking) the momentum boundary layer for an Ag-water nanofluid is greater than that of a Cu-water nanofluid. When $\lambda = 2$ (stretching) the opposite is true. This indicate that the thermal boundary for an Ag-water nanofluid is higher than that of a Cu-water nanofluid. Figures 5.14 (a) and (b) show that the solutal concentration increases up to a certain value of η . We observe that in the case of an Ag-water nanofluid the increase is less than that of Cu-water nanofluid, beyond this critical value the concentra-

tion profile decreases. We observe that in the case a Cu-water nanofluid the increase is greater than that of an Ag-water nanofluid when $\lambda = -2, 0$, but when $\lambda = 2$ (stretching) the opposite is true (see Figure 5.14 (b)). Therefore, the solutal concentration boundary layer thickness increases at a certain point with the value of η increasing before it tends to decrease. The results show good agreement with those obtained by Bhattacharyya [188]. Figure 5.15 shows the effect of the stretching/shrinking parameter λ on the shear stress, while Figures 5.16 (a) and (b) depict the effect of λ on the wall heat and mass transfer rates respectively. It can be seen from Figure 5.15 that the shear stress increases with increase in a stretching/shrinking parameter. It can also be seen that the change in the shear stress decreases with increases in ξ . From Figures 5.16 (a) we also note that the heat transfer rate increases with λ and the change in the heat transfer rate increases with ξ . Moreover, from Figure 5.16 (b) it is clear that the mass transfer rate decreases with the increase in λ . Furthermore, from Figure 5.16 (a) and (b), we observe that, for the wall heat transfer rate, in the case of an Ag-water nanofluid the increase is less than that of a Cu-water nanofluid, while the opposite is true for the wall mass transfer rate. From the above numerical investigations we found that the velocity profile decreases with an increase in nanoparticle volume fraction, while the opposite is true in the case of temperature profile. Moreover, the, concentration profile increases at certain critical value of dimensionless variable, but beyond these critical values it decreases with an increase in nanoparticle volume fraction. The findings above show good agreement with previously published results.

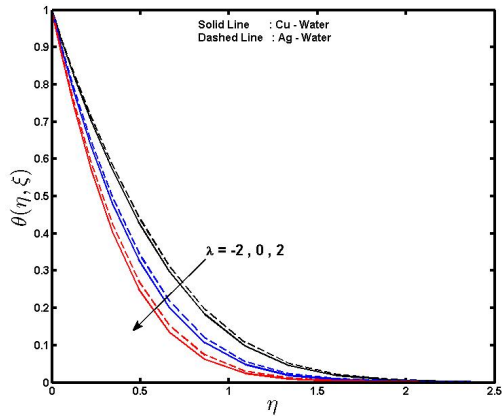


(a)

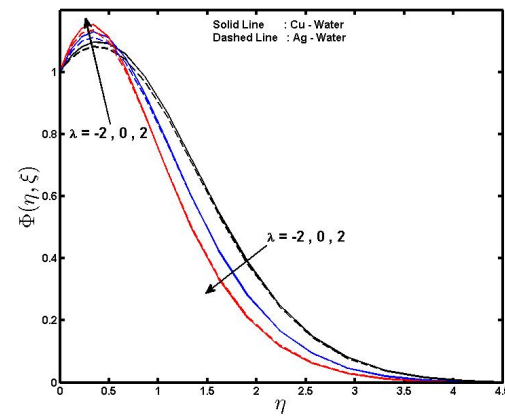


(b)

Figure 5.13: Effect of various a stretching/shrinking parameter values λ on (a) axial velocity and (b) tangential velocity profiles respectively, for $D_f = 0.01$, $\phi = 0.3$, $Gr_t = 0.01$, $Gr_c = 0.01$, $Ha = 2$, $\delta = 0.1$, $Sc = 1$, $Sr = 1$, $f_w = 1$, $\gamma = 0.1$ and $\xi = 0.5$.



(a)



(b)

Figure 5.14: Effect of various a stretching/shrinking parameter values λ on (a) the temperature profiles and (b) the concentration profiles for $D_f = 0.01$, $\phi = 0.3$, $Gr_t = 0.01$, $Gr_c = 0.01$, $Ha = 2$, $\delta = 0.1$, $Sc = 1$, $Sr = 1$, $f_w = 1$, $\gamma = 0.1$ and $\xi = 0.5$.

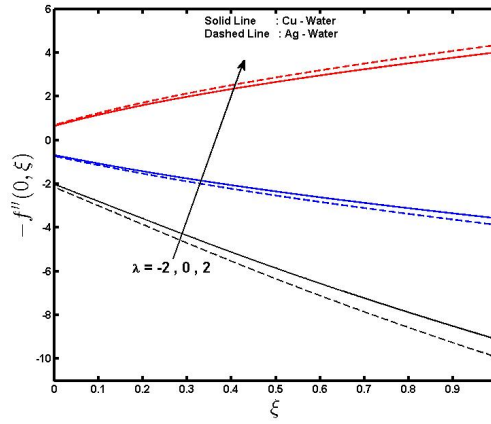
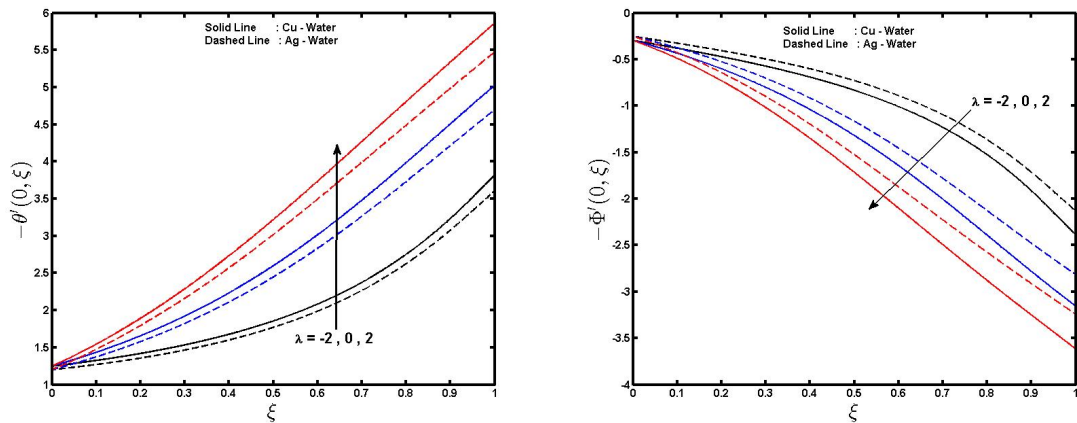


Figure 5.15: Effect of various a stretching/shrinking parameter values λ on the skin friction coefficient for $D_f = 0.01$, $\phi = 0.3$, $Gr_t = 0.01$, $Gr_c = 0.01$, $Ha = 2$, $\delta = 0.1$, $Sc = 1$, $Sr = 1$, $f_w = 1$ and $\gamma = 0.1$.



(a)

(b)

Figure 5.16: Effect of various a stretching/shrinking parameter values λ on (a) the heat transfer coefficient and (b) the mass transfer coefficient for $D_f = 0.01$, $\phi = 0.3$, $Gr_t = 0.01$, $Gr_c = 0.01$, $Ha = 2$, $\delta = 0.1$, $Sc = 1$, $Sr = 1$, $f_w = 1$ and $\gamma = 0.1$.

5.6 Summary

In this chapter we investigated unsteady MHD mixed convection, heat and mass transfer in a nanofluid over a stretching/shrinking sheet in the presence of Soret and Dufour effects, heat generation, magnetic field and chemical reaction parameter, for both Cu-water nanofluid and Ag-water nanofluid. The transformed nonlinear partial differential equations are solved numerically using the spectral relaxation method (SRM), our results, although using innovative methods, are found in to be in good agreement with previously published results. Thus we conclude that the methods employed provide a relatively easy means of simulating the behaviour of nanofluids, even under the influence of other complicating phenomena. From the simulations we now understand better the behaviour of nanofluids with regards to our dissertation in terms of enhancing thermal conductivity of fluid and heat transfer, In particular we highlight the new finding about parameters in our problem.

Chapter 6

Conclusion

In this study, we presented an analysis of double-diffusive convection and flow in a porous medium saturated with a nanofluid. Numerical results for the skin friction, heat and mass transfer rates have been presented for different physical parameters. We transformed the set of nonlinear governing equations and boundary conditions into nonlinear non-similar forms suitable for numerical simulations. The numerical simulations were run using values of thermophysical properties and parameter values found in the literature. We considered both Cu-water and Ag-water nanofluids. Results showing the effects of the physical and fluid parameters on the fluid properties were tabulated and presented graphically in each Chapter. Here, we highlight some of the results and conclusions that have been drawn from this study, and discuss them in relation to prior work, and their application in practice.

In Chapter 3 we studied double-diffusive convection in a nanofluid flow over a stretching sheet with heat generation, Soret effects and a chemical reaction term. The influence of the physical parameters on the double-diffusive convection was presented graphically. Exact solutions were

obtained in the particular cases $\xi = 0$ and $\xi = 1$. From the numerical study, the following conclusions could be drawn;

- The tangential velocity, temperature and the local Sherwood number increases with an increase in the nanoparticle volume fraction. The opposite is true in the case of the solute concentration, local skin friction factor and local Nusslet number.
- Increasing the Soret number tends to increase the concentration profiles, while the local Sherwood number decreases.
- When the chemical reaction parameter increases, the solute concentration profiles decreases but the reverse was noted for the local Sherwood number.
- In the limiting cases of initial steady and final steady states, we found good agreement between our results and previous results in the literature. This suggested that the methods used give accurate results.

In Chapter 4 we studied mixed convection in a nanofluid flow over a non-isothermal wedge subject to Soret and Dufour effects. We applied the spectral relaxation method (SRM) to obtain numerical solutions. A comparison of our results with those from previous studies was again showed good agreement. We determined the influence of the physical parameters, and found the following:

- The velocity profile increases with the nanoparticle volume fraction, thermal radiation parameter and the Dufour number.
- The concentration profiles decrease with an increase in the nanoparticle volume fraction, Dufour number, chemical reaction parameter and the Soret number.

- The skin friction decreased with an increase in nanoparticle volume fraction but the opposite is true as the thermal radiation parameter increased.
- The heat transfer coefficient reduces with an increase in the nanoparticle volume fraction and the Dufour number, whereas it increased as the thermal radiation parameter increased.
- Increasing the nanoparticle volume fraction, Dufour number, Soret number and chemical reaction increased the mass transfer coefficient. The opposite is true in the case of the thermal radiation parameter.
- The fluid temperature increased when the nanoparticle volume fraction, thermal radiation parameter and the Dufour number are increased.

In Chapter 5 we extended the study presented in Chapter 4 to include unsteady MHD mixed convection with suction/injection. The system of partial differential equations, were solved numerically using the spectral relaxation method (SRM). Once again, there was good correspondence between our results and those in the literature, giving us assurance of the reliability and accuracy of our findings. The following conclusions could drawn from the study:

- The velocity profiles are reduced by an increase in the nanoparticle volume fraction. The opposite is true in the case of the fluid temperature.
- The velocity of the nanofluid increases with the Hartmann number, suction/injection parameter and stretching/shrinking parameter.
- The skin friction factor increases with an increase in nanoparticle volume fraction and stretching/shrinking parameter λ .

- Regarding stretching/shrinking and suction/injection parameters, the Cu-water nanofluid has a higher skin friction coefficient than the Ag-water nanofluid.
- Increases in nanoparticle volume fraction lead to a decrease in the wall mass transfer rate.
- The wall heat transfer rate increases with the Hartmann number, suction/injection parameter f_w and stretching/shrinking parameter λ , but it reduces with the nanoparticle volume fraction.
- The fluid temperature decreases when the suction/injection and a stretching/shrinking parameters increase.

We have, in this work, shown that nanoparticles contribute significantly to an increase in the thermal conductivity of common fluids and enhance heat transfer. The comparison between the SRM and the SQLM shown in Chapter 3 showed that both methods are computationally efficient and reliable for finding solutions of highly non-linear differential equations.

Bibliography

- [1] J. Bear and Y. Bachmat. Introduction to modeling of transport phenomena in porous media. Kluwer Academic Publishers, Dordrecht, Netherlands, 1990.
- [2] T. Corey. Mechanics of immiscible fluids in porous media. Water Resources, Colorado, Highlands Ranch, USA, 1994.
- [3] D. Ingham and I. Pop. Transport phenomena in porous media. Elsevier Science, London, England, 2005.
- [4] J. Vazquez. The porous medium equations. *Clinical Microbiology Reviews*, 471-495, 2007.
- [5] J. H. Strange and J.B. W. Webber. Multidimensionally resolved pore size distributions. *Applied Magnetic Resonance*, 12:231–245, 1997.
- [6] D. Nield and A. Bejan. Convection in porous media. Springer Verlag, New York, 1999.
- [7] J. H. Lethr and J. K. Lethr. Standard handbook in environmental science, health and technology. McGraw-Hill, New York, USA, 2000.
- [8] X. Feng. Fluid flow and transport in porous media. American Mathematical Society, 524, 2002.

- [9] K. Vafai. Handbook of porous media. CRC Press, New York, 2005.
- [10] P. Ranganatha and R. Viskanta. Mixed convection boundary layer flow along a vertical surface in a porous medium. *Numerical Heat Transfer*, 7(5):305–317, 1984.
- [11] D. A. Nield and A. V. Kuznetsov. The Cheng-Minkowycz problem for natural convection boundary layer flow in a porous medium saturated by a nanofluid. *International Journal of Heat and Mass Transfer*, 52:5792–5795, 2009.
- [12] D. A. Nield and A. V. Kuznetsov. Thermal instability in a porous medium layer saturated by a nanofluid. *International Journal of Heat and Mass Transfer*, 52:5796–5801, 2009.
- [13] M. Kumari and G. Nath. Natural convection from vertical cone in a porous medium due to the combined effects of heat and mass diffusion with non-uniform wall temperature/concentration or heat/mass flux and suction/injection. *International Journal of Heat and Mass Transfer*, 52:3064–3069, 2009.
- [14] A. Behzadmehr and H. Azarkish. Sampels of theoretical investigations in convective heat transfer of nanofluids. *University Sistan and Baluchestan*, 7:141–150, 2009.
- [15] J.P. Holman. Heat transfer. McGraw-Hill Series in Mechanical Engineering, Mishawaka, 1986.
- [16] L. Burmeister. Convection heat transfer. John Wiley and Sons, Canada, 1993.
- [17] S. Thirumale. Fundamentals of heat and mass transfer. Dorling Kindersley, India, 2006.
- [18] J. Welty, C. Wicks, and R. Wilson. Fundamentals of momentum heat and mass transfer. McGraw-Hill Series in Mechanical Engineering, 1984.

- [19] W. Kays and M. Crawford. Convective heat and mass transfer. McGraw-Hill, New York, 1993.
- [20] Y. Jaluria. Natural convection heat and transfer. Pergamon Press, Oxford, 1980.
- [21] R. S. Gorla and A. Zinolabedini. Free convection from a vertical plate with non-uniform surface temperature and embedded in a porous medium, transactions of asme. Journal of Energy Resources Technology, 109(1):26–30, 1987.
- [22] R. S. Gorla and A. Zinolabedini. Free convection from a vertical plate with non-uniform surface heat flux and embedded in a porous medium. Transport in Porous Medium Journal, 3:95–106, 1988.
- [23] B. Gebhart, Y. Jaluria, R. Mahajan, and B. Sammakia. Buoyancy-induced flows and transport springer. Springer, New York, 1988.
- [24] M. M. Rathore and R. Kapuno. Engineering heat transfer. Jones and Bartlett, Ontario, Canada, 2010.
- [25] Y. Jaluria and B. Gebhart. Stability and transition of buoyancy induced flows in a stratified medium. Journal of Fluid Mechanics, 12:593–612, 1974.
- [26] P. Cheng and W. J. Minkowycz. Free convection about a vertical flat plate embedded in a porous medium with application to heat transfer from a dike. Journal of Geophysical Research, 82(14):2040–2044, 1977.
- [27] Y. Jaluria and K. Himasekhar. Buoyancy induced two dimensional vertical flows in a thermally stratified environment. Computers and Fluids, 11(1):39–49, 1983.

- [28] R. Rudramoorthy and K. Mayilsamy. Heat and mass transfer. Dorling Kindersley, India, 2010.
- [29] R. Wooding. Rayleigh instability of a thermal boundary layer in flow through a porous medium. *Journal of Fluid Mechanics*, 9:183–192, 1960.
- [30] F. Lai. Coupled heat and mass transfer by natural convection from a horizontal line source in saturated porous medium. *International Communications in Heat and Mass Transfer*, 17:489–499, 1990.
- [31] J. Liyod and M. Sparrow. Combined force and free convection flow on vertical surfaces. *International Journal of Heat and Mass Transfer*, 13:434–438, 1970.
- [32] E. W. Mureithi and D.P. Mason. On the stability of a forced free boundary layer flow with viscous heating. *Fluid Dynamics Research*, 31(4):65–78, 2002.
- [33] W. Siegmann and L. Rubinfeld. A nonlinear model for double diffusive convection. *Journal on Applied Mathematics*, 29:540–557, 1975.
- [34] M. Bourich, M. Hasnaoui, and A. Amahmid. Double diffusive natural convection in porous enclosure partially heated from below and differentially salted. *International Journal of Heat and Fluid Flow*, 25:1034–1046, 2004.
- [35] M. Benzeghiba, A. Campo, and S. Chikh. Thermosolutal convection in a partly porous vertical annular cavity. *Journal of Heat Transfer*, 125(4):703–715, 2003.
- [36] A. Mojtabi and M. C. C. Mojtabi. Double diffusive convection in porous media. *Handbook of Porous Media*, 7:269–320, 2005.

- [37] B.B. Beya and T. Lili. Oscillatory double diffusive mixed convection in a two-dimensional ventilated enclosure. *International Journal of Heat and Mass Transfer*, 50:4540–4553, 2007.
- [38] M. Mamou. Stability analysis of double diffusive convection in porous enclosures. Institute for Aerospace Research, National Research Council Canada, Ottawa, 11:113–154, 2002.
- [39] A. Akbarzadeh and P. Manins. Convection layers generated by side walls in solar ponds. *Solar Energy*, 41:521–529, 1988.
- [40] D. Nield. Onset of thermohaline convection in a porous medium. *Water Resources Research*, 4(3):553–560, 1968.
- [41] P. G. Baines and A. E. Gill. On thermohaline convection with linear gradients. *Journal of Fluid Mechanics*, 37:289–306, 1969.
- [42] D. Gershuni, E. Zhukhovisskii, and D. Lyubimov. Thermal concentration instability of a mixture in a porous medium. *Sovling Physic Dokl*, 21:375–377, 1976.
- [43] A.A. Khan and A. Zebib. Double diffusive instability in a vertical layer of a porous medium. *Journal of Heat Transfer*, 103(3):179–181, 1981.
- [44] A. Raptis, G. Tzivanidis, and N. Kafousias. Free convection and mass transfer flow through a porous medium bounded by infinite vertical limiting surface with constant suction. *Letters in Heat and Mass Transfer*, 8:417–424, 1981.
- [45] D. A. Nield, D. M. Manole, and J. L. Lage. Convection induced by inclined thermal

- and solutal gradients in a shallow horizontal layer of porous medium. *Journal of Fluid Mechanics*, 257:559–574, 1993.
- [46] A. Amahmid, M. Hasnaoui, and P. Vasseur. On the transition between aiding and opposing double diffusive flows in a vertical porous matrix. *Solar Energy*, 3:123–137, 2000.
- [47] Z. Alloui, P. Vasseur, L. Robillard, and A. Bahloul. Onset double-diffusive convection in a horizontal Brinkman cavity. *Chemical Engineering Communications*, 197(3):387–399, 2010.
- [48] Y.S. Li, Z.W. Chen, and J.M. Zhan. Double-diffusive marangoni convection in a rectangular cavity: transition to chaos. *International Journal of Heat and Mass Transfer*, 53:5223–5231, 2010.
- [49] T. Okedayo, Gideon, and S. O. Abah. Plane stagnation double-diffusive MHD convective flow with convective boundary condition in a porous media. *American Journal of Computational Mathematics*, 2:223–227, 2012.
- [50] Ch. RamReddy, P.V.S.N. Murthy, A.J. Chamkha, and A.M. Rashad. Influence of viscous dissipation on free convection in a non-Darcy porous medium saturated with nanofluid in the presence of magnetic field. *The Open Transport Phenomena Journal*, 5:20–29, 2013.
- [51] J.A. Eastman, S.U.S. Choi, S. Li, W. Yu, and L.J. Thompson. Anomalously increased effective thermal conductivities containing copper nanoparticles. *Applied Physics Letters*, 78(6):718–720, 2001.

- [52] S.U.S. Choi, Z.G. Zhang, W. Yu, F.E. Lockwood, and E.A. Grulke. Anomalous thermal conductivity enhancement on nanotube suspensions. *Applied Physics Letters*, 79:2252–2254, 2001.
- [53] P. Vassallo, R. Kumar, and S. D. Amico. Pool boiling heat transfer experiments in silica-water nanofluids. *International Journal of Heat and Mass Transfer*, 47:407–411, 2004.
- [54] S.M. You, J.H. Kim, and K.H. Kim. Effect of nanoparticles on critical heat flux of water in pool boiling heat transfer. *Applied Physics Letters*, 83:3374–3376, 2003.
- [55] J. Routbort. Argonne National Laboratory. Michellin North America, 2009.
- [56] K. V. Wong and O. D. Leon. Applications of nanofluids current and future. *Advances in Mechanical Engineering*, 2010:11, 2010.
- [57] J. Boungiorno, HU Lin-Wen, S.J. Kim, H. Ryan, T. Bao, and F. Eric. Nanofluids for enhanced economics and safety of nuclear reactors an evaluation of the potential features issues and research gaps. *Nuclear Technology*, 162(1):80–91, 2008.
- [58] E. H. Herbert and J. S. Turner. Double-diffusive convection and its implications for the temperature and salinity structure of the ocean and lake Vanda. *Journal of Physical Oceanography*, 2(1):456–461, 1972.
- [59] B. Bai, L. Zhang, L. Zhang, and H. Li. Experimental study on double-diffusive convection during solidification of $n\text{h}_{4\text{CL}} - \text{h}_{2\text{O}}$ hypereutectic in cylindrical cavity. *Heat Transfer Conference, collocated with the Fluids Engineering, Energy Sustainability, and 3rd Energy Nanotechnology Conference, Heat Transfer: Jacksonville, Florida, USA, ASME*, 1:713–718, 2008.

- [60] S. Mergui, S. Geoffroy, and C. Benard. Ice block melting into a binary solution, coupling of the interfacial equilibrium and the flow structures. *Journal of Heat Transfer*, 124(6):1147–1157, 2002.
- [61] N. Barman and P. Dutta. Studies on macrosegregation and double-diffusive convection during directional solidification of binary mixture. *Materials Science and Technology*, 24(10):1230–1237, 2008.
- [62] R.W. Griffiths. Layered double-diffusive convection in porous media. *Journal of Fluid Mechanics*, 102:221–248, 1981.
- [63] C. Beckermann, C. Fan, and J. Mihailovic. Numerical simulations of double-diffusive convection in a Hele-Shaw cell. *International Video Journal of Engineering Research*, 1:71–82, 1991.
- [64] S. Webb, D. Reneta, P. Suhas, and H.J.S. Fernando. Double-diffusive convection in narrow aspect cylinders experimental data and CFD simulations. *American Physical Society, 62nd Annual Meeting of the APS Division of Fluid Dynamics*, 11, 2009.
- [65] B. Gebhart and L. Pera. The nature of vertical natural convection flow resulting from the combined buoyancy effects of thermal and mass diffusion. *International Journal of Heat and Mass Transfer*, 14:2025–2050, 1971.
- [66] W.J. Minkowycz, P. Cheng, and F. Moalem. The effect of surface mass transfer on buoyancy induced Darcian flow adjacent to a horizontal heated surface. *International Journal of Heat and Mass Transfer*, 12:55–65, 1985.
- [67] A. J. Chamkha and S. M. M. El-Kabeir. Unsteady heat and mass transfer by MHD mixed

- convection flow over an impulsively stretched vertical surface with chemical reaction and Soret and Dufour effects. *Chemical Engineering Communications*, 200:1220–1236, 2013.
- [68] F.C. Lai. Coupled heat and mass transfer by mixed convection from a vertical plate in a saturated porous medium. *International Communications in Heat and Mass Transfer*, 18:93–106, 1991.
- [69] K.A. Yih. Coupled heat and mass transfer in mixed convection over a wedge with variable wall temperature and concentration in porous media. *International Communications in Heat and Mass Transfer*, 25:1145–1158, 1998.
- [70] C. Cheng. Transient heat and mass transfer by natural convection from vertical surface in porous media. *Journal physics D: Applied Physics*, 33:1425–1430, 2000.
- [71] Md.S. Khan, I. Karim, L.E. Ali, and A. Islam. Unsteady MHD free convection boundary layer flow of a nanofluid along a stretching sheet with thermal radiation and viscous dissipation effects. *International Nano Letters*, 24(2), 2012.
- [72] A. Mahdy. Unsteady mixed convection boundary layer flow and heat transfer of nanofluids due to stretching sheet. *Nuclear Engineering and Design*, 249:248–255, 2012.
- [73] T. Chen, C. Yuh, and A. Moutsoglou. Combined heat and mass transfer in mixed convection along vertical and inclined plates. *International Journal of Heat and Mass Transfer*, 23:527–537, 1980.
- [74] M. Acharya, G.C. Dash, and L.P. Singh. Magnetic field effects on the free convection and mass transfer flow through porous medium with constant suction and constant heat flux. *Indian Journal of Pure Applied Mathematics*, 31(1):1–18, 1999.

- [75] A. Ishak, R. Nazar, and I. Pop. Heat transfer over an unsteady stretching permeable surface with prescribed wall temperature. *Nonlinear Analysis: Real World Applications*, 10(5):2909–2913, 2009.
- [76] N. Joshi, M. Kumar, and S. K. Budhani. Numerical solution of heat and mass transfer with thermal radiation and MHD boundary layer flow over a stretching surface with suction/injection. *International Journal of Computational Engineering Research*, 2:2250–3005, 2012.
- [77] S. Manjunatha, B. Gireesha, and C. Bagewadi. Effect of thermal radiation on boundary layer flow and heat transfer of dusty fluid over an unsteady stretching sheet. *International Journal of Engineering, Science and Technology*, 4(4):36–48, 2012.
- [78] K. Bhattacharyya, S. Mukhopadhyay, and G.C. Layek. Unsteady MHD boundary layer flow with diffusion and first order chemical reaction over a permeable stretching sheet with suction or blowing. *Chemical Engineering Communications*, 200:379–397, 2013.
- [79] G. Adomian. A review of the decomposition method and some recent results for nonlinear equation. *Mathematical and Computer Modelling: International Journal*, 7(13):17–43, 1990.
- [80] J. C. Williams and T. B. Rhyne. Boundary layer development on a wedge impulsively set into motion. *Journal of Applied Mathematics*, 38(2):215–224, 1980.
- [81] S. S. Motsa, P. Dlamini, and M. Khumalo. Solving hyperchaotic systems using the spectral relaxation method. *Mathematical Problems in Engineering*, 2012:18, 2012.
- [82] S. S. Motsa. A new spectral relaxation method for similarity variable nonlinear boundary layer flow systems. *Chemical Engineering Communications*, 201(2):241–256, 2014.

- [83] L. N. Trefethen. Spectral methods in matlab. Society for Industrial and Applied Mathematics, Philadelphia, USA, 165, 2000.
- [84] C. Canuto, M. Hussaini, A. Quarteroni, and T. Zang. Spectral methods in fluid dynamics. Springer-Verlag, Berlin, 1988.
- [85] S. S. Motsa and Z. G. Makukula. On spectral relaxation method approach for steady von kármán flow of a Reiner-Rivlin fluid with joule heating, viscous dissipation and suction/injection. Central European Journal of Physics, 78:718–720, 2013.
- [86] S. Shateyi. A new numerical approach to MHD flow of a maxwell fluid past a vertical stretching sheet in the presence of thermophoresis and chemical reaction. Boundary Value Problems, 2013(1):196, 2013.
- [87] S. Shateyi and O. D. Makinde. Hydromagnetic stagnation-point flow towards a radially stretching convectively heated disk. Mathematical Problems in Engineering, 2013:8, 2013.
- [88] S. Shateyi and G. T. Marewo. A new numerical approach of MHD flow with heat and mass transfer for the UCM fluid over a stretching surface in the presence of thermal radiation. Mathematical Problems in Engineering, 2013:8, 2013.
- [89] S. S. Motsa and S. Shateyi. Successive linearisation analysis of unsteady heat and mass transfer from a stretching surface embedded in a porous medium with suction/injection and thermal radiation effects. Canadian Journal of Chemical Engineering, 13:113, 2011.
- [90] R. E. Bellman and R. E. Kalaba. Quasilinearization and nonlinear boundary-value problems. Elsevier, New York, 1965.

- [91] S. S. Motsa and P. Sibanda. Spectral method based numerical solutions of partial differential equations. Sixth Annual Workshop on Computational Applied Mathematics and Mathematical Modelling in Fluid flow, University of Kwazulu-Natal, Pietermaritzburg, South Africa, July, 1–7, 2013.
- [92] P. Dlamini, S. S. Motsa, and M. Khumalo. On the comparison between compact finite difference and pseudospectral approaches for solving similarity boundary layer problems. *Mathematical Problems in Engineering*, 2013:15, 2013.
- [93] S. S. Motsa and P. Sibanda. On extending the quasilinearization method to higher order convergent hybrid schemes using the spectral homotopy analysis method. *Journal of Applied Mathematics*, 2013:9, 2013.
- [94] S. S. Motsa. New iterative methods for solving non-linear boundary value problems. Fifth Annual Workshop on Computational Applied Mathematics and Mathematical Modelling in Fluid flow, University of Kwazulu-Natal, Pietermaritzburg, South Africa, July, 1–63, 2012.
- [95] H. Blasius. Grenzschichten in flüssigkeiten mit kleiner reibung. *Zeitschrift für Angewandte Mathematik and Physik*, 56:1–37, 1908.
- [96] L. Howarth. On the solution of the laminar boundary layer equations. *The Royal Society of London Series A : Mathematical and Physical Sciences*, 164(919):547–579, 1938.
- [97] B. C. Sakiadis. Boundary layer behaviour on continuous solid surfaces: boundary layer equations for two-dimensional and axisymmetric flow. *American Institute of Chemical Engineers Journal*, 7:26–28, 1961.

- [98] L. J. Crane. Flow past a stretching plate. *Zeitschrift for Angewandte Mathematik and Physik*, 21:645–647, 1970.
- [99] P. S. Gupta and A. S. Gupta. Heat and mass transfer on a stretching sheet with suction or blowing. *Canadian Journal of Chemical Engineering*, 55:744–746, 1977.
- [100] T. S. Chen and F. A. Strobel. Buoyancy effects in boundary layer adjacent to a continuous moving horizontal flat plate. *Journal of Heat Transfer*, 102:170–172, 1980.
- [101] L. J. Grubka and K. M. Bobba. Heat transfer characteristics of a continuous, stretching surface with variable temperature. *Journal of Heat Transfer*, 107(1):248–250, 1985.
- [102] B.J. Gireesha, G.K. Ramesh, H.J. Lokesh, and C.S. Bagewadi. Boundary layer flow and heat transfer of a dusty fluid over a stretching vertical surface. *Applied Mathematics*, 2:475–481, 2011.
- [103] Y.M. Aiyesimi, S.O. Abah, and G.T. Okedayo. The analysis of hydromagnetic free convection heat and mass transfer flow over a stretching vertical plate with suction. *American Journal of Computational and Applied Mathematics*, 1:20–26, 2011.
- [104] K. Bhattacharyya and K. Vajravelu. Stagnation point flow and heat transfer over an exponentially shrinking sheet. *Communications in Nonlinear Science and Numerical Simulation*, 17:2728–2734, 2012.
- [105] G. K. Ramesh, B. J. Gireesha, and C. S. Bagewadi. Heat transfer in MHD dusty boundary layer flow over an inclined stretching sheet with non-uniform heat source/sink. *Advances in Mathematical Physics*, 2012:13, 2012.
- [106] N. Joshi, M. Kumar, and S. Budhani. Numerical solution of heat and mass transfer

- with thermal radiation and MHD boundary layer flow over a stretching surface with suction/injection. *International Journal of Computational Engineering*, 2(2):496–500, 2012.
- [107] H. Mondal and D. Pal. Non-Darcian buoyancy driven heat and mass transfer over a stretching sheet in a porous medium with radiation and Ohmic heating. *International Journal of Nonlinear Science*, 14(1):115–123, 2012.
- [108] K. Vajravelu. Viscous flow over a nonlinearly stretching sheet. *Applied Mathematics and Computation*, 124:281–288, 2001.
- [109] H.I. Andersson, J.B. Aarseth, and B. S. Dandapat. Heat transfer in a liquid film on an unsteady stretching surface. *International Journal of Heat and Mass Transfer*, 43(1):69–74, 2000.
- [110] A. Ali and A. Mehmood. Homotopy analysis of unsteady boundary layer flow adjacent to permeable stretching surface in a porous medium. *Communications in Nonlinear Science and Numerical Simulation*, 13(2):340–349, 2008.
- [111] A. Ishak, R. Nazar, and I. Pop. Unsteady mixed convection boundary layer flow due to a stretching vertical surface. *Arabian Journal for Science and Engineering*, 31(2):165–182, 2006.
- [112] A. Ishak, R. Nazar, and I. Pop. Boundary layer flow and heat transfer over an unsteady stretching vertical surface. *Meccanica*, 44(7):369–375, 2009.
- [113] T. Hayat, Z. Abbas, and T. Javed. Mixed convection flow of a micropolar fluid over a nonlinearly stretching sheet. *Physics Letters A*, 372(5):637–647, 2008.

- [114] R. Sharma, R. Bhargava, and I. V. Singh. A numerical solution of MHD convection heat transfer over an unsteady stretching surface embedded in a porous medium using element free Galerkin method. *International Journal of Applied Mathematics and Mechanics*, 8(10):83–103, 2012.
- [115] R. Sharma. Effect of viscous dissipation and heat source on unsteady boundary layer flow and heat transfer past a stretching surface embedded in a porous medium using element free Galerkin method. *Applied Mathematics and Computation*, 219(12):976–987, 2012.
- [116] N. Bachok, A. Ishak, and I. Pop. Unsteady three-dimensional boundary layer flow due to a permeable shrinking sheet. *Applied Mathematics and Mechanics*, 31(11):1421–1428, 2010.
- [117] K. Bhattacharyya. Heat transfer analysis in unsteady boundary layer stagnation point flow towards a shrinking/stretching sheet. *Ain Shams Engineering Journal*, 4:259–264, 2013.
- [118] S. Manjunatha, B.J. Gireesha, and C. S. Bagewadi. Effect of thermal radiation on boundary layer flow and heat transfer of dusty fluid over an unsteady stretching sheet. *International Journal of Engineering, Science and Technology*, 4(4):36–48, 2012.
- [119] K. Bhattacharyya, S. Mukhopadhyay, and G. C. Layek. Unsteady MHD boundary layer flow with diffusion and first order chemical reaction over a permeable stretching sheet with suction or blowing. *Chemical Engineering Communications*, 200(3):379–397, 2013.
- [120] S. Liao. Series solutions of unsteady boundarylayer flows over a stretching flat plate. *Studies in Applied Mathematics*, 117:239–263, 2006.

- [121] H. Xu, S.J. Liao, and I. Pop. Series solutions of unsteady three-dimensional MHD flow and heat transfer in the boundary layer over an impulsively a stretching plate. *European Journal of Mechanics Fluids*, 26:15–27, 2007.
- [122] S.U.S. Choi and J. A. Eastman. Enhancing thermal conductivity of fluids with nanoparticles. *International Mechanical Engineering Congress and Exposition*, (1):12–17, 1995.
- [123] D. Yulong, H. Chen, L. Wang, C.Y. Yang, Y. He, W. Yang, W.P. Lee, L. Zhang, and R. Huo. Heat transfer intensification using nanofluids. *Kona Powder and Particle Journal*, (25), 2007.
- [124] M. Sheikholeslami, M. Gorji-Bandpy, D.D. Ganji, S. Soleimani, and S.M. Seyyedi. Natural convection of nanofluids in an enclosure between a circular and a sinusoidal cylinder in the presence of magnetic field. *International Communications in Heat and Mass Transfer*, 39(9):1435–1443, 2012.
- [125] S. U. S. Choi. Enhancing thermal conductivity of fluids with nanoparticles. *International Mechanical Engineering Congress and Exposition*, 231:99–105, 1995.
- [126] W. A. Khan and I. Pop. Boundary-layer flow of a nanofluid past a stretching sheet. *International Journal of Heat and Mass Transfer*, 53:2477–2483, 2010.
- [127] K. Das. Slip flow and convective heat transfer of nanofluids over a permeable stretching surface. *Computers and Fluids*, 64:34–42, 2012.
- [128] L. Zheng, C. Zhang, X. Zhang, and J. Zhang. Flow and radiation heat transfer of an a nofluid over a stretching sheet with velocity slip and temperature jump in porous medium. *Journal of the Franklin Institute*, 350(5):990–1007, 2013.

- [129] M. Mustafa, T. Hayat, I. Pop, S. Asghar, and S. Obaidat. Stagnation point flow of a nanofluid towards a stretching sheet. *International Journal of Heat and Mass Transfer*, 54:5588–5594, 2011.
- [130] P.K. Kameswaran, S. Shaw, P. Sibanda, and P.V.S.N. Murthy. Homogeneous heterogeneous reactions in a nanofluid flow due to a porous stretching sheet. *International Journal of Heat and Mass Transfer*, 57:465–472, 2013.
- [131] A.M. Rohni, S. Ahmad, and I. Pop. Flow and heat transfer over an unsteady shrinking sheet with suction in nanofluids. *International Journal of Heat and Mass Transfer*, 55:1888–1895, 2012.
- [132] M. Narayana and P. Sibanda. Laminar flow of a nanoliquid film over an unsteady stretching sheet. *International Journal of Heat and Mass Transfer*, 55:7552–7560, 2012.
- [133] N. Bachok, A. Ishak, and R. Nazar. Flow and heat transfer over an unsteady stretching sheet in a micropolar fluid with prescribed surface heat flux. *International Journal of Mathematical Models and Methods in Applied Sciences*, 4(3), 2010.
- [134] A.J. Chamkha, A.M. Rashad, and E. Al-Meshaie. Melting effect on unsteady hydro-magnetic flow of a nanofluid past a stretching sheet. *International Journal of Chemical Reactor Engineering*, 9:113, 2011.
- [135] M. Mustafa, T. Hayat, and A. Alsaedi. Unsteady boundary layer flow of nanofluid past an impulsively a stretching sheet. *Journal of Mechanics*, 29(3):423–432, 2013.
- [136] S. S. Motsa, P.G. Dlamini, and M. Khumalo. Solving hyperchaotic systems using the spectral relaxation method. *Mathematical Problems in Engineering*, 2012:18, 2012.

- [137] H. C. Brinkman. The viscosity of concentrated suspensions and solution. *The Journal of Chemical Physics*, 20:571–81, 1952.
- [138] E. Abu-Nada. Application of nanofluids for heat transfer enhancement of separated flows encountered in a backward facing step. *International Journal of Heat and Fluid Flow*, 29:242–249, 2008.
- [139] S. J. Liao. An analytic solution of unsteady boundary layer flows caused by an impulsively stretching plate. *Communications in Nonlinear Science and Numerical Simulation*, 11:326–329, 2006.
- [140] H. F. Oztop and E. Abu-Nada. Numerical study of natural convection in partially heated rectangular enclosures filled with nanofluids. *International Journal of Heat and Fluid Flow*, 29:1326–1336, 2008.
- [141] A. A. Afify. Similarity solution in MHD effects of thermal diffusion and diffusion thermo on free convective heat and mass transfer over a stretching surface considering suction or injection. *Communications in Nonlinear Science and Numerical Simulation*, 14(5):2202–2214, 2009.
- [142] J. A. Gbadeyan, A. S. Idowu, A. W. Ogunsola, O. O. Agboola, and P.O. Olanrewaju. Heat and mass transfer for Soret and Dufours effect on mixed convection boundary layer flow over a stretching vertical surface in a porous medium filled with a viscoelastic fluid in the presence of magnetic field. *Global Journal of Science Frontier Research*, 11(8):2249–4626, 2011.
- [143] Y. Hasegawa and N. Kasagi. The effect of Schmidt number on air-water interface mass

- transfer. Proceeding of the 4th International Conference on Multiphase Flow, May 27 to June 1, New Orleans, Louisiana, USA, 2001.
- [144] N. G. Kafoussias and E. W. Williams. Thermal-diffusion and diffusion-thermo effects on mixed free-forced convective and mass transfer boundary layer flow with temperature dependent viscosity. *International Journal Engineering Science*, 33:1369–1384, 1995.
- [145] K. Vajravelu, K.V. Prasad, J. Lee, C. Lee, I. Pop, and Robert A. Van Gorder. Convective heat transfer in the flow of viscous Ag-water and Cu-water nanofluids over a stretching surface. *International Journal of Thermal Sciences*, 50:843–851, 2011.
- [146] P. K. Kameswaran, P. Sibanda, and A.S.N. Murti. Nanofluid flow over a permeable surface with convective boundary conditions and radiative heat transfer. *Mathematical Problems in Engineering*, 2013:11, 2013.
- [147] P. K. Kameswaran, M. Narayana, P. Sibanda, and P. V. S. N. Murthy. Hydromagnetic nanofluid flow due to a stretching or shrinking sheet with viscous dissipation and chemical reaction effects. *International Journal of Heat and Mass Transfer*, 55:7587–7595, 2012.
- [148] Md. S. Alam and Md. S. H. Mollah. Influence of Chemical reaction and heat generation/absorption on MHD free convective heat and mass transfer flow along an inclined stretching sheet considering Dufour and Soret effects. *Asian Transactions on Basic and Applied Sciences*, 02:2221–4291, 2012.
- [149] M. M. Ali, R. Akhter, N. A. Azim, and M. A. Maleque. The effects of radiation and heat generation on MHD natural convection flow along vertical flat plate in presence of

- viscous dissipation. *Daffodil International University Journal of Science and Technology*, 6(2), 2011.
- [150] S. Abel and P. H. Veena. Visco-elastic liquid flow and heat transfer in a porous medium over a stretching sheet. *International Journal Nonlinear Mechanics*, 33(3):531–540, 1998.
- [151] K.V. Prasad, M.S. Abel, and A. Joshi. Oscillatory motion of a visco-elastic liquid over a stretching sheet in porous media. *Journal of Porous Media*, 3:61–68, 2000.
- [152] N. Aminreza, R. Pourrajab, and M. Ghalambaz. Effect of partial slip boundary condition on the flow and heat transfer of nanofluids past stretching sheet prescribed constant wall temperature. *International Journal of Thermal Sciences*, 54:253–261, 2012.
- [153] M. A.A. Hamad and M. Ferdows. Similarity solution of boundary layer stagnation-point flow towards a heated porous stretching sheet saturated with a nanofluid with heat absorption/generation and suction/blowing: A li2 group analysis. *Communications in Nonlinear Science and Numerical Simulation*, 17:132–140, 2012.
- [154] P. Dulal and H. Mondal. Influence of thermophoresis and Soret-Dufour on magnetohydrodynamic heat and mass transfer over a non-isothermal wedge with thermal radiation and Ohmic dissipation. *Journal of Magnetism and Magnetic Materials*, 331:250–255, 2013.
- [155] H. Masuda, A. Ebata, K. Teramae, and N. Hishinuma. Alteration of thermal conductivity and viscosity of liquid by dispersing ultra-fine particles. *Netsu Bussei, Institute of Fluid Science*, 7(4):227–233, 1993.
- [156] J. Buongiorno. Nanofluid coolants for advanced nuclear power plants. *Journal of Applied Physics Proceedings*, 05:15–19, 2005.

- [157] J.A. Gbadeyan, A.S. Idowu, A.W. Ogunsola, O.O. Agboola, and P.O. Olanrewaju. Heat and mass transfer for Soret and Dufours effect on mixed convection boundary layer flow over a stretching vertical surface in a porous medium filled with a viscoelastic fluid in the presence of magnetic field. *Global Journal of Science Frontier Research*, 11:5975–5896, 2011.
- [158] M. A. Seddeek. Finite-element method for the effects of chemical reaction, variable viscosity, thermophoresis and heat generation/absorption on a boundary-layer hydromagnetic flow with heat and mass transfer over a heat surface. *Acta Mechanica*, 177:1–18, 2005.
- [159] M. J. Subhakar and K. Gangadhar. Soret and Dufour effects on MHD free convection heat and mass transfer flow over a stretching vertical plate with suction and heat source/sink. *International Journal of Modern Engineering Research*, 2:3458–3468, 2012.
- [160] K.Md. Shakhaoath, Md.M. Alam, and M. Ferdows. Effects of magnetic field on radiative flow of a nanofluid past a stretching sheet. *Procedia Engineering*, 56:316–322, 2013.
- [161] P. Singh, D. Sinha, and N. S. Tomer. Oblique stagnation-point Darcy flow towards a stretching sheet. *Journal of Applied Fluid Mechanics*, 5(3):29–37, 2012.
- [162] J. Buongiorno. A benchmark study on the thermal conductivity of nanofluids. *Journal of Applied Physics Proceedings*, 9(1):15–19, 2009.
- [163] D.C. Venerus, J. Buongiorno, R. Christianson, J. Townsend, I.C. Bang, G. Chen, S.J. Chung, M. Chyu, H. Chen, Y. Ding, F. Dubois, G. Dzido, D. Funfschilling, Q. Galand, J. Gao, H. Hong, M. Horton, Lin wen Hu, C.S. Iorio, A.B. Jarzebski, Y. Jiang, S. Kabelac, M.A. Kedzierski, C. Kim, Ji-Hyun Kim, S. Kim, T. McKrell, R. Ni, J. Philip,

- N. Prabhat, P. Song, S. Van Vaerenbergh, D. Wen, S. Witharana, Xiao-Zheng Zhao, and Sheng-Qi Zhou. Viscosity measurements on colloidal dispersions (nanofluids) for heat transfer applications. *Applied Rheology*, 20:4(7):44582, 2010.
- [164] P. E. Gharagozloo, J. K. Eaton, and K.E. Goodson. Diffusion, aggregation, and the thermal conductivity of nanofluids. *Applied Physics Letters*, 93(1):103110, 2008.
- [165] J. Philip, P. Shima, and B. Raj. Boundary layer flow of a nanofluid past a stretching sheet. *International Journal of Heat and Mass Transfer*, 53:2477–2483, 2010.
- [166] K. A. Yih. MHD forced convection flow adjacent to a non-isothermal wedge. *International Communications in Heat and Mass Transfer*, 26(6):819–827, 1999.
- [167] R. K. Tiwari and M. K. Das. Heat transfer augmentation in a two-sided lid-driven differentially heated square cavity utilizing nanofluids. *International Journal of Heat and Mass Transfer*, 50:2002–2018, 2007.
- [168] P. K. Kameswaran and P. Sibanda. Thermal dispersion effects on convective heat and mass transfer in an Ostwald de Waele nanofluid flow in porous media. *Boundary Value Problems*, 10:1687–2770, 2013.
- [169] A. V. Kuznetsov and D.A. Nield. Natural convective boundary layer flow of a nanofluid past a vertical plate. *International Journal of Thermal Sciences*, 49:243–247, 2010.
- [170] C. H. Chen. Laminar mixed convection adjacent to vertical, continuously stretching sheets. *Heat and Mass Transfer*, 33:471–476, 1988.
- [171] Emad M. Abo-Eldahab and Mohamed A. El Aziz. Blowing/suction effect on hydromagnetic heat transfer by mixed convection from an inclined continuously stretching surface

- with internal heat generation/absorption. *International Journal of Thermal Sciences*, 43:709–719, 2004.
- [172] M. Abd El-Aziz. Thermal-diffusion and diffusion-thermo effects on combined heat and mass transfer by hydromagnetic three-dimensional free convection over a permeable stretching surface with radiation. *Physics Letters*, 372(3):263–272, 2008.
- [173] F.M. Hady, F.S. Ibrahim, S.M. Abdel-Gaied, and M.R. Eid. Radiation effect on viscous flow of a nanofluid and heat transfer over a nonlinearly stretching sheet. *Nanoscale Research Letters*, 7:229, 2012.
- [174] N. Bachok, A. Ishak, and I. Pop. Unsteady boundary layer flow and heat transfer of a nanofluid over a permeable a stretching/shrinking sheet. *International Journal of Heat and Mass Transfer*, 55:2102–2109, 2012.
- [175] A.M. Rohni, S. Ahmad, A. Ismail, and I. Pop. Flow and heat transfer over an unsteady shrinking sheet with suction in a nanofluid using Buongiorno’s model. *International Communications in Heat and Mass Transfer*, 43:75–80, 2013.
- [176] J. Buongiorno. Convective transport in nanofluids. *Journal of Heat Transfer*, 128(3):240–250, 2005.
- [177] K. B. Pavlov. MHD flow of an incompressible viscous fluid caused by deformation of a surface. *Journal Magnetohydrodynamics*, 4:146–147, 1974.
- [178] K. Jafar, R. Nazar, A. Ishak, and I. Pop. MHD flow and heat transfer over stretching/shrinking sheets with external magnetic field, viscous dissipation and Joule effects. *The Candian Journal of Chemical Engineering*, 90:1336–1346, 2012.

- [179] A. J. Chamkha. MHD flow of a uniformly stretched vertical permeable surface in the presence of heat generation/absorption and a chemical reaction. *International Communications in Heat and Mass Transfer*, 30(3):413–422, 2003.
- [180] R. Kandasamy and P. G. Palanimani. Effects of chemical reactions, heat and mass transfer on nonlinear magnetohydrodynamic boundary layer flow over a wedge with a porous medium in the presence of Ohmic heating and viscous dissipation. *Journal of Porous Media*, 10:489–502, 2007.
- [181] S. P. Anjali and M. Thiyagarajan. Steady nonlinear hydromagnetic flow and heat transfer over a stretching surface of variable temperature. *Heat Mass Transfer*, 42:671–677, 2006.
- [182] S. S. Motsa, P. Dlamini, and M. Khumalo. A new multistage spectral relaxation method for solving chaotic initial value systems. *Nonlinear Dyn*, 72:265–283, 2013.
- [183] M. Suali, N.M.A. Long, and A. Ishak. Unsteady stagnation point flow and heat transfer over a stretching/shrinking sheet with prescribed surface heat flux. *Applied Mathematics and Computation*, 1:1–11, 2012.
- [184] K. T. Yang. Unsteady laminar boundary layers in an incompressible stagnation flow. *Journal of Applied Mechanics*, 25:421–427, 1958.
- [185] X. Q. Wang and A. S. Mujumdar. Heat transfer characteristics of nanofluids. *International Journal of Thermal Sciences*, 46:1–19, 2007.
- [186] M.A.A. Hamad and I. Pop. Scaling transformations for boundary layer flow near the stagnation-point on a heated permeable stretching surface in a porous medium saturated

- with a nanofluid and heat generation/absorption effects. *Transport in Porous Medium*, 87:25–39, 2011.
- [187] S. S. Motsa and S. Shateyi. Soret and Dufour effects on steady MHD natural convection flow past a semi-infinite moving vertical plate in a porous medium with viscous dissipation in the presence of a chemical reaction. *Evaporation, Condensation and Heat Transfer*, 16:582, 2011.
- [188] K. Bhattacharyya. Boundary layer flow and heat transfer over an exponentially shrinking sheet. *Chinese Physics Letters*, 28(7):074701, 2011.